High resolution mechanics of viruses studied by Atomic Force Microscopy

Ivanovska-Surtcheva, I.L.

2007

document version
Publisher's PDF, also known as Version of record

High resolution mechanics of viruses studied by Atomic Force Microscopy

Irena L. Ivanovska

This thesis is reviewed by:

prof.dr. J.L. Carrascosa
dr. A. Evilevitch
prof.dr. R. van Grondelle
prof.dr. F.C. MacKintosh
dr. S. Tans
prof.dr. Th. Schmidt

The work described in this thesis was performed in the group of Physics of Complex Systems at Vrije Universiteit. The project was financially supported by the "Nederlandse organisatie voor Wetenschappelijk Onderzoek (NWO)".

ISBN 97-890-8659-117-6

Cover design by I.L. Ivanovska
Printed in Bulgaria by GRAFIX Ltd, Sofia
2007

VRIJE UNIVERSITEIT

High resolution mechanics of viruses studied by Atomic Force Microscopy

ACADEMISCH PROEFSCHRIFT

ter verkrijging van de graad Doctor aan
de Vrije Universiteit Amsterdam,
op gezag van de rector magnificus
prof.dr. L.M. Bouter,
in het openbaar te verdedigen
ten overstaan van de promotiecommissie
van de faculteit der Exacte Wetenschappen
op donderdag 5 juli 2007 om 10.45
in het auditorium van de universiteit,
de Boelelaan 1105

door

Irena Lambrova Ivanovska-Surtcheva

geboren te Sofia, Bulgarije

promotor: prof.dr. C.F. Schmidt
copromotor: dr.ir. G.J.L. Wuite

CONTENTS

CHAPTER 1

"The chief difficulty Alice found at first was in managing her flamingo: she succeeded in getting its body tucked away, comfortably enough, under her arm, with its legs hanging down, but generally, just as she had got its neck nicely straightened out, and was going to give the hedgehog a blow with its head, it WOULD twist itself round and look up in her face, with such a puzzled expression that she could not help bursting out laughing: and when she had got its head down, and was going to begin again, it was very provoking to find that the hedgehog had unrolled itself, and was in the act of crawling away."

From ***Alice's Adventures in Wonderland***
by ***Lewis Carroll***

Introduction

Nature uses complex paths and mechanisms for material design and synthesis in living organisms on all scales. Specifically interesting for investigation are biological objects which are minimalistic in design and display surprising combinations of physical properties like robustness and resilience, while only rather weak intermolecular forces are responsible for their structural integrity. Examples of such objects are virus shells – they are self-assembled nanocontainers made of proteins which carry the genetic information of the virus from host to host for further infection. Some viruses, for example the bacteriophages, carry very long strands of DNA (a few microns long) compacted into a shell with sizes of tens of nanometers. The highly stressed DNA is kept inside under considerable pressure, tens of atmospheres, without rupturing. Detailed studies of the structure and protein organization in these shells in combination with knowledge of their mechanical properties could inspire new engineering materials which mimic the resistance to deformation and fracturing of those bioassemblies. Scanning Force Microscopy has been demonstrated to be a very powerful method both for manipulating these protein assemblies and for imaging them under different conditions.

Viruses

Viruses are microscopic particles containing a genome in a protein shell, which infects cells. There are several explicit properties which define an organism as a virus (1). Viruses carry genomic material either as RNA or as DNA containing all the information for its replication. They cannot replicate themselves and are using the host protein-synthesizing machinery for reproduction. Within an appropriate host cell, the viral genome is replicated and directs the synthesis using its cellular systems. Progeny virions are formed by self-assembly from newly synthesized components within the host cell. Those virions leave the host to transmit their viral genome to the next one and begin a new life cycle. Viruses may infect plants, animals or bacteria (called bacteriophages). They carry their genome in protective protein shells called capsids or nucleocapsids which self-assembly from one type or small amount of different types of subunits in a highly organized manner. The viral capsids are, besides their role to protect their genome against hostile environment, also actively involved in diverse mechanisms of genome delivery to the host cell. For example, plant viruses such as CCMV (2, 3) are known to disassemble and release their RNA inside the cell and bacteriophages such as ϕ 29 and lambda phage inject their DNA into the host cell using the pressure stored in their capsids due to the highly confined DNA molecule (4).

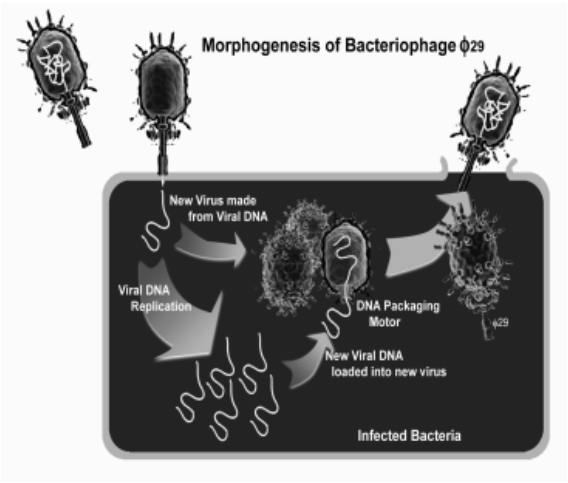

Fig. 1. Bacteriophage life cycle. Picture from M. Rossmann, Purdue University.

DNA is injected into the host cell while the empty phage remains outside; newly replicated DNA is packed into preformed proheads (5-8); the tail is attached; the new virions are lised from the host cell.

Icosahedral symmetry

A regular icosahedron is a symmetric structure with 12 pentagonal vertices and 20 equilateral triangular faces. It has a defined set of symmetry elements: 6 fivefold axes through the 12 vertices, 10 threefold axes through the 20 triangles and 15 twofold axes through the edges. To build an icosahedron out of protein, each face must be made of at least three proteins, because an individual protein does not normally have intrinsic threefold symmetry. The minimal amount of protein subunits to interact through the exact 2- 3- and 5 fold axes in identical ways is 60, but it turns out that most of the viruses are built from T (integer) times the number of 60, where T is called the triangulation number. The arrangement of a large number of small chemically identical units in icosahedral symmetry provides a genetically economical way to build up viral capsids. In that way only small fraction of the viral genome will be used for coding the virus protective shell and will produce large enough space for encapsulation of its genomic material. Self-assembly requires specificity of interactions among the proteins and a way to accomplish this is to allow them subsequently to form identical bonds with their neighbours. If more then 60 subunits interact to form a closed shell, (which is true for most of the viruses) not all of them can have identical environments. To address this issue Caspar and Klug proposed their principle of quasi-equivalence (9). Their hypothesis is that shells built from more than 60 subunits will be formed from identical subunits with slight but regular changes in the bonding, referred to as quasiequivalent. Their environments will be not any longer identical but very similar. The T number of the capsid counts the number of different environments which a subunit can have, hence a virus such as CCMV, with T=3, will have 180 subunits which will be involved in three slightly different but distinct types of bonding. The T number is a geometrical concept which describes how a closed structure can be built from a flat hexagonal lattice by replacing specific hexamers with pentamers. The pentamers themselves are obtained from a hexamer by cutting one of the 6 equilateral triangles of the hexamer and bringing together the free edges (Fig. 3). Hence the pentamers become convex and introduce the curvature needed to construct a closed shell. For large structures the position of the hexamers converted to pentamers can be described using a net with a

fix origin (O) at the center of a hexamer and coordinates (h, k) along the 60° axes of the net. Then T = h2 + hk+ k2, (h and k are any integers), describes the position of adjacent hexamer to be converted to pentamer (1, 10-12).

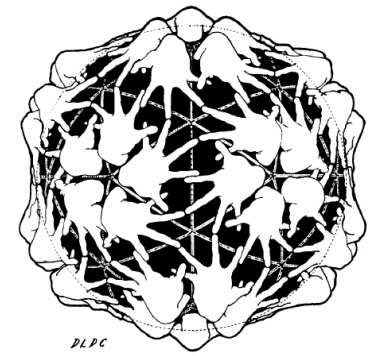

Fig.2 An icosahedral arrangement of hands.- illustration of the principles of quasi-equivalent molecular interactions. Illustration by Donald Caspar.

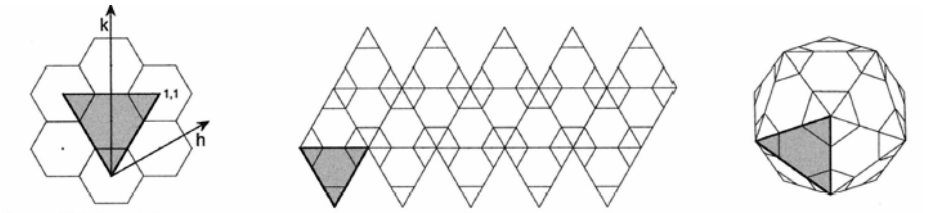

Fig 3. Geometric principles of constructing icosahedral lattices of defined T (triangulation) number. Example of T= 1 closed shell. The structure is generated by inserting 12 pentamers at appropriate positions in the hexamer net as specified by (*h,k*) lattice points that mark the centers of the original hexagons in the sheet.

Bacteriophage ϕ 29

ϕ 29 is a well characterized double-stranded DNA bacteriophage that infects Bacillus subtilis. The capsid is a prolate icosahedron, elongated along the 5-fold axis, with a triangulation number T = 3, Q = 5 (see Fig. 4). During its life circle the viral genome is packed into a preformed capsid, the prohead, using a portal motor which consist of the head-tail connector protein (gp10), a specific viral-coded RNA (pRNA) and the ATPase protein gp16 (14-17) The capsid furthermore consists of only one type structural protein gp8, head fibers (gp8.5), and its assembly require the presence of the gp10 connector and a scaffold protein (gp7) (13, 18, 19-21).

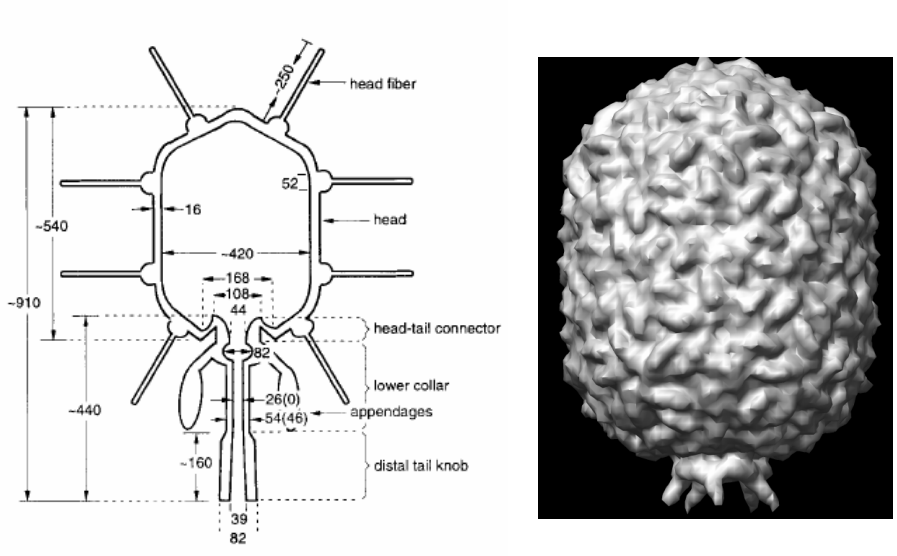

Fig. 4 A). Schematic diagram of Phi29 bacteriophage (Tao et al, *Cell*, **95**, 413). B) Pseudo-atomic reconstruction of Phi 29 prohead (European Bioinformatics B.A.L., McMurray, C.T., Anderson, D.L., and Rossmann, M.G. EMD-1117)

Gp8 is organized in pentamers and hexamers following the Caspar and Klug quasi–equivalence organization (9). The shape of the elongated prohead stems from a ring of 10 hexamers inserted between the two hemispheres of the icosahedron. The resulting structure is 45 nm wide and 54 nm long with a thickness of only 1.6 nm (14, 17, 20, 22). This tiny structure accommodates a 19.3 kb genome. The connector complex which replaces one of the gp8 pentamers, actively packages this 19.3 kb (6.6-μm) piece of DNA using an ATPase. Once packaged, the DNA is kept under high pressure (~ 6 MPa = 60 atm) inside the viral shell. No change in the head volume is observed during maturation, so the prohead and mature head have the same dimensions.

Bacteriophage λ

Wild-type (wt) phage *λ* (see .. 5) infects E. coli cells. It contains a double-stranded DNA (48,502 bp) in an icosahedral T=7 capsid to which a flexible, noncontractile tail is attached. The tail is 173 nm long, separately assembled and attached to one of the icosahedral 5-fold vertices of the capsid (23). The mature capsid has an outer diameter of 63 nm and shell thickness between 1.8

and 4.1 nm. It is built of 415 copies of the gpE protein (40 kDa) and 405-420 copies of the gpD protein (11.4 kDa). gpE forms the actual shell and is clustered in hexamers and pentamers. gpD decorate the shell and six gpD trimers surround each hexamer (24, 25). DNA packaging is accompanied by an expansion of the shell and the addition of gpD. λ phages can package DNA ranging in length from 78 to 106% of wt λ-DNA and remain infectious (26) If the genome is shorter than 78% DNA the phage fails to infect. When the DNA is longer than 106% of wt length packaging does not occur.

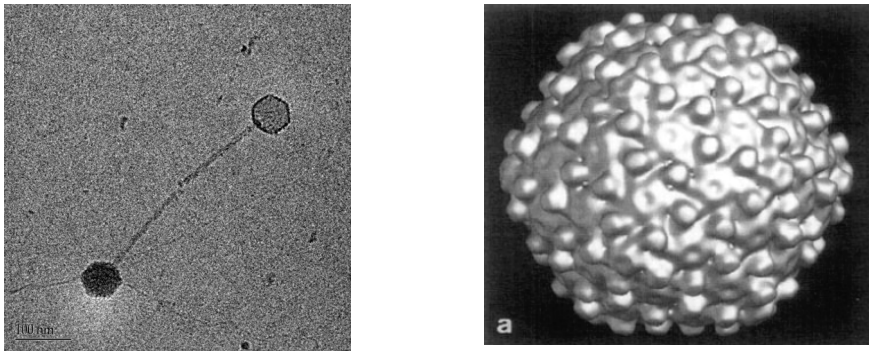

Fig. 5 A) Cryo EM image of empty and full with DNA λ phages. The tails of the two phages are oriented in one line (Evilevitch A. et al., (2005) *Biophys. J.* **88 (1),** 751-756). Pseudo-atomic reconstruction of the λ phage capsid outer surface (Dokland, T. & Murialdo, H. (1993) *J Mol Biol* **233**, 682)

CCMV

The CCMV capsid is an icosahedral shell with an outer diameter of 28 nm and an average thickness of 3.8 nm (Fig. 6a) (27). It is made of 180 copies of a single 190-residue long protein that is organized into two structural units (capsomers), pentamers and hexamers (28). The CCMV capsid consist of 12 pentamers and 20 hexamers arranged in a T = 3 organization (29) The CCMV genome consists of four single-stranded RNAs: RNAs 1 and 2, each about 3000 bases long, are packaged separately; RNAs 3 and 4 (2000 and 1000 bases, respectively) are packaged together (30) Capsids that contain these different parts of the genome are morphologically indistinguishable (31). Under the proper pH conditions and with the appropriate ionic strength of the buffer, mixtures of capsid proteins and RNA will spontanously self-assemble in vitro

into infectious viruses, indistinguishable from those obtained from diseased plants (30, 31). Under different conditions, it is also possible to let the proteins self-assemble into empty capsids that are structurally indistinguishable from full capsids (31).

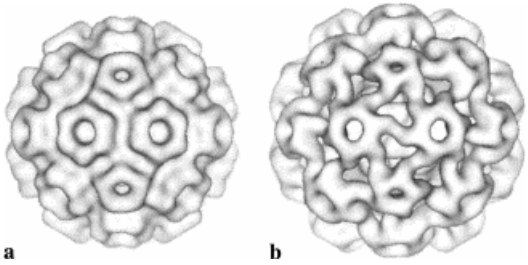

Fig.6. Cryo-EM image reconstructions of (a) native CCMV and (b) swollen CCMV particles. The capsids are placed with icosahedral twofold axis perpendicular to the page. The picture is adapted from H Liu, Vol 142, Issue 3 , 2003, 356

A number of mutants of CCMV (32-35) have been made by substitution or deletion of single residues in the capsid protein. Among them is the salt-stable (ss) mutant, which does not dissociate at pH 7.5 in high ionic strength buffer (I > 1 M). The stability stems from a single substitution in the capsid protein of Lys-42 to an Arginine. Another mutant, SubE, has the same substitution, but, in addition, the nine basic residues (Lysine and Arginine) at the N-terminus have been replaced by Glutamic acid. These substitutions result in a charge inversion and RNA cannot be packaged into this capsid. The native CCMV virion has divalent metal ions bound to its shell surface, which can be removed at pH 5 with EDTA without any visible change of the particles. When the metal ions are removed at pH 7 or if metal-free particles at pH 5 are transferred to a buffer of pH 7, then the capsid swell and increase their diameter by 10% (Fig. 6b). The phenomenon was interpreted by Bancroft in 1970 as a result of electrostatic repulsion of charged carboxyl clusters which exists in the absence of divalent metal ions at pH 7, but are protonated at pH5.

Scanning Probe Microscopy (36)

Scanning Probe Microscopy (SPM) is a microscopic technique used to study surface topology and properties. SPM uses a very sharp probe (tip) to scan a surface to generate an image based on tip-sample interactions. The Scanning Tunnelling Microscope has been invented first (1981). It is based on the detection of a tunnelling current between a metal needle and a conducting

sample. This current is used to control the tip-sample distance After the STM development, several other devices based on different interactive forces between the tip and the sample have been developed. The basic principle of these devices is that there is a parameter *(P)* which depends of the tip-sample distance with a well defined and unique function $P = P(z)$. This parameter can then be used in a feedback system which control this distance. During lateral movement of the tip across the surface, the sample topography changes the interaction parameter *P*. When the tip-sample distance changes, the feedback system restores the preset value in real time. In that way the surface topography $Z = f(x, y)$ can be obtained from the recorded feedback signal during the scanning.

Atomic Force Microscopy

Atomic Force Microscopy (AFM) was invented in 1986 by Bining, Quate and Herber (39) The detection probe of an AFM is a tip with a radial apex of 10-100 nm mounted on the end of a flexible cantilever with a length of several micrometers. The cantilever will bent due to the forces exerted on the tip due to the interaction with the sample. The cantilever bending can be precisely evaluated from the deflection of a laser beam focused on the free end of the cantilever. The position of the deflected laser beam is detected with a photodiode. The signal from the photodiode is used as a feedback parameter to control the tip-sample interaction. The tip (or the sample) can be controlled with an accuracy level of angstroms.

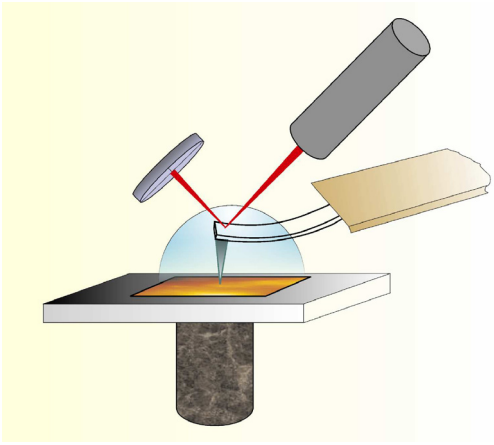

Fig.7. Simplified scheme of AFM set up.

Scanners

The cantilever movement has been achieved with special transducers (scanners) made from piezoelectric materials. Piezoelectric materials are known to change their size in an external electric field. Tubular piezoelements are widely used for AFM scanners since they allow large movement with relatively small input voltages.

Detectors

The optical detection system is aligned in a way that the beam deflected from the cantilever is positioned on the centre of four segmented photodiode. Differential currencies detected due to laser spot displacement after a change in the cantilever position due to tip-sample interactions indicate the bending and the torsion of the cantilever.

Cantilevers AFM cantilevers are typically produced by photolithography and etching processes. The common materials used are silicon, SiO_2 or Si_3N_4 layers on a silicon base. Cantilevers can be triangular or rectangular in shape. The most important parameters of a cantilever are: its spring constant which can vary from 10^{-3} N/m to 10 N/m and its resonance frequency which depend on the material properties (such as Young's modulus) and the geometrical dimensions of the cantilever. The probing tip is located on the free end of the cantilever. Typically the tips are pyramid shaped with an angle between 60 and 70 degrees and apex radius of curvature from 1 nm to 100 nm. The tip size is the most important parameter for the obtainable imaging resolution. The finite tip size results in a convolution between the sample topography and the tip shape, so the lateral dimensions of the scanned features appeared broadened in comparison to the actual size.

AFM modes

There are two methods to acquire images and properties of a sample: contact modes (quasi-static) and non-contact (oscillatory) modes (36). In **contact mode** the tip apex is in direct mechanical contact with the sample surface during scanning. The interaction force between the tip and sample is counterbalanced by the elastic force produced by the deflected cantilever. The scan can be performed at constant force or at constant tip-sample (average)

distance. The first case gives information of the surface topography and the second one about the spatial distribution of the interaction forces. In **non-contact mode** the cantilever is forced to oscillate with small amplitude (~1nm). Oscillations close to the surface are affected by an additional force due to van der Waals interactions with the sample. In this mode phase contrast images are acquired. The most common used oscillatory mode is the so-called **intermittent-contact** mode or **tapping mode** in which the cantilever is excited near its resonance frequency with amplitude of about 10 to 100 nm. The cantilever is moved to the surface till the tip makes "semi" contact with the sample. The resulting interactions are then a superposition of van der Waals and elastic forces on the cantilever.

Jumping mode

Jumping mode (40) or pulse force mode (41-43) scanning is essentially the same. In the first case the characteristic features are implemented by software while in the other case they are incorporated by electronics. These modes can be added as an external module to any AFM that allows access to the feedback signal from the photo detector. In this mode a sinusoidal voltage is used to modulate the Z piezo of the AFM with amplitude of 20 to 500 nm at a frequency of 100 Hz–2 kHz. The average distance between tip and sample is adjusted such that the tip is out of contact with the sample at the lowest point of the oscillation. At the highest point of the oscillation the cantilever reaches a defined maximum deflection. In principle this method allows recording force curves with high frequency. To avoid overloading the system with data only selected points of the force curves are recorded and evaluated. During each cycle, the AFM tip gets pushed onto the sample surface till the exerted force reaches a fixed maximum value. At that point the tip is retracted from the surface again. The sample is moved in lateral dimension when it is out of contact with the cantilever, hence shear forces on the sample are avoided. Since the analysis of the cantilever deflection signal is done in real-time, and the values can be feed into the channels of the AFM, high resolution images of adhesion or mechanical properties of the sample can be recorded in parallel with sample topography. Scanning performed in liquid almost eliminate the capillary forces, hence the tip can easily be detached from the sample surface

without pulling on it. All those features make jumping mode scanning very suitable for studying biological objects.

Force Distance curves

During force measurements (43, 44) a sample is moved up and down by applying a voltage to the piezoelectric translator, onto which the sample is mounted. The cantilever deflection, versus position of the piezo, normal to the surface is recorded with preset steps, which define the speed of the force versus distance (FZ) curve acquisition. To obtain a real FZ curve, the measured quantities have to be converted into force and distance. This requires calibration of the piezo, knowledge of the spring constant of the cantilever and the sensitivity of the cantilever bending. The later value can be obtained from the cantilever deflection when it is pushed on a surface much harder then itself. A FZ curve has the following characteristic regions: i) approach ii) jump to contact iii) deflection iv) retraction. If two FZ curves, one made on an "infinitely" hard surface and the other made on soft sample are matched at their initial position of bending (contact point), then the distances between two of them in vertical direction gives information about the indentation on the sample (Fig. 8)

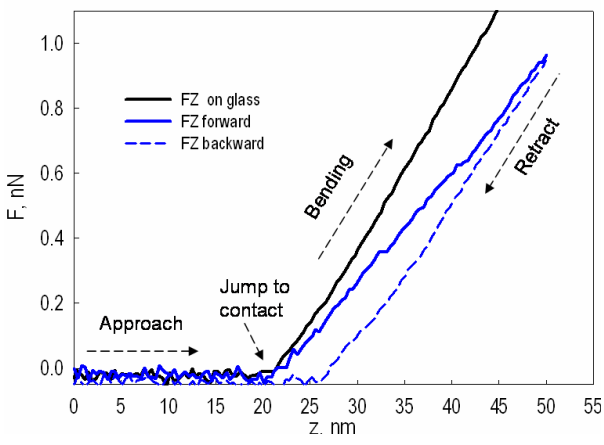

Fig.8. Force versus distance curve.

Theoretical background (45)

Under applied forces solid bodies exhibit deformation i.e. they change in shape and/or volume. When a body is deformed, the distances between its points change. The change in an element of length when the body is deformed is given by the *strain tensor*.

$$u_{ik} = \frac{1}{2}\left(\frac{\partial u_i}{\partial x_k} + \frac{\partial u_k}{\partial x_i} + \frac{\partial u_i}{\partial x_i}\frac{\partial u_i}{\partial x_k} \right) \qquad [1]$$

where $\boldsymbol{u}$ is the displacement vector $u_i = x_i^{'} - x_i$

When a deformation occurs, the arrangement of the molecules is changed and forces which therefore arise tend to return to their equilibrium. Then the total force can be written as the volume integral $\int \boldsymbol{F}\, dV$ where $\boldsymbol{F}$ is the force per unit volume and $\boldsymbol{F}\, dV$ the force on the volume element dV. Then

$$\int F dV = \int \frac{\partial \sigma_{ik}}{\partial x_k} dV = \oint \sigma_{ik}\, df_k \qquad [2]$$

The tensor σ_{ik} is called the *stress tensor* and the $\sigma_{ik}\, df_k$ is the i th component of the force on the surface element df. The continuum elastic theory describes only deformations small in respect to the dimensions of the deformed body.

The general expression for the free energy F of a deformed isotropic body is given by expanding F in powers of u_{ik}

$$F = F_0 + \frac{1}{2}\lambda {u_{ii}}^2 + \mu {u_{ik}}^2, \qquad [3]$$

where λ and μ are called *Lame coefficients*.

If the volume of the body is unchanged by the deformation, but only its shape then such deformation is called *pure shear*. The other ultimate case is when the shape remains unchanged and deformation change only the body's volume, then it is called *hydrostatic compression*. Any deformation can be represented as a linear combination of pure shear and pure compression and then the free energy can be rewritten as

$$F = \mu\left(u_{ik} - \frac{1}{3}\delta_{ik}\, u_{ik} \right)^2 + \frac{1}{2} K {u_{ii}}^2 \qquad [4]$$

The quantities *K* and μ are called respectively the *bulk modulus* or *modulus of compression* and *shear modulus* or *modulus of rigidity*. Hence the stress tensor can be calculated from [4] using the general thermodynamic relation which gives the relation between the stress tensor and the free energy for constant entropy and temperature by $\sigma_{ik} = (\partial F / \partial u_{ik})_T$.

$$\sigma_{ik} = K u_{ll} \delta_{ik} + 2\mu \left(u_{ik} - \frac{1}{3} \delta_{ik} u_{ll} \right) \qquad [5]$$

The converse formula which gives the strain tensor in terms of the stress tensor is

$$u_{ik} = \frac{\delta_{ik} \sigma_{ll}}{9K} + \frac{\left(\sigma_{ik} - \frac{1}{3} \delta_{ik} \sigma_{ll} \right)}{2\mu} \qquad [6]$$

When strain tensor u_{ik} is a linear function of the stress tensor σ_{ik} then Hook's law is valid, which generalised form is given by [5].

For some simple cases of homogeneous deformations two other important quantities can be derived. If we consider simple extension of a rod along the z axis due to the forces applied to its ends, it stretches in both directions. From [6] the non zero components (all u_{jk} with $i \neq k$ are zero) can be found:

$$u_{xx} = u_{yy} = -\frac{1}{3} \left(\frac{1}{2\mu} - \frac{1}{3K} \right) p, \qquad u_{zz} = \frac{1}{3} \left(\frac{1}{3K} + \frac{1}{\mu} \right) p, \qquad [7]$$

where with *p* is denoted the force per unit area. The coefficient of *p* is called coefficient of extension and the reciprocal value is called *modulus of extension* or *Young's modulus E:*

$$u_{zz} = p / E \qquad [8]$$

where

$$E = 9K\mu / (3K + \mu) \qquad [9]$$

Another widely used material parameter is the ratio of the transverse compression to the longitudinal extensions, which is called Poisson ratio, ν :

$$u_{xx} = -\nu u_{zz} \qquad [10]$$

where

$$\nu = \frac{1}{2}(3K - 2\mu)/(3K + \mu) \qquad [11]$$

Deformation of shells

The total free energy of a thin spherical shell with radius *R* surface element *dA* under deformation can be written as sum of two terms: its stretching and its bending energy

$$F = \frac{1}{2}\kappa \int (c - c_0)^2 \, dA + \frac{1}{2} E \int \sigma_{ik} u_{ik} \, dA \qquad [12]$$

where *c* is the shell mean curvature, c_0 its spontaneous curvature and κ is the bending rigidity

$$\kappa = \frac{E h^3}{12\left(1 - \nu^2\right)} \qquad [13]$$

The balance between the stretching and bending energies is characterised by a dimensionless number called the Foppl von Karman number

$$\gamma = \frac{E R^2}{\kappa} \qquad [14]$$

The Foppl von Karman number is an intrinsic characteristic of a closed shell and can be used to determine the equilibrium shape of icosahedral shells.

Linear regime

According to the thin shell theory (45) indentations of a spherical shell with an amplitude on the order of the shell thickness *h* are linearly related to the point force ***P*** need for that indentation. The indentation ζ is predicted to scale as $\zeta(P)/R \propto P/\sqrt{\kappa E}$. For close shells the stretching is a first order effect, the corresponding stress tensor is ~ $E\zeta/R$ and the stretching energy per unit is of order of $Eh\,(\zeta/R)^2$. On the other hand the bending energy is of the order of $Eh^3\,(\zeta/R^2)^2$ so the ratio between them is rather large (in the order of $(R/h)^2$). If we consider a shell as a deformed spring then the force *P* divided by the indentation along the axis on which the force is acting gives the linear spring

constant, *k*. In general, the linear spring constant *k* of a homogeneous shell of radius *R* can only depend on the Young's modulus *E*, the Poisson ratio ν of the material, and on the geometric quantities *h* and *R*. In fact, on dimensional grounds, the spring constant must be given by *E* multiplied by a length. For thin spherical shells, it is expected that k_{shell} is proportional to Eh^2 / R.

$$k = \alpha E\, h^2/R \qquad [15]$$

where the proportionality coefficient α is a geometrical prefactor and can be extracted from numerical calculations for a given geometry. Beyond this regime, non-linear buckling is predicted due to coupling of in-plane compression and out-of-plane bending. The buckling is predicted to occur under a uniform external pressure p_{cr},

$$p_{cr} \sim Eh^2/R \qquad [16]$$

Outline of the thesis

The thesis consists mainly of a collection of published and submitted publications. In chapter 2 describes the study of empty viral shells with Scanning Force Microscopy. We probe the mechanical properties of bacteriophage ϕ29 shells by applying point forces and obtain their Young's moduli. The extent of the elastic response is investigated and the forces which empty shells can withstand are shown. We also show that after repetitive pushing with low forces the capsids break. Chapter 3 presents a similar study on a plant virus - cowpea chlorotic mottle virus (CCMV). Bacteriophages and plant viruses have very different mechanisms of self assembly and genome delivery. We therefore like to compare the particles with eachother. In this chapter we investigate CCMV wild-type capsids, both with and without the RNA genome, as well as full capsids of a salt-stable mutant and empty capsids of the subE mutant. In chapter 4 we report a combined theoretical and experimental study of the structural failure of viral shells under mechanical stress. Discontinuities in the force-indentation curves which are associated with virus shell failure are connected with its intrinsic physical properties described with the Föppl-von Kármán (FvK) number. In chapter 5 I describe a detailed study of the fracturing of ϕ29 bacteriophage capsids. Finally, in

chapter 6 we investigate the correlation between packaged DNA length in phage λ (78 – 100 % of wt DNA) and capsid strength and elasticity. The results are explained and supported with a theoretical model. Chapter 7 is organized as a review of AFM studies of viruses. It makes comparisons between different virus shells and draws some conclusions based on their specific properties.

References

1. S.J. Flint, L. W. E., R.M. Krug, V.R. Racaniello, A. M. Skalka (2004) *Principles of Virology: Molecular Biology, Pathogenesis, and Control of Animal Viruses* (ASM Press, Washington, DC,).
2. Motoyosh.F, Bancroft, J. B., Watts, J. W. & Burgess, J. (1973) *Journal of General Virology* **20,** 177-193.
3. Bancroft, J. B. & Lane, L. C. (1973) *Journal of General Virology* **19,** 381-389.
4. Ponchon, L., Mangenot, S., Boulanger, P. & Letellier, L. (2005) *Biochimica Et Biophysica Acta-General Subjects* **1724,** 255-261.
5. Earnshaw, W. C. & Casjens, S. R. (1980) *Cell* **21,** 319-331.
6. Bazinet, C. & King, J. (1985) *Annual Review of Microbiology* **39,** 109-129.
7. Black, L. W. (1989) *Annual Review of Microbiology* **43,** 267-292.
8. Casjens, S. & King, J. (1975) *Annual Review of Biochemistry* **44,** 555-611.
9. Caspar, D. L. D. & Klug, A. (1962) *Cold Spring Harbor Symposia on Quantitative Biology* **27,** 1-&.
10. Baker, T. S., Olson, N. H. & Fuller, S. D. (1999) *Microbiology and Molecular Biology Reviews* **63,** 862-+.
11. Johnson, J. E. & Speir, J. A. (1997) *Journal of Molecular Biology* **269,** 665-675.
12. Zlotnick, A. (2004) *Proceedings of the National Academy of Sciences of the United States of America* **101,** 15549-15550.
13. Tao, Y., Olson, N.H., Xu, W., Anderson, D.L., Rossmann, M.G., and Baker, T.S. (1998) *Cell* **95,** 431-437.
14. Ibarra, B., Caston, J. R., Llorca, O., Valle, M., Valpuesta, J. M. & Carrascosa, J. L. (2000) *Journal of Molecular Biology* **298,** 807-815.
15. Simpson, A. A., Tao, Y. Z., Leiman, P. G., Badasso, M. O., He, Y. N., Jardine, P. J., Olson, N. H., Morais, M. C., Grimes, S., Anderson, D. L., Baker, T. S. & Rossmann, M. G. (2000) *Nature* **408,** 745-750.
16. Valpuesta, J. M. & Carrascosa, J. L. (1994) *Quarterly Reviews of Biophysics* **27,** 107-155.
17. Guasch, A., Pous, J., Ibarra, B., Gomis-Ruth, F. X., Valpuesta, J. M., Sousa, N., Carrascosa, J. L. & Coll, M. (2002) *Journal of Molecular Biology* **315,** 663-676.
18. Morais, M. C., Kanamaru, S., Badasso, M. O., Koti, J. S., Owen, B. A. L., McMurray, C. T., Anderson, D. L. & Rossmann, M. G. (2003) *Nature Structural Biology* **10,** 572-576.
19. Morais, M. C., Choi, K. H., Koti, J. S., Chipman, P. R., Anderson, D. L. & Rossmann, M. G. (2005) *Molecular Cell* **18,** 149-159.

20. Tao, Y. Z., Olson, N. H., Xu, W., Anderson, D. L., Rossmann, M. G. & Baker, T. S. (1998) *Cell* **95,** 431-437.
21. Morais, M. C., Kanamaru, S., Badasso, M. O., Koti, J. S., Owen, B. A. L., McMurray, C. T., Anderson, D. L. & Rossmann, M. G. (2003) *Nature Structural Biology* **10,** 572-576.
22. Wikoff, W. R. & Johnson, J. E. (1999) *Current Biology* **9,** R296-R300.
23. Hendrix, R. W. (1983) (Cold Spring Harbor, N.Y. : Cold Spring Harbor Laboratory.
24. Yang, F., Forrer, P., Dauter, Z., Conway, J. F., Cheng, N., Cerritelli, M. E., Steven, A. C., Pluckthun, A. & Wlodawer, A. (2000) in *Nat Struct Biol*, Vol. 7, pp. 230-7.
25. Dokland, T. & Murialdo, H. (1993) in *J Mol Biol*, Vol. 233, pp. 682-94.
26. Feiss, M., Fisher, R. A., Crayton, M. A. & Egner, C. (1977) in *Virology*, Vol. 77, pp. 281-93.
27. Reddy, V. S., Natarajan, P., Okerberg, B., Li, K., Damodaran, K. V., Morton, R. T., Brooks III, C. L. & Johnson, J. E. (2001) *J. Virol.* **75,** 11943-11947.
28. Speir, J. A., Munshi, S., Wang, G., Baker, T. S. & Johnson, J. E. (1995) *Structure* **3,** 63-78.
29. Baker, T. S., Olson, N. H. & Fuller, S. D. (1999) *Micro. Mol. Biol. Rev.* **63,** 862-922.
30. Bancroft , J. B. H., R. W. (1977) *Atlas of Insect and Plant Viruses* (Academic Press, New York, NY).
31. Fox, J. M., Wang, G., Speir, J.A., Olson, N. H., Johnson, J. E., Baker, T. S. & Young, M. J. (1988) *Virology* **244,** 212-218.
32. Douglas, T., Strable, E., Willits, D. Aitouchen, A., Libera, M. & Young, M. (2002) *Adv. Mater.* **14,** 415 - 418.
33. Fox, J. M., Zhao, X., Speir, J. A. & Young, M. J. (1990) *Virology* **222,** 115-122.
34. Fox, J. M., Albert, F. G., Speir, J. A. & Young, M. J. (1997) *Virology* **227,** 229-233.
35. Zhao, X., Fox, J. M., Olson, N. H., Baker, T. S. & Young, M. J. (Virology) **207,** 486 - 494.
36. Mironov, V. L. (2004) *Fundamentals of Scanning Probe Microscopy* (Russian academy of science, Institute of Physics of microstructures, Nizhni Novgorod).
37. Binnig, G. & Rohrer, H. (1982) *Helvetica Physica Acta* **55,** 726-735.
38. Binnig, G., Rohrer, H., Gerber, C. & Weibel, E. (1982) *Applied Physics Letters* **40,** 178-180.
39. Binnig, G., Quate, C. F. & Gerber, C. (1986) *Physical Review Letters* **56,** 930-933.
40. de Pablo, P. J., Colchero, J., Gomez-Herrero, J. & Baro, A. M. (1998) *Applied Physics Letters* **73,** 3300-3302.
41. RosaZeiser, A., Weilandt, E., Hild, S. & Marti, O. (1997) *Measurement Science & Technology* **8,** 1333-1338.
42. Krotil, H. U., Stifter, T., Waschipky, H., Weishaupt, K., Hild, S. & Marti, O. (1999) *Surface and Interface Analysis* **27,** 336-340.
43. Butt, H. J., Cappella, B. & Kappl, M. (2005) *Surface Science Reports* **59,** 1-152.
44. Cappella, B. & Dietler, G. (1999) *Surface Science Reports* **34,** 1.
45. L.D.Landau, E. M. L. *Theory of elasticity* (Institute of Physical Problems, USSR Academy of science, Moskow USSR, Moscow).

CHAPTER 2

"What do you know about this business?' the King said to Alice.

'Nothing,' said Alice.

'Nothing WHATEVER?' persisted the King.

'Nothing whatever,' said Alice.

'That's very important,' the King said, turning to the jury."

From *Alice's Adventures in Wonderland*
by *Lewis Carroll*

Bacteriophage capsids: tough nano-shells with complex elastic properties

I.L. Ivanovska[*†], P.J. de Pablo[*†§], B. Ibarra[‡], G. Sgalari[*¶], F.C. MacKintosh[*], J.L. Carrascosa[‡], C.F. Schmidt[*] and G.J.L. Wuite[*‖]

[*]Faculty of Exact Sciences, Department of Physics and Astronomy, Vrije Universiteit, Amsterdam, 1081 HV, The Netherlands.

[‡]Department of Structure of Macromolecules, Centro Nacional de Biotecnología, CSIC. Campus Universidad Autónoma de Madrid, Madrid, Spain.

Abbreviations: SFM, Scanning Force Microscopy; FZ, force-distance.

Published in ***PNAS, 2004*, vol. 101,** 7600

Abstract

The shell of bacteriophages protects the viral DNA during host-to-host transfer and serves as a high-pressure container storing energy for DNA injection into a host bacterium. Here, we probe the mechanical properties of nanometer-sized bacteriophage ϕ29 shells by applying point forces. We show that empty shells withstand nanonewton forces while being indented up to 30% of their height. The elastic response varies across the surface, reflecting the arrangement of shell proteins. The measured Young's modulus (~1.8 GPa) is comparable to that of hard plastic. We also observe fatigue and breakage of capsids after probing them repetitively. These results illustrate the mechanoprotection viral shells provide while also suggesting new design principles for nanotechnology.

The protective proteinaceous shells (capsids) of viruses are striking examples of biological materials engineering. These highly regular, self-assembled, nanometer sized containers are minimalistic in design, but combine complex passive and active functions. Besides chemical protection, they are involved in the selective packing and the injection of the viral genetic material (1, 2). *Bacillus subtilis* phage ϕ29 is a relatively small virus built of only seven different structural polypeptides, including a scaffolding protein directing the assembly. Its capsid assembles as a 54x42 nm precursor (prohead; Fig. 1A, B), which consists of four proteins, but most of the mechanically coherent shell is made of only one protein (gp8), the presence of one additional component (the fiber protein) being dispensable for structural integrity (3-6). The organization of these proteins within a prohead is known from cryo-electron microscopy (EM) (3, 4, 7-10). A prolate shell is constructed from 235 gp8 subunits form in a T = 3 lattice with 11 pentameric plus 20 hexameric units forming icosahedral end caps and 10 hexameric units forming the cylindrical equatorial region. In one of the end caps the central pentamer is replaced by the connector complex consisting of a dodecamer of gp10 subunits. The connector complex actively packages a 6.6-μm piece of DNA using an ATPase (10, 11). Once packaged, the DNA is kept under high pressure (~ 6 MPa = 60 atm) inside the viral shell (1, 12, 13).

The structure of many viral capsids is rather well known from scanning force microscopy (SFM), X-ray crystallography and EM studies (3, 5, 14-18), but very little is as yet known about their dynamic mechanical properties from direct measurements. Understanding the mechanical properties of such nanometer-scale shells is not only important for virus biology but may also provide inspiration for future nanotechnology. Here, we use SFM to directly probe the mechanical strength and elastic response of ϕ29 capsids. We measured a Young's modulus of about 1.8 GPa, and found evidence for local structure in the mechanical response of the shells. We also studied the breakage and slow disintegration of the viral capsids by deforming them repeatedly with the SFM tip. This method naturally extends to studying other viral shells as well as the mechanical consequences of filling the shells with DNA.

Materials and Methods

Sample preparation.

The proheads used for our experiments were purified from *Bacillus subtilis* bacteria infected with a ϕ29 mutant in genes 14 and 16 (ATPase), which results in the formation of stable empty proheads (4). The buffer used for imaging is TMS (50 mM Tris-HCl pH = 7.8, 10 mM $MgCl_2$, 100 mM NaCl). The prohead stock solution (c = 6 µg/µl) is diluted 100-fold into the same buffer. A droplet of 20 µl was deposited on a glass disk mounted on the piezo holder. After waiting 20 minutes for the adsorption of the proheads, the surface is gently rinsed with TMS to remove unbound objects while keeping the surface wet. The glass disks themselves were first cleaned in a solution of 10% KOH and 90% ethanol, dried in vacuum and made hydrophobic in vapor of hexamethyldisilazane (Sigma-Aldrich) in order to attach the proheads.

SFM measurements.

All SFM images were taken with a Nanotec™ SFM operated in "jumping mode" in liquid (19). The relevant feature of this mode is that the lateral displacement of the tip occurs always when it is not in contact with the sample so that shear forces are avoided. During imaging with jumping mode the tip performs a rapid succession of force-distance (FZ) curves, each taken in several milliseconds in a raster scanning fashion. The maximal applied force is well defined, since each individual approach is stopped at the cantilever deflection corresponding to the set force. Force-distance curves were recorded by measuring cantilever deflection (force) as a function of the vertical position of the piezo to which the sample was mounted. The experiments were performed in liquid in order to investigate the proheads under physiological conditions, and to reduce surface tension forces. The cantilevers used (OMCL-RC800PSA, Olympus, Japan) had nominal spring constants of 0.05 N/m, which allowed us to apply low loads (<100pN) on the viral shells. The tip-radii of the cantilevers were <20 nm. The spring constant of the cantilevers were calibrated using a thermal oscillations method (20), and within the used wafer unit they were 0.052 ± 0.007 N/m.

Results and Discussion

Imaging proheads. We imaged surface-attached proheads using jumping mode SFM which allowed us to accurately control maximal tip-sample forces (see Material and Methods) (19). Imaging was first performed at low resolution (128 or 64 pixels/micron) and low maximal force (<100 pN) in order to determine the prohead position and orientation (Fig. 1C). The distribution of the measured heights of the proheads (Fig. 1D) shows two distinct peaks centered at 42 nm (std. dev. = 2nm, N = 50) and 54 nm (std. dev. = 2nm, N = 43). These values are consistent with width (R_s) and height (R_l) of proheads as determined by EM (3, 5). Therefore, about half of the shells were deposited on their side and the other half standing upright on the surface. For testing their mechanical properties, we have focused on the proheads deposited on their side since the upright shells likely represent two different, hard to distinguish populations, i.e. attached through either the connector end or the opposite end of the capsid. In addition, probing these upright objects led to erratic results.

High-resolution scans of individual proheads showed that they were intact and not measurably perturbed by consecutive imaging at low maximal forces of up to 100 pN (Fig. 1E). When a surface is scanned in contact mode, instead of in jumping mode, lateral forces are exerted on the deposited capsids. We could detach proheads from the surface in contact mode while no evidence of shell rupture (i.e. leftover debris) was observed. These observations show that the binding strength to the surface was smaller than the protein-protein interactions within the proheads. Both results indicate that the surface does not significantly affect the shell. Nevertheless, the proheads were firmly enough attached to not move with respect to background markers after successive scans. Also features visible on the exterior of the proheads were stationary in consecutive high-resolution images of the same object. They thus seemed to be an attribute of the shells, i.e. the gp8 surface topology, and not a scanning artifact. In some images, the connector could be observed in the expected location and with the expected size (~19 nm), matching EM and X-ray studies (7-9).

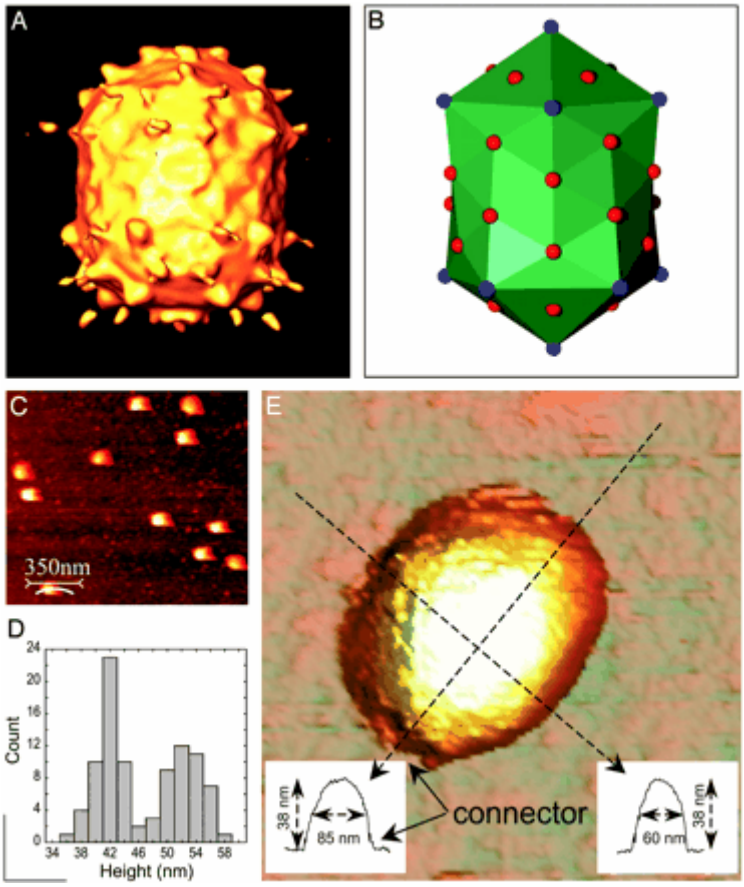

Fig. 1. Bacteriophage ϕ29 prohead shape and structure. (A) 3D cryo-electron microscopy reconstruction of an empty prohead. (B) Schematic model of the protein organization within a prohead as reconstructed from cryo-electron microscopy. (C) Low resolution SFM image of ϕ29 proheads in buffer (2x2 μm scan area; 128x128 pixels). The proheads were attached to a glass surface by hydrophobic interaction. Topography is recorded using jumping mode with a loading force of ~100 pN. (D) Bimodal distribution of the measured heights of the attached objects (N = 93). (E) High resolution 3D-image of a prohead (loading force ~120 pN) with the corresponding cross-section profiles along both axes of the prohead.

Imaging shells with the SFM at different maximal loading force showed the deformability of ϕ29 shells under uniaxial pressure (Fig. 2A). Shells appeared progressively flattened with higher maximal scan forces and were eventually destroyed. Shells also appeared laterally narrower due to the

reduction in the apparent lateral dilation caused by the tip. This is likely due to a combination of vertical and lateral deformation under large load. In figure 2A (panel 4) it can be seen that up to a certain critical force the induced deformations were reversible – the shell responded elastically. The decrease in measured height of proheads was approximately proportional to force up to a critical force of ~0.6 nN (Fig. 2B). Above that critical force, the rapid repetitive indentation inherent to the imaging procedure caused them to break apart (Fig. 2A, 6). Subsequent low-force images of such broken capsids typically showed that large fragments of virus shell remained intact (Fig. 2A, 7).

Indenting shells. The topographical maps of ϕ29 proheads made in imaging mode at fixed maximal load forces are, for every image, the result of more than 2000 tip-sample interactions. To investigate quantitatively the elastic response of the viral shells we recorded single FZ curves (see Material and Methods) after positioning the SFM tip above the center of individual proheads. We roughly located the center of a prohead by stopping the cantilever in the middle of a topographical scan of a prohead. We then fine-tuned the tip position by making a profile scan and by re-directing the tip to the middle of the virus cross-section. This method made sure that the equatorial region of the prohead was probed and that pushing near the end-caps where the shell curvature can cause slipping of the tip was avoided. FZ curves were recorded in two different modes. In the first mode, curves were recorded slowly (~1 sec) after repositioning the tip to within a few nanometers of the shell center following each contact. This procedure corrected for slow stage drift and allowed us to repeatedly probe a region within the equatorial band (Fig. 3a); the other procedure consisted of recording fast sequences of force-distance curves each taken within 8 msec, to approximately linear response of the proheads to tip forces of up to several nanonewtons. From the slope of the linear sections of the FZ curves, we could therefore calculate a spring constant of the prohead (k_{shell}) using $k_{shell} = k_c k_{eff} \left(k_c - k_{eff}\right)^{-1}$, where k_{eff} is the effective (measured) spring constant due to both cantilever bending and shell deformation acting as two springs in series, and k_c is the spring constant of the cantilever.

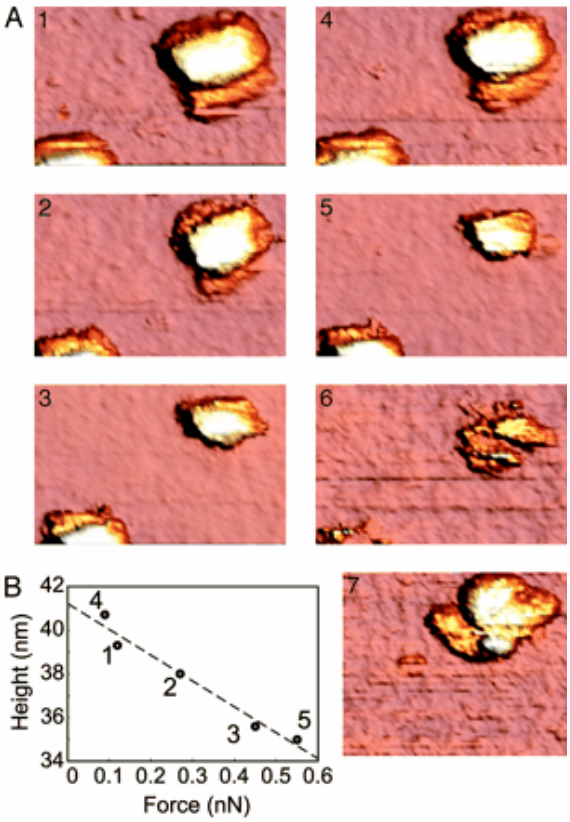

Fig. 2. Force dependence of the appearance of proheads. (A) 3D-topographical SFM images each taken with a different maximal loading force. Panel 1, the applied maximal loading force, $F_{applied}$, was 120 pN, the maximal measured height, h_{max}, (= 39 nm) corresponds to a slightly deformed shell. Panel 2, F_{max} = 270 pN; h_{max} = 38 nm. Panel 3, F_{max} = 450 pN; h_{max} = 35.5 nm. Panel 4, F_{max} = 90 pN; h_{max} = 40.5 nm – when lowering the maximal force, the shell recovered to its original shape. Panel 5, F_{max} = 550 pN; h_{max} = 35 nm. Panel 6, in the process of taking a topographical image with a maximal loading force of 600 pN the shell was destroyed. Imaging involved thousands of individual tip-sample contacts, which probably started to weaken the structure. Panel 7, lowering the loading force again to 90 pN showed that the broken shell consisted of large fragments, with h_{max} = 27 nm. (B) The dependence of the measured height on applied force (the dashed line is a linear regression).

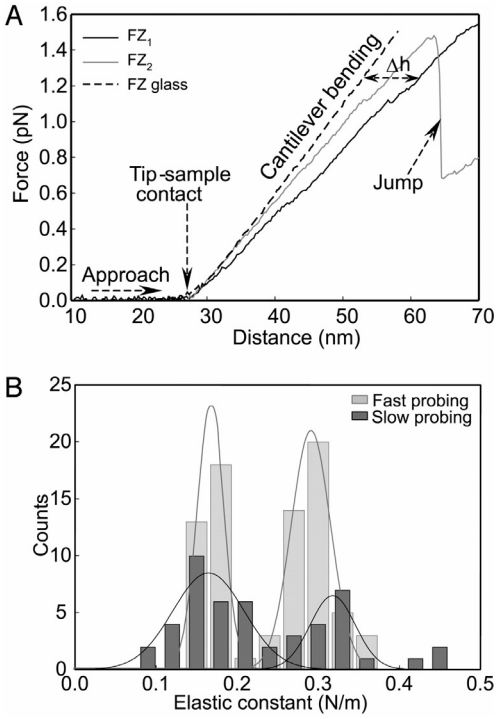

Fig. 3. Determining the elastic response of proheads. (A) Two typical FZ curves taken in sequence in slightly different locations on a single shell, and a FZ curve taken on the glass surface. The glass curve was shifted along the z-axis to match the tip-sample contact points of FZ1 and FZ2, to allow a direct readout of the indentation of the shell due to the applied force. Sudden discontinuities sometimes occurred in the FZ curves as seen in FZ2 at 1.4 nN. This is probably due to a fracture in the shell. (B) Histograms of measured spring constants. Red: 13 intact shells, each measured several times (N_{total} = 48). The tip was re-centered before each FZ curve. Gray: two rapid series of FZ curves (8 ms per curve), taken at two locations on a prohead (N = 77).

Modeling thin virus shells. The observed linear behavior is expected from thin shell mechanics, which predicts a linear elastic response for the indentation of a homogeneous spherical shell up to an indentation amplitude on the order of the shell thickness, *h* (21). Beyond this regime, non-linear buckling is predicted due to coupling of in-plane compression and out-of-plane bending. In general, the linear spring constant *k* of a homogeneous shell of radius *R* can only depend on the Young's modulus *E*, the Poisson ratio ◎◎

of the material, and on the geometric quantities h and R. In fact, on dimensional grounds, the spring constant must be given by E multiplied by a length. For thin spherical shells, it is expected that k_{shell} is proportional to Eh^2/R (21). We have calculated analytically the deformation of a homogeneous, spherical, elastic shell subject to equal and opposite forces applied at the poles, by expanding the shape of the deformed sphere in spherical harmonics. This procedure allowed us to calculate the full elastic energy by standard methods (22, 23). Assuming the shell is composed of a linear elastic material with a Poisson ratio of 0.3[††], we reproduced the expected $E\,h^2/R$ scaling of the spring constant for thin shells, with a coefficient of approximately 4.5 for h/R = 0.1. Thus the effective spring constant for the total pole-to-pole indentation becomes,

$$k = 2.25\,E\,h^2/R \qquad (1)$$

With this expression and the measured k_{shell}, we can estimate the Young's modulus of the virus shell, taking the values of h and R from EM studies (3).

Mechanically inhomogeneous shells. We found, surprisingly, by pushing on different intact proheads on the center area of the equatorial band, that a bimodal distribution emerged for the elastic constant of the shells (Fig. 3B, red bars). The two spring constants were 0.31 N/m (std. dev. = 0.03, N = 18) and 0.16 N/m (std. dev. = 0.04, N = 30), respectively. To rule-out the possibility that the soft response could be due to damaged structures, we included only objects in the histogram that were sampled in at least 2 locations, and for which we measured at least one high spring constant after softer ones. Elasticity measurements after irreversible behavior (breakage) were excluded from the histogram as well. Pushing rapidly and up to 100 times on two different locations on a prohead (Fig. 3B, gray bars), we found again a bimodal distribution in the spring constant with similar mean values and standard deviations as when different objects were sampled and compared[‡‡].

[††]Most materials have a Poisson ratio between 0.2-0.5. The dependence of our result on the precise value of the Poisson ratio within this range is very weak ~5%.

[‡‡]Surface effects are considered an unlikely source for such bimodal distribution. Since it would require that a single virus has two modes of interaction with the surface between which it can reproducibly shift back and forth. Moreover, such sticking/un-sticking mechanism should be independent of the applied indentation force, and would have to be reproducible from virus to virus as well.

The bimodal distribution can be explained by the inhomogeneous structure of the shell on the scale of the subunits (gp8), which is comparable to the size of the tip contact region (~5 nm) (3, 24, 25). Given these scales, we expect to be able to resolve some local structure of the shells with the SFM. The observed variation of the elastic response can arise either from inhomogeneity of the material (e.g., its thickness) or from variations in local curvature (26) – it is harder, for instance, to indent a convex area than a flat one. It may be surprising, however, to find a bimodal distribution of spring constants instead of a broad distribution. Considering the way a shell deforms under point forces can provide a possible explanation for this phenomenon. Although stress is concentrated near the tip in a local indentation, there is always a dominating (by amplitude) long-wavelength deformation corresponding to a global flattening of the spheroidal shell. This mode averages over local inhomogeneities in the surface. Only if the local elastic response becomes as soft or softer than the response due to the global mode will the local softness be apparent. The overall compliance observed with the SFM in the linear regime can therefore roughly be modeled by two springs in series: one corresponding to the local mode and the other to the global mode. Based on this picture, the highest measured spring constants should reflect primarily the properties of the shell as a whole (the global mode), and in particular should be observed whenever the tip is in contact with a locally stiff region. The appearance of a weaker resistance to the tip on the other hand suggests a soft local area. Thus, the observed bimodal distribution points to the presence of a particularly soft mode of local deformation. Considering the structure of the proheads (fig 1B) a plausible candidate for such soft spots could be the central area of the hexagonal regions within the equatorial band, which are weakly curved and of order of ~15 nm diameter. Based on this model, we have used the larger spring constant in the analytical and finite element analysis of the global shell properties.

Extracting material properties. Treating the empty prohead as homogeneous and as a sphere, we obtain Young's moduli E from Eq. (1) of 1.2 or 1.6 GPa, inserting for R either one of the two radii of the more realistic ellipsoidal shape and using an h of 1.6 nm. The result underestimates/overestimates E for

the short/long radius. Apart from neglecting the actual prolate shape, this calculation also does not take into account the geometrical constraint due to the deposition of the proheads on a flat surface which could result in an overestimation of the *E*. Therefore, for comparison, we have modeled our experiments using finite element methods.

The finite element model (CADRE, cadrepro4.2TM) of the virus shell consisted of 9000 elements each 1.6 nm thick with a Poisson ratio of 0.3, arranged in a hollow 20x27 nm geodesic ellipsoid resting on a surface. A point loading force, perpendicular to the surface, is applied on top of the equatorial region, mimicking the SFM experiments. We again assume that the structure is homogeneous. The modulus *E* can now be adjusted in order to match the experimental $k_{shell,1}$. This resulted in an estimate of $E = 1.8 \pm 0.2$ GPa, consistent with the analytical result, if one reasonably assumes that the long axis is dominant for the elastic response of the prohead. This value of the Young's modulus is close to the values of hard plastics and similar to values measured for other structural proteins such as actin, tubulin or collagen (27).

The finite element analysis also quantifies the stresses for every element of the object. According to our analysis the maximal in-plane stresses (compression/extension) at 1 nN applied point force for a prohead are found to be on the order of 0.3 GPa[§§]. Reliably determining maximal stresses at higher forces would require a more sophisticated model incorporating the inhomogeneous features of the prohead. Nevertheless, 0.3 GPa is a lower estimate for the tensile stresses the empty prohead can still withstand when indented by a force acting from the outside of the structure. The minimal rupture strength of the shells due to internal pressure has been theoretically estimated to be 0.1-0.3 GPa (1, 13, 28, 29)[¶¶]. Since indentation reorders the monomers even more than expansion of the shell, it seems that the tensile strength due to internal pressure of the proheads could even be higher than 0.3 GPa.

[§§]Modeling assumes a point force with an idealized shell that doesn't change its thickness, in reality the tip will indent into the surface (Hertz contact), which spreads the force and prevents divergent stresses and breakthrough. For Hertz behavior to be observable, however, the tip radius would have to be smaller than the thickness of the shell.

[¶¶]The estimate of the tensile strength by Smith et al. (2001) is based on proheads filled with DNA while our measurements are based on empty proheads. While proheads do not seem to increase in size or change shape when filled with DNA, there may be some maturation occurring during DNA packaging. This could conceivably change the shell properties during packing process, resulting in an alteration of the tensile strength.

Exploring the limits of proheads. To probe the limits of the elasticity and the resilience of the prohead we applied loads of up to several nanonewtons (Fig. 4A), and we found that proheads still responded linearly up to forces of 2.8 ± 0.3 nN (N = 11). At these forces they were indented by 12 ± 3 nm (N = 11). This is a deformation of almost 30% of the total height of a prohead. Nevertheless, proheads would still recover to their normal height after such large deformations, even after pushing repetitively, tens of times, on the same location. Height recovery took place faster than 4 ms, thus the relaxation time of the proheads was less than that. At forces beyond ~2.8 nN there were significant deviations from linearity, with the slope of the force-distance curves decreasing (Fig. 4A). This non-linearity has the opposite sign from the non-linear response observed when indenting solids, usually modeled by the Hertz model (30, 31). It is expected that a thin shell will undergo a buckling transition where curvature gets inverted under the point of pressure and stresses will be concentrated in a ring of finite radius around the emerging dent (21). The predicted decrease in stiffness is qualitatively observed in our experiments.

We also observed irreversible breakage after repeatedly pushing on a prohead (Fig. 4B), presumably due to material fatigue. After such an event, a prohead often still responded linearly to applied force, but with a permanently lower elastic constant. Continued pushing on a shell with high force caused severe fracturing of the structure and eventually caused it to fall apart (Fig. 2B, triangles). Severely destroyed shells also started to react in a plastic manner to applied force. An upper limit for the energy dissipated in a small shell rupture can be estimated by calculating the area between two up-curves before and after a rupture event up to the indentation at which the rupture had occurred. For instance, from the blue curves shown in figure 4c, using numerical parameters from Purohit et al (2003) (12), it can be estimated that the loss of energy (~1.3 10^{-18} Nm) is about the energy it would cost to dislodge a single monomer from the shell or form a crack of ~25 nm. Larger breakage events were also observed, which could mean that entire oligomeric forms were removed.

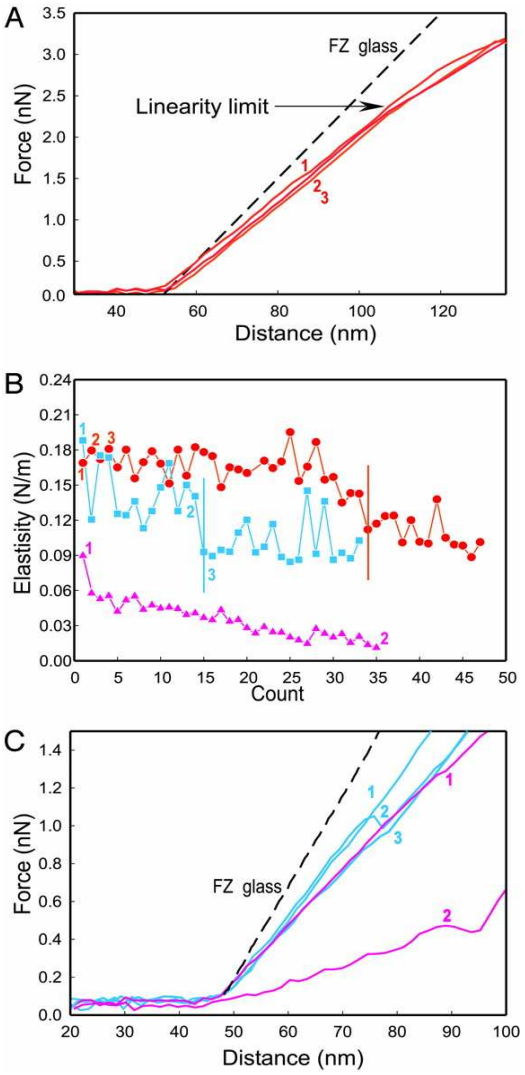

Fig. 4. Pushing the limits of the capsids. (A) Three consecutive FZ curves taken in rapid succession (8 msec) on a prohead. This shell responded linearly to applied forces up to ~2.5 nN. At higher forces a softer reaction to applied force was observed. The elastic constant was calculated from the linear region of each curve in this figure. (B). The change of the measured spring constant with repeated indentations on three different proheads (red, blue and magenta). The red curve (related to the curves in panel *A*) shows a gradual change of the elasticity after about 30 indentations whereas the blue curve shows a sudden decrease. Both show that the rigidity of the object is permanently lowered after the decrease (marked by the vertical lines). This decrease was an indication of the destruction of the viral shell. The magenta curve illustrates how repeated indentation of a prohead can eventually completely disintegrate it. This prohead appeared broken at the first scan and its rigidity decreased further with each consecutive indentation. (C) The magenta and blue curves relate to the ones in panel *B*. The blue curves display a discrete breakage event in the prohead, which resulted in a permanently lower spring constant of the object. The magenta FZ curves represent the first and last curves of a shell, which disintegrated with every consecutive push.

Conclusions.

Our results show that one can probe nano-scale shells and quantitatively extract their mechanical properties. We find that the capsid of bacteriophage ϕ29 is remarkably dynamic yet resilient and tough enough to easily withstand the known packing pressure of DNA (~60 atmospheres). These capsids thus not only provide a chemical shield, but also significant mechanical protection for their genetic contents. Viral shells are a remarkable example of nature's solution to a challenging materials engineering problem—they self-assemble to form strong shells of precisely defined geometry (32), using a minimum amount of different proteins. These biological construction principles suggest possible approaches for manmade nano-scale containers. The method developed here provides a new window on viral structural biology, focusing on the mechanics. Important areas to be explored in the future include the effects of packing DNA, the state of the packed DNA inside the shells and maturation of viral particles.

Acknowledgments

We like to thank T. Smit for stimulating discussions. This work was supported by a NWO Vernieuwingsimpuls grant (2000) (to G.J.L.W.), by grants from the Dutch Foundation for Fundamental Research on Matter (FOM) (to F.C.M. and C.F.S.) and partly supported by grant BMC2002-00996 (to J.L.C.).

References

1. Smith, D. E., Tans, S. J., Smith, S. B., Grimes, S., Anderson, D. L. & Bustamante, C. (2001) *Nature* **413,** 748-752.
2. Earnshaw, W. C. & Casjens, S. R. (1980) *Cell* **21,** 318-31.
3. Tao, Y. Z., Olson, N. H., Xu, W., Anderson, D. L., Rossmann, M. G. & Baker, T. S. (1998) *Cell* **95,** 431-437.
4. Ibarra, B., Caston, J. R., Llorca, O., Valle, M., Valpuesta, J. M. & Carrascosa, J. L. (2000) *J. Mol. Biol.* **298,** 807-815.
5. Rossmann, M. G., Bernal, R. & Pletnev, S. V. (2001) *J. Struct. Biol.* **136,** 190-200.
6. Wikoff, W. R. & Johnson, J. E. (1999) *Curr. Biol.* **9,** R296-R300.
7. Valpuesta, J. M., Fernandez, J. J., Carazo, J. M. & Carrascosa, J. L. (1999) *Struct. Fold. Des.* **7,** 289-296.
8. Simpson, A. A., Tao, Y. Z., Leiman, P. G., Badasso, M. O., He, Y. N., Jardine, P. J., Olson, N. H., Morais, M. C., Grimes, S., Anderson, D. L., Baker, T. S. & Rossmann, M. G. (2000) *Nature* **408,** 745-750.

9. Guasch, A., Pous, J., Ibarra, B., Gomis-Ruth, F. X., Valpuesta, J. M., Sousa, N., Carrascosa, J. L. & Coll, M. (2002) *J. Mol. Biol.* **315,** 663-676.
10. Valpuesta, J. M. & Carrascosa, J. L. (1994) *Q. Rev. Biophys.* **27,** 107-155.
11. Guo, P., Peterson, C. & Anderson, D. (1987) *J. Mol. Biol.* **197,** 229-36.
12. Purohit, P. K., Kondev, J. & Phillips, R. (2003) *Proc. Natl. Acad. Sci. USA.* **100,** 3173-3178.
13. Tzlil, S., Kindt, J. T., Gelbart, W. M. & Ben-Shaul, A. (2003) *Biophys. J.* **84,** 1616-1627.
14. Baker, T. S., Olson, N. H. & Fuller, S. D. (2000) *Microbiol. Mol. Biol. Rev.* **64,** 237-237.
15. Johnson, J. E. & Speir, J. A. (1997) *J. Mol. Biol.* **269,** 665-675.
16. Moody, M. F. (1999) *J. Mol. Biol.* **293,** 401-433.
17. Kuznetsov, Y. G., Malkin, A. J., Lucas, R. W., Plomp, M. & McPherson, A. (2001) *Journal of General Virology* **82,** 2025-2034.
18. Kuznetsov, Y. G., Victoria, J. G., Robinson, W. E. & McPherson, A. (2003) *Journal of Virology* **77,** 11896-11909.
19. de Pablo, P. J., Colchero, J., Gomez-Herrero, J. & Baro, A. M. (1998) *Appl. Phys. Lett.* **73,** 3300-3302.
20. Burnham, N. A., Chen, X., Hodges, C. S., Matei, G. A., Thoreson, E. J., Roberts, C. J., Davies, M. C. & Tendler, S. J. B. (2003) *Nanotechnology* **14,** 1-6.
21. Landau, L. D. & Lifshitz, E. M. (1986) *Theory of elasticity* (Pergamon Press, New York).
22. Niordson, F. I. (1985) *Shell Theory* (North-Holland, Amsterdam).
23. Zhang, Z., Davis, H. T. & Kroll, D. M. (1993) *Physical Review E* **48,** R651-R654.
24. Caspar, D. L. D. & Klug, A. (1962) *Cold Spring Harbor Symp. Quant. Biol.* **27,** 1-24.
25. Johnson, K. L. (2001) *Contact Mechanics* (Cambridge University Press, Cambridge.
26. Bausch, A. R., Bowick, M. J., Cacciuto, A., Dinsmore, A. D., Hsu, M. F., Nelson, D. R., Nikolaides, M. G., Travesset, A. & Weitz, D. A. (2003) *Science* **299,** 1716-1718.
27. Howard, J. (2001) *Mechanics of Motor Proteins and the Cytoskeleton* (Sinauer Associates, Inc., Massachusetts).
28. Kindt, J., Tzlil, S., Ben-Shaul, A. & Gelbart, W. M. (2001) *Proc. Natl. Acad. Sci. USA.* **98,** 13671-13674.
29. Cordova, A., Deserno, M., Gelbart, W. M. & Ben-Shaul, A. (2003) *Biophys. J.* **85,** 70-74.
30. Hertz, H. (1882) *J. Reine Angew. Mathematik* **92,** 156-171.
31. Sneddon, I. N. (1965) *Int. J. Eng. Sci.* **3,** 47-57.
32. Lidmar, J., Mirny, L. & Nelson, D. R. (2003) *cond-mat/0306741*.

CHAPTER 3

"What **is** *the use of repeating all that stuff,'* the Mock Turtle interrupted, *`if you don't explain it as you go on? It's by far the most confusing thing I ever heard!'"*

From *Alice's Adventures in Wonderland*
by Lewis Carroll

Nanoindentation studies of full and empty viral capsids and the effects of capsid protein mutations on elasticity and strength

I. L. Ivanovska[2], J. P. Michel[1], M. M. Gibbons[3], W. S. Klug[3], C. M. Knobler[1], G. J. L. Wuite[2] and C. F. Schmidt[2]

[1] Department of Chemistry and Biochemistry, University of California Los Angeles, Los Angeles, CA 90095-1569, USA;
[2] Faculty of Exact Sciences, Department of Physics and Astronomy, Vrije Universiteit, 1081 HV Amsterdam, The Netherlands;
[3] Department of Mechanical and Aerospace Engineering, University of California Los Angeles, Los Angeles, CA 90095-1597, USA;

Abbreviations: AFM, atomic force microscopy; CCMV, cowpea chlorotic mottle virus; wt, wild type; ss, salt stable; *FZ*, force-distance.

Published in ***PNAS, 2006*, vol. 103,** 6184

Abstract

The elastic properties of capsids of the cowpea chlorotic mottle virus (CCMV) have been examined at pH 4.8 by nano-indentation measurements with an atomic force microscope. Studies have been carried out on wild-type capsids, both empty and containing the RNA genome, as well as on full capsids of a salt-stable mutant and empty capsids of the subE mutant. Full capsids resisted indentation more than empty capsids but all of the capsids were highly elastic. There was an initial reversible linear regime that persists up to indentations varying between 20 and 30 % and applied forces of 0.6 to 1.0 nN; it is followed by a steep drop in force that is associated with irreversible deformation. A single point mutation in the capsid protein increased the capsid stiffness. The experiments are compared with calculations by finite element analysis of the deformation of a homogeneous elastic thick shell. These calculations capture the features of the reversible indentation region, and allow Young's moduli and relative strengths to be estimated for the empty capsids.

Viral genomes are surrounded and protected by a protein shell, the capsid. X-ray diffraction and cryo-electron microscopy have allowed the structures of viral capsids to be determined to high resolution (1, 2). Many capsids have highly symmetric structures that exhibit icosahedral symmetry; they range in diameter from about 30 to 100 nm. Capsids are composed of multiple copies of just a few proteins, often only one, which are arranged into pentameric and hexameric structural units called capsomers. The forces between the proteins are typical of those associated with protein secondary and tertiary structures and are therefore relatively weak. Yet it has been shown that the capsids of bacterial viruses such as ϕ29 and λ, which contain highly stressed DNA genomes, are capable of withstanding internal pressures of tens of atmospheres without rupturing (3-5). It is therefore of interest to investigate the mechanical properties of viral capsids and to determine how their strength and elasticity depend on the capsid structure. Atomic Force Microscopy (AFM) nanoindentation measurements are a convenient method to probe the mechanical properties of biological objects (6-8) and, in a recent paper (9), this technique was employed to study procapsids of the bacteriophage ϕ29. Here we use the same methodology to examine the plant virus CCMV (cowpea chlorotic mottle virus).

The CCMV capsid (Fig. 1) is an icosahedral shell with an outer diameter of 28 nm and an average thickness of 3.8 nm (1). It is made up of 180 copies of a single 190-residue long protein that are organized into two structural units (capsomers), pentamers and hexamers (10); CCMV capsids consist of 12 pentamers and 20 hexamers [Caspar-Klug triangulation number T = 3 (2)]. Each pentamer is surrounded by six hexamers and each hexamer is surrounded symmetrically by three pentamers and three hexamers. The CCMV genome is multipartite; it consists of four single-stranded RNAs: RNAs 1 and 2, each about 3000 bases long, are packaged separately; RNAs 3 and 4 (2000 and 1000 bases, respectively) are packaged together (11). Capsids that contain these different parts of the genome are morphologically indistinguishable (12). Beyond its relative simplicity and its symmetric structure, CCMV has a number of properties that make it an appealing target for study. The virus is able to self-assemble in vitro. Under the proper conditions of pH and ionic strength, mixtures of the capsid protein and RNA

will spontaneously form infectious viruses, indistinguishable from those obtained from infected plants (11, 12). Moreover, under other conditions, the protein alone can self-assemble into empty capsids that are structurally indistinguishable from full capsids (12). Thus, by comparing the properties of empty and full capsids it is possible to assess the effect of the protein-RNA interaction on capsid elasticity and strength. CCMV capsids can also assemble spontaneously around a wide variety of anionic polymers (13, 14) and this property has raised the possibility of their use as nanocontainers (15). Because of the broad interest in CCMV, a number of mutants have been obtained in which substitutions and/or deletions of residues in the capsid protein have been performed (15-18), making it possible to explore the effects of the protein primary structure on the mechanical properties. This, in turn, opens the possibility of custom-tailoring shells for technical purposes.

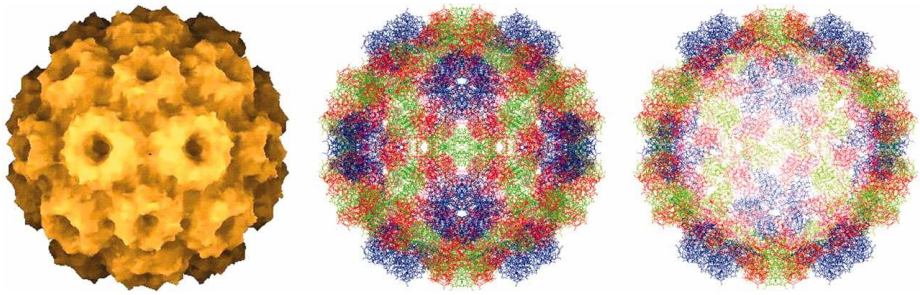

Fig. 1. Structure of CCMV capsid from x-ray diffraction studies (1). Left: "depth-cued" showing outer surface. The other images show the detailed structure as viewed down a two-fold axis (center) and the cross section of the capsid at the midplane showing the capsid wall (right).

Materials and Methods

The wt viruses were prepared at UCLA from infected plants following the procedures previously described (19). Two mutants were kindly provided to us by the group of M. Young and T. Douglas (MSU, Bozeman, MT). The salt stable (ss) mutant does not dissociate at pH 7.5 at high ionic strength (*i* >1M) (16). Sequence analysis shows that there is a single substitution of lysine 42 of the capsid protein to arginine. The *SubE* mutant has the same

substitution but, in addition, the nine basic residues (lysine and arginine) at the N-terminus have been replaced by glutamic acid (15). As a result of the charge inversion, RNA cannot be packaged into subE capsids. Solutions of the mutants were studied in virus buffer (0.1 M sodium acetate pH 4.8, 1 mM EDTA) without further treatment.

Empty wt capsids were prepared by disassembly of native virions at high salt concentration (~ 1M) above pH 7. A sample of full CCMV capsids solution (3 ml at 2 mg/ml in virus buffer) was dialyzed overnight at 4°C against disassembly buffer (0.9 M NaCl, 0.02 M Tris-HCl pH 7.4, 1 mM DTT, 0.5 mM PMSF) in dialysis cassettes with a 3.5 kDa molecular weight cut-off membrane (Pierce Slide-A-Lyser, Fisher Scientific). The mixture of RNA and coat protein was then diluted at least two times against disassembly buffer and centrifuged at 4°C in swinging buckets (Beckman rotor SW41) at 99,000 g for 25 hours. The collected upper supernatant was then concentrated using a Centriplus YM-3 filter (Millipore polyethersulfone membrane with a nominal molecular weight cut-off of 3,000) by centrifugation at 4°C for 2 hr at 3,000 g. UV measurement of the concentrate shows a spectrum characteristic of a pure protein solution with a maximum at 277 nm. The absorbance ratio A_{260}/A_{280} was typically of the order of 0.6-0.7. The concentration of CCMV protein monomers was determined spectroscopically (20): c = 0.2-0.3 mg/ml. The coat protein solution was then dialyzed overnight at 4°C against the *reassembly* buffer (0.9 M NaCl, 0.1 M sodium acetate pH 4.8, 10 mM $MgCl_2$, 0.5 mM PMSF). The reassembled empty wt CCMV capsids were finally dialysed and stored in buffer (0.1 M sodium acetate pH 4.8, 1mM $MgCl_2$, 0.5 mM PMSF).

For AFM, virus particles were adsorbed onto microscope cover slips. The circular glass substrates were first cleaned in a saturated solution of KOH in ethanol, then dried in vacuum and made hydrophobic by silanization with 1,1,1,3,3,3-hexamethyldisilazane ($C_6H_{19}NSi_2$, 99.9% pure, Sigma Aldrich) vapor. Initial stock solutions (~1mg/ml) of each type of CCMV capsid were diluted 100-fold in the corresponding buffer. A 100-µl droplet of viral solution was deposited on the hydrophobic substrate and allowed to stand for 20 min to allow the capsids adsorb. Another 100 µl of buffer was then added to insure complete immersion of the cantilever.

All the imaging and force measurements were performed at the Vrije Universiteit with an AFM (Nanotec, Madrid, Spain) in jumping mode (21). In this mode, imaging is achieved by a succession of force-distance measurements executed in several milliseconds in a raster scan fashion. Lateral displacements occur only when the tip is not in contact with the sample, thereby minimizing shear forces. A complete description of the apparatus and the measurement procedures can be found in an earlier paper (9). Silicon nitride, gold-coated cantilevers (Olympus Research) with nominal spring constants, of 0.05 Nm^{-1}, were calibrated by the method described by Sader, et al. (22). The four-sided pyramidal-shaped tip radii were 20 nm, so the tip apex can be approximated as a sphere with a diameter of about 40 nm. Imaging and force measurements were all performed at room temperature in virus buffer at pH 4.8.

Results

The capsids were first imaged in a large field of view (1µm x 1µm or 2µm x 2µm), low resolution (128 pixels per µm) and low maximal force (≤100 pN) in order to determine their position on the substrate. When the imaging was performed with loads above 150-200 pN, there was irreversible deformation of the capsids and some local damage could be observed.

Under conditions in which there was low thermal drift, both empty an full wt capsids were observed with three distinct shapes shapes, hexagonal, pentagonal and round (Fig. 2). In a sample of 35 full wt capsids, all measured with the same tip, 15 were distinctly pentagonal, 12 hexagonal and 8 round. For the 37 empty wt capsids imaged, the corresponding numbers were 19, 9 and 9. The average height of the pentagonal objects was distinctly lower than those that are hexagonal and circular, which were closely similar, Table 1. These differences in shape and height are consistent with the structure of the icosahedral CCMV capsid, which has axes that display 2-, 3- and 5-fold symmetry. X-ray structural analyses of wt capsids (10) show that the external diameters along these axes are, respectively, 24.0, 28.6 and 29.1 nm and image reconstructions show that capsid cross sections perpendicular to 2-fold axes appear pentagonal and those perpendicular to the 3-fold and 5-fold axes appear, respectively, hexagonal and circular (1). We are therefore able to

associate the smaller diameter with capsids that adsorb onto the substrate at a 2-fold site and the higher, hexagonal and circular cross-section capsids with those that adsorb onto 3-fold sites (hexamer faces) and 5-fold sites (pentamer faces). For an icosahedron, the numbers of 2-, 3- and 5-fold sites are in the ratio 30:20:12 and if the adsorption occurs randomly, this distribution would be expected in the capsid images and heights. As shown in Table 1, relative numbers of each type of image and their heights are roughly in accord with this expectation.

The AFM images of both the subE and ss mutants do not show such clear distinctions and the height distributions are unimodal. The average height of the empty subE capsids is 28.2 ± 0.2 nm (n = 41) and that of the ss mutant is 27.5 ± 0.2 nm (n = 29), essentially indistinguishable from the larger height for the wt capsids.

After individual objects were imaged, indentation measurements were performed. In these measurements, the applied force (measured in volts) was obtained as a function of the displacement of the Z-piezo upon which the sample is mounted. The relation between the voltage output and the force was first determined by making force-distance (FZ) measurements on the incompressible substrate surface next to the capsid. The tip was then centered above the capsid and a series of three to five successive FZ curves was generated, after which the capsid is reimaged and its height redetermined. If there was no obvious change, additional FZ curves were obtained on the same capsid.

The FZ curves for an empty SubE capsid are shown in Figs. 3A and 3B. The black curves are the FZ curves performed on the substrate surface next to the capsid; they have been translated to match the contact points and the horizontal differences between this line and successive FZ curves correspond to the extent of indentation of the capsid. At pH 5, all capsids exhibited the same qualitative behavior. In each case there was a linear regime extending to relative indentations ranging from 20 to 30% and forces from 0.6 to 1 nN. The curves were highly reproducible, as evidenced by the overlap of the curves for repeated indentations in Fig. 3A. The retraction curves under these conditions show, at most, only a very small hysteresis (Fig. 3B). The resilience, the fraction of the indentation energy returned upon retraction, is > 90%.

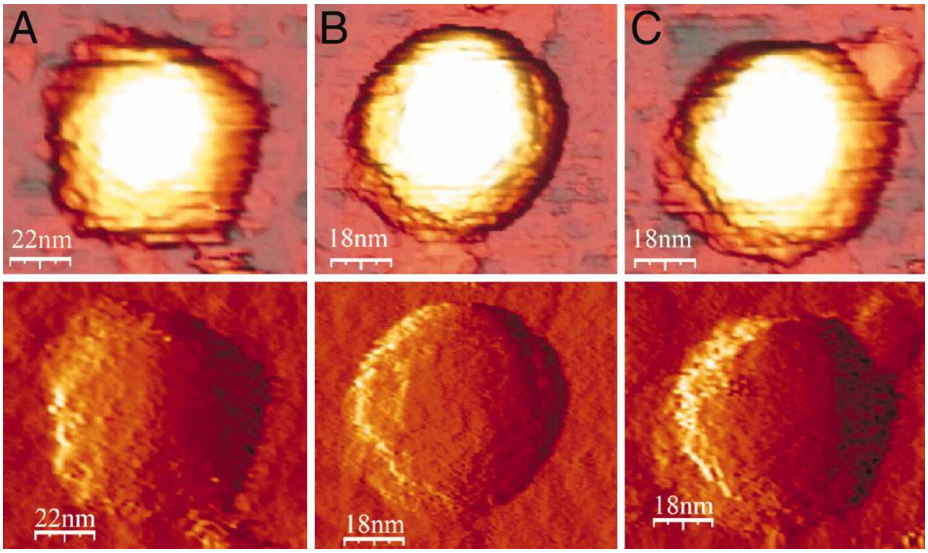

Fig. 2. AFM images of wt capsids. The direct images are shown in the upper row and the lower row shows derivative images obtained from them, which show the shapes more clearly. A. Empty capsid, adsorption on a 2-fold site B. Full capsid, adsorption on a 3-fold site C. Full capsid, adsorption on a 5-fold site. The loading forces were approximately 100 pN.

Table 1. Capsid heights, spring constants and threshold forces

Capsid type		Height (nm)			
Wt	Pentagonal	Hexagonal	Circular	k (N/m)	f (nN)
Full	25.4 ± 0.3*	27.7 ± 0.2	27.5 ± 0.3	0.20 ± 0.02	0.81 ± 0.04
	n = 15	n = 12	n = 8	n = 32	n = 28
Empty	24.6 ± 0.3	28.6 ± 0.3	28.7 ± 0.2	0.15 ± 0.01	0.6 ± 0.04
	n = 19	n = 9	n = 9	n = 31	n = 27
Mutants					
Full ss		27.5 ± 0.2		0.31 ± 0.02	1.06 ± 0.03
		n = 29		n = 29	n = 29
Empty subE		28.2 ± 0.2		0.19 ± 0.02	0.77 ± 0.02
		n = 41		n = 41	n = 35

* Uncertainty is standard error of the mean

There is no detectable loss in height, and images taken immediately after indentation show no evidence of damage. No significant dependence of the linear behavior on the indentation rate has been observed in indentations at rates ranging from 20 to 2000 nm/s.

The linear regime typically ended with a catastrophic drop in the force (Fig. 3C), which occurs for deformations of 20 – 30% corresponding to ratios of the deformation to the wall thickness of about 2. The values of the force at which the jump occured range from 0.6 to 1 nN and were slightly sensitive to the indentation rate: an increase of two orders of magnitude in speed resulted in an increase in the extent of the linear regime by about 10%. The force then increased with further indentation, Fig. 3D, but additional smaller drops often occurred. At high indentations the *FZ* curve asymptotically approaches that of the incompressible surface. Reversibility was lost once the threshold at which the force plummets had been exceeded. In subsequent indentations the linear region became smaller or disappeared, the initial slope tended to decrease and the force drop was smeared out. Capsids that had been indented beyond the threshold force showed losses in height of up to 10 nm and are deformed. A partial restoration of the height could be observed after relaxation for ~ 20 min.

Spring constants for the capsids can be obtained from the slopes of the forward curves in the linear regime. The capsid and cantilever can be considered as two harmonic springs in series. The spring constant k_{cap} of the capsid is then related to k_{eff}, the slope of the *FZ* curve, and k_c, the cantilever spring constant by: $k_{cap} = k_c\, k_{eff}\, (k_c - k_{eff})^{-1}$. Mean values of the spring constant distributions for each type of capsid are shown in Table 1. The spring constants in successive low-force indentations of a single capsid with the same cantilever differed by less than 1%; the generally larger spread in values for an array of capsids may represent capsid variability. Unlike the height distributions, the spring constant distributions for the wt capsids were not bimodal and there are no significant differences in the averages taken separately over the three capsid shapes.

Both the wt and mutant full capsids were more resistant to indention than empty capsids. The onset of the catastrophic drop in the force occurred

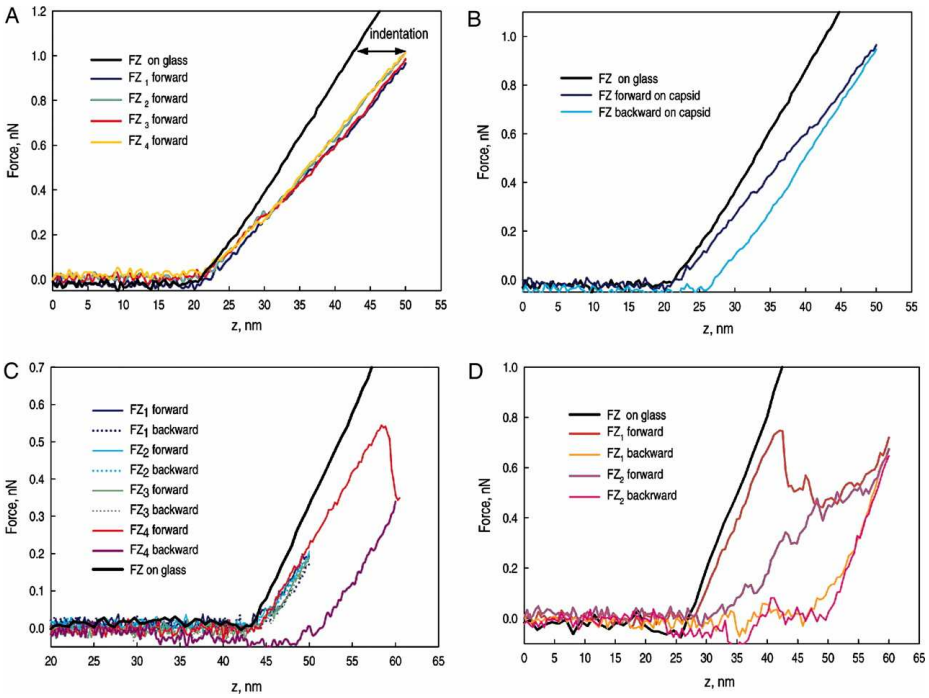

Fig. 3. FZ indentation curves. A. Empty SubE capsid in the linear regime. The black curve shows the cantilever on the glass surface; it has been translated to match the contact point of the capsid. Four successive force curves are shown. B. Empty SubE capsid showing some hysteresis. The dark blue line is the forward curve (indentation), and the light blue one is the backward (retraction) curve. C. Force-distance curve for an empty wt capsid showing repeated small indentations followed by a larger indentation beyond the reversible region. The red blue curve shows the large hysteresis upon retraction. D. Full wt capsid showing successive indentations beyond the reversible region. All of the capsids examined exhibited the same qualitative behavior.

at essentially the same deformation for all of the capsids. Hence the forces at the threshold were proportional to the force constants.

If one adopts a continuum model for the capsid as a first approximation, the spring constant can be related to the Young's modulus, *E*, of the protein shell. The simplest model for the elastic response is to assume the capsid to be an elastic thin spherical shell undergoing small deformations.

In that case,

$$k_{cap} = \alpha E h^2/R, \qquad [1]$$

where h is the wall thickness, R is the outer radius and α is a geometry-dependent proportionality factor (23). For CCMV, however, the thin-shell approximation $h/R << 1$ is clearly marginal and, moreover, the deformations that have been investigated are not small. We can therefore have gone to the next level of approximation and modeled the capsid as a homogeneous elastic *thick* shell subject to large deformations. To model the shells, we carried out finite-element analyses using the program ABAQUS (ABAQUS, Inc.). The calculations allow us to follow the shape of the capsid as it is indented and to determine the local stresses in its wall. The calculated curves all scale with E so for a fixed tip shape and size the only input parameters are h, R, and the Poisson ratio σ, which we take as 0.4. (The results are rather insensitive to the value of σ) A typical calculated indentation curve F/E versus tip displacement is shown in Fig. 4 for R = 14.3 nm, h = 3.8 nm and a spherical tip of radius 14 nm. The insets in the figure show how the capsid shape changes with indentation and the color is an indication of the von Mises stress, which is a combination of the principal stresses (24).

The effect of the thicknes of the shell is obvious only at very small indentations d, where the curve is not linear but rises as $d^{2/3}$ in accord with the Hertz model (23). The calculated stress distributions suggest that this non-linear behavior is associated with the radial spread of the stress through the capsid wall as the indentation begins. The tip radius and the shell thickness limit this initial Hertzian regime to the indentation depth at which the shell contact area has spread to about the shell thickness. Beyond this initial region, the curve is linear until the decrease in slope around d = 7- 8 nm. At this point, the top of the capsid buckles away from the end of the tip (see inset). Buckling is found in all of our calculations, which have been performed with a large range of tip diameters and for indentation between flat plates. This is in accord with experiments on macroscopic thin shells (ping-pong balls!) compressed between plates, for which a buckling transition was observed at deformations corresponding to $2h$ (25). Moreover, the slope of the linear region is insensitive to the tip radius. It increases by about 10% when the tip

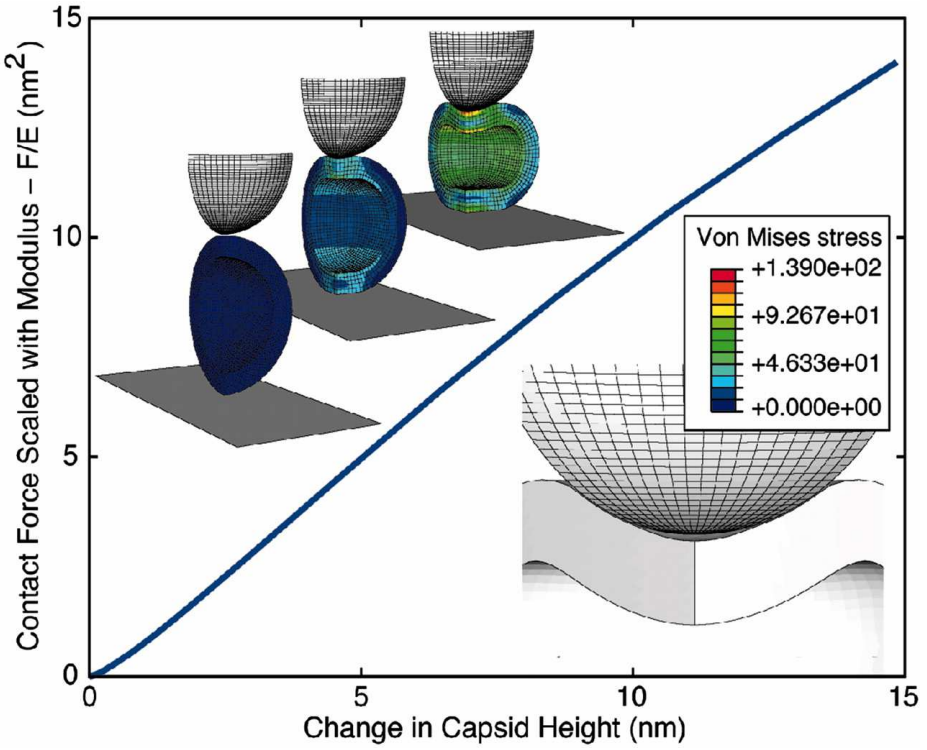

Fig. 4. Calculated dependence of F/E on capsid deformation for R = 14.3 nm, h = 3.8 nm, ◎ = 0.4. The insets above the curve show a one-quarter segment of the capsid at indentations d = 0, 5.6 and 14 nm and the von Mises stress is indicated by the color. The inset below the curve shows the buckling of the capsid away from the tip that is mirrored by a decrease in the slope.

radius is increased from 7 to 28 nm; an increase from 14 nm to an infinite radius, indentation between two planes, leads to an increase of 25 %.

The result, then, of the thick-shell analysis for CCMV is that the thin-shell formula [1] holds for indentations ranging from a few percent up to about 30% and estimates of the slope of the linear region in Fig. 4 give $\alpha = 1$. Using this expression with the values h = 3.8 nm and R = 14.3 nm, we find Young's moduli of 140 and 190 MPa for the empty wt and subE capsids, respectively. To the extent that the wall thicknesses are the same for the two capsids, the relative values of the Young's modulus can be expected to be reliable to 10%. The absolute values are more uncertain because there is some

arbitrariness in the choice of the capsid dimensions (mainly the shell thickness) and because the calibration of the cantilever spring constant may be uncertain by as much as 10%. These Young's moduli are comparable in magnitude to those of soft plastics such as Teflon (26).

Discussion

The CCMV capsid is clearly not a homogeneous spherical shell. Nevertheless, until the onset of irreversible deformation the response of the capsid to indentation closely resembles that expected for this idealized model, demonstrating that the experiment provides a measure of the average properties of the protein assembly. The higher Young's modulus, and therefore greater strength of the subE mutant, is not unexpected, given that it shares the same point mutation with the more stable ss mutant. The enhanced stability is seen as well in the full mutant capsids, where the ss mutant has a higher spring constant than the wt. Clearly higher forces are required to irreversibly damage both mutants.

The elasticities that we have measured for CCMV can be compared to those reported by Ivanovska, et al. for the ϕ29 procapsid (9). In that study a bimodal distribution of spring constants was observed, with average values of 0.31 and 0.16 N/m (9). The larger value was attributed to an average over the inhomogenous shell and the smaller to a locally soft region. In contrast, we see no evidence of a bimodal stiffness distribution for CCMV. Tama and Brooks (27) concluded from a normal mode analysis that the pentamer faces of CCMV were more flexible than the hexamer faces. On the other hand, Hespenheide, et al. (28), on the basis of the rigidity percolation method, argue that pentamers are stiffer than hexamers. Our results cannot resolve this contradiction but measurements made with sharper tips may have a chance of settling it.

In order to determine the Young's moduli from the *k's* for ϕ29, Ivanovska, et al. performed a finite element analysis for a point loading force on a homogeneous hollow geodesic ellipsoid. They obtained a Young's modulus for ϕ29 of 1.8 GPa, an order of magnitude greater than those for CCMV. Since the yield stress is generally proportional to *E*, the phage should therefore be able to resist much higher internal stresses than CCMV. The

force exerted by the DNA in ϕ29 corresponds to an internal pressure on the order of 60 atm and a packaging motor is required for assembly (4). In CCMV, which self assembles, it is highly unlikely that the RNA exerts a large internal pressure, which is consistent with the difference in the Young's moduli.

The positively charged N-termini of the capsid protein are known to interact strongly with the RNA and this will enhance the stability of the full capsids. Although the x-ray analysis does not resolve the portion of the RNA within the capsid, Monte Carlo simulations of a coarse-grained model for RNA within a CCMV capsid find that the RNA forms a shell bound to the capsid (27). If one assumes that a protein/RNA composite has a Young's modulus similar to that of the capsid alone, then the difference in the k's between the full and empty capsids could be attributed to a 10% increase in the wall thickness, a value comparable to that found in the simulations.

The qualitative features of the force curves we have measured are very similar to those that have been observed for microtubules by de Pablo, et al. (7), who found a linear regime followed by a catastrophic drop in force that arises for indentations greater than 20%. The diameter of the microtubule cylinders and the wall thickness are closely similar to those of CCMV. From an analysis of the indentations accompanying the abrupt drops in force, de Pablo, et al. argued that the microtubules could collapse into double or single layers of protein. In the case of CCMV, the minimum following an initial drop in force generally occurs at a indentation of about 50 %, which does not correspond to a flattening that brings the capsid walls in contact. The resolution in the images of the deformed capsids is not sufficiently high to allow us to determine the nature of the capsid failure.

We cannot expect finite element calculations on spherical shells to describe the sharp decline in the force because failure may well be localized at specific sites such as pentamer faces that one might expect to be more weakly bound than hexamer faces. However, we can attempt to use the calculations to provide an estimate of the force at which failure is likely to occur. It is known that the tensile strengths of many materials are 5 – 10% of their Young's moduli (26). When the stress is not purely uniaxial, this criterion is often expressed in terms of the von Mises stress (24). The finite element

calculations show that at a indentation of 30%, the maximum von Mises stress in the capsid is about 100 MPa, close to half the Young's modulus, and therefore well in excess of the 5 – 10% rule of thumb. Such relatively high tensile strengths are found for highly elastic materials such as rubber and elastin, which also have low Young's moduli (30).

The success of a continuum elastic model in describing the properties of a protein array may be interpreted as evidence for the fact that the relaxation of the capsomer protein conformations is very slow compared to the rate at which the capsid is indented in our measurements. If the deformation that accompanies the sharp drop in force is associated with changes in the organization of the capsomers and not the result of a complete loss of one or more proteins, then it is possible that the very slow rate at which the deformed capsids regain their height is a measure of this slow relaxation. If this were true, the mechanical properties and response that we obtain would not be those of a capsid that was indented in an equilibrium fashion. It could be argued, for example, that frequency dependence of the elastic constants accounts for the very large difference between the Young's moduli of tubelin microtubules determined from AFM measurements (7, 32) and those obtained from osmotic compression measurements (31), which are four orders of magnitude smaller. On the other hand, estimates of E made from an analysis of thermal fluctuations of a microtubule, an equilibrium measurement, are in good accord with the AFM studies (32) and recent high-indentation measurements on ϕ 29 shows that the capsids regain their initial heights within milliseconds.

Our measurements have revealed that a single point mutation in the viral capsid protein is able to enhance the mechanical stability of a capsid and, as might be expected, that the strength of a plant virus capsid is considerably lower than that of a phage, which must be able to withstand a high internal pressure. The fact that we are able to distinguish different capsid orientations for both the empty and full wt capsids and not for either of the mutants, suggests that the point mutation that the mutants share has an effect on the capsid geometry that has not been noted in cryoelectron microscopy images but might be determined by x-ray crystal analysis.

Acknowledgments

We thank Trevor Douglas, Mark Young and Debbie Willits for providing the mutant viruses and Jack Johnson, Jeffrey Speir and Robijn Bruinsma, Bill Gelbart and Fred MacKintosh for helpful discussions. This work was supported by grant CHE-04 00363 from the US National Science Foundation, a NWO Vernieuwingsimpuls grant (2000) (to G.J.L.W.) and grants from the Dutch Foundation for Fundamental Research on Matter (FOM) (to C.F.S.). Melissa Gibbons is supported by a fellowship from the UCLA Dean of Engineering.

References

1. Reddy, V.S., Natarajan, P., Okerberg, B., Li, K., Damodaran, K. V., Morton, R. T., Brooks III, C. L. & Johnson, J. E. (2001) *J. Virol.* **75**, 11943-11947.
2. Baker,T. S., Olson, N. H. & Fuller, S. D. (1999) *Micro. Mol. Biol. Rev.* **63**, 862-922.
3. Anderson, F. T., Rappaport, C. & Muscatine, A. N. (1953) *Ann. Inst. Pasteur* **84**, 5 – 14.
4. Smith, D. E., Tans, S. J., Smith, S. B., Grimes, S. Anderson, D. L. & Bustamante, C. (2001) *Nature* **413**, 748-752.
5. Evilevitch, A., Lavelle, L., Knobler, C. M., Raspaud, E. & Gelbart, W. M. (2003) *PNAS* **100**, 9292 - 9295.
6. Arnoldi, M., Fritz, M., Bäuerlein, E., Radmacher, M., Sackmann, E. & Boulbitch, A. (2000) *Phys. Rev. E* **62**, 1034-1044.
7. dePablo, P.J., Schaap, I. A. T., MacKintosh, F. C. & Schmidt, C. F. (2003) *Phys. Rev. Lett.* **91**, 098101-1 – 098101-4.
8. Yao, X., Walter, J., Burke, S., Stewart, S., Jericho, M. H., Pink, D., Hunter, R. & Beveridge, T. J. (2002) *Colloids Surf. B: Biointerfaces* (2002) **23,** 213-230.
9. Ivanovska, I. L., de Pablo, P. J., B. Ibarra, B., Sgalari, G., F. C. MacKintosh, F. C., Carrascosa, J. L., Schmidt, C. F. & Wuite, G. J. L. (2004) *Proc. Natl. Acad. Sci. USA* **101**, 7600-7605.
10. Speir, J. A., Munshi, S., Wang, G., Baker, T. S. & Johnson, J. E. (1995) *Structure* **3**, 63-78.
11. Bancroft , J. B. & Horne, R. W. (1977) *Atlas of Insect and Plant Viruses* vol. 8 387-302 (Academic Press, New York, NY).
12. Fox, J. M., Wang, G., Speir, J.A., Olson, N. H., Johnson, J. E., Baker, T. S. & Young, M. J. (1988)*Virology* **244**,212-218.
13. Bancroft, J. B. *Advances in Virus Research*, vol. 16 (1970) 99-134 (Academic Press, New York, NY).
14. Douglas, T. & Young, M. (1998) *Nature* ***393****,152-155.*
15. Douglas, T., Strable, E., Willits, D. Aitouchen, A., Libera, M. & Young, M. (2002) *Adv. Mater.* **14**, 415 - 418.
16. Fox, J. M., Zhao, X., Speir, J. A. & Young, M. J. (1990) *Virology* **222**, 115-122.

17. Fox, J. M., Albert, F. G., Speir, J. A. & Young, M. J. (1997) *Virology* **227**, 229-233.
18. Zhao, X., Fox, J. M., Olson, N. H., Baker, T. S. & Young, M. J. *Virology* **207**, 486 - 494.
19. Michel, J. P., Gingery, M. & Lavelle, L. (2004) *J. Virolog. Meth.* **122,** 195-198.
20. Gill, S. C. & von Hippel, P. H. (1989) *Anal. Biochem.* **182**, 319-326.
21. dePablo, P.J., Colchero, J., Gomez-Herrero, J. & Barro, A. M. (1998) *Appl. Phys. Lett.* **73**, 3300-3302.
22. Sader, J. E. , Chon J. W. M. & Mulvaney, P. (1999) *Rev. Sci. Instrum* **70**, 3967-9.
23. Landau, L. D. & Lifshitz, E. M. (1986) *Theory of Elasticity* (Pergamon, New York).
24. Ugural, A. C. & Fenster, S. K. (2003) *Advanced Strength and Applied Elasticity* (Prentice Hall, Saddle River, NJ).
25. Pauchard, L. & Rica, S. (1998) *Phil. Mag*.**78**, 225-233.
26. Howard, J. (2001) *Mechanics of Motor Proteins and the Cytoskeleton* (Sinauer Associates, Sunderland, MA).
27. Tama, F. & Brooks III, C. L.(2005) *J. Mol. Biol.* **345**, 299-314.
28. Hespenheide, B. M., Jacobs, D. J. & Thorpe, M. F. (2004) *J. Phys.: Condens. Matter*, **16**, S5055–S5064.
29. Zhang, D., Konecny, R., Baker, N, A, & McCammon, J. A. (2004) *Biopolym.***75**,325-337.
30. Kis, A., Kasa, S., Babic', B., Kulik, A.J., Benoît, W., Briggs, G.A.D., Schönenberger, C., Catsicas, S. & Forró, L. (2002) *Phys. Rev. Lett.* **89,** 248101-1-248101-4.
31. Needleman, D. J., Ojeda-Lopez, M. A., Raviv, U., Ewert, K., Jones, J. B., Miller, H. P., Wilson, L. & Safinya, C. R. (2004) *Phys. Rev. Lett.* **93**, 198104-1-198104-4.
32. Mickey, B. & Howard, J. (1995) *J. Cell. Biol.* **130,** 909-917.

CHAPTER 4

*"When **I** use a word,*' Humpty Dumpty said, in rather a scornful tone, *`it means just what I choose it to mean -- neither more nor less.'*

*`The question is,*' said Alice, *`whether you **can** make words mean so many different things.'*

`The question is,*' said Humpty Dumpty, *`which is to be master -- that's all.'"

From *Through The Looking Glass*
by Lewis Carroll

Failure of Viral Shells

William S. Klug*, Robijn F. Bruinsma**, Jean-Philippe Michel***, Charles M. Knobler***,

University of California, Los Angeles, CA 90095, USA

*Department of Mechanical and Aerospace Engineering

**Department of Physics

*** Department of Chemistry and Biochemistry

and

Irena L. Ivanovska[+], Christoph F. Schmidt[+§] and Gijs J. L. Wuite[+]

[+]Department of Physics and Astronomy, Vrije Universiteit, 1081 Amsterdam, The Netherlands

[§] III. Physikalisches Institut, Fakultät für Physik, Georg-August Universität, 37077 Göttingen, Germany

Published in ***Phys. Rev. Lett***. 2006, **97**, 228101

Abstract:

We report a combined theoretical and experimental study of the structural failure of viral shells under mechanical stress. We find that discontinuities in the force-indentation curve associated with failure should appear when the so-called Föppl-von Kármán (FvK) number exceeds a critical value. A nano-indentation study of a viral shell subject to a soft-mode instability, where the stiffness of the shell decreases with increasing pH, confirms the predicted onset of failure as a function of the FvK number.

A range of micro-mechanical probes have become available that can be used to study the mechanical properties of both individual proteins and of protein aggregates [1]. One of the interesting outcomes of these studies is that the *linear response* of protein assemblies such as actin filaments, microtubules, and viral shells to an applied force is well described by continuum theory, despite the fact that the dimensions of these assemblies may not be much larger than those of the (structurally complex) constituting protein units. This poses the question as to whether the continuum description applies as well to the *non-linear* response of protein assemblies. The threshold for structural failure under applied force is, for instance, a non-linear property that is of considerable importance for materials applications of protein assemblies [2]. The failure threshold of bulk materials normally is determined by the presence of structural defects, such as cracks, that are enlarged under the action of the external force [3]. Thin shell structures are a special case: they normally fail because of localized, nonlinear instabilities [4] that typically are excited at sub-critical loads by structural and geometric imperfections. Small protein assemblies such as viral shells or microtubules can be *structurally perfect*, which allows for the possibility that failure thresholds of these systems are determined by intrinsic and fundamental physical properties.

In this letter, we report on a combined theoretical and experimental study of the structural failure of a viral shell. Our central result is that the nature of structural failure is determined by a simple and universal physical characteristic, namely the *Föppl-von Kármán (FvK) number*. The FvK number is a dimensionless control parameter that emerges from the continuum theory of thin shells. For a closed spherical shell of radius R, it is defined as $\gamma = YR^2/\kappa$, with Y the 2D Young's modulus of the "in-plane" elasticity of the shell, and κ the "out-of-plane" bending energy. The FvK number is thus the dimensionless ratio of stretching and bending stiffnesses. Lidmar, Mirny, and Nelson[5] studied the shape of closed *icosahedral* shells and found that γ acts as a control parameter for the morphology of the shell. For γ smaller than a certain value γ_B (the "buckling threshold" [6]) the shell shape is nearly spherical, while for γ greater than γ_B, the shell shape is nearly polyhedral.

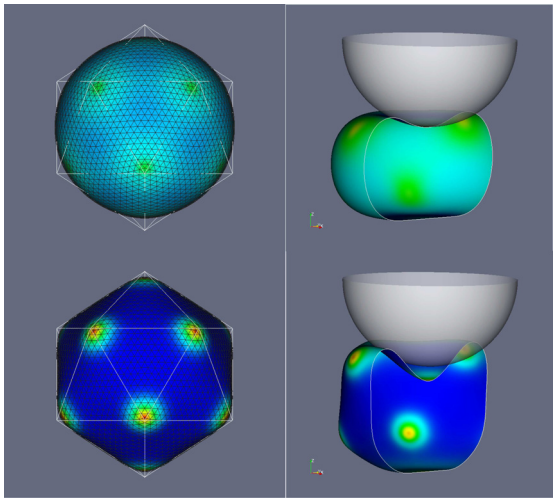

FIG 1: Shapes of icosahedral shells under external force calculated numerically by finite-element analysis [9] with FvK numbers $\gamma = 100$ (top) and $\gamma = 1200$ (bottom). Initial shapes are shown on the left side, deformed shapes on the right side. On the initial shapes, white edges represent the reference icosahedron, and black edges are the triangular finite element control mesh. Cut-away views of the deformed shapes are shown. Color contours indicate the combined strain energy density due to stretching and bending. The ratio ς / R of indentation to radius is 0.35, just beyond the discontinuity in the force-indentation curve for $\gamma = 1200$ (see FIG.2) where a five-fold apex of the icosahedron has inverted. Inversion does not occur for $\gamma = 100$.

FIG. 1 shows, on the left side, numerically computed shape profiles with FvK numbers below γ_B (top) and above γ_B (bottom). Contours of strain energy density are color-coded. The reference state for the calculation of the elastic energies is that of a perfect icosahedron (indicated by the white outlines in FIG. 1). The in-plane stretching energy is zero in this reference state, but the total energy is high due to bending along the icosahedral edges. In the final state, this bending energy is relaxed at the expense of a certain level of in-plane stretching as determined by γ. Note that the elastic energy (and hence, stress) in the relaxed shells is focused on the five-fold symmetry sites.

In the linear-response regime, the indentation ζ of a spherical shell induced by an infinitesimal applied force F is predicted [7] to scale as $\zeta(F)/R \propto F/\sqrt{\kappa Y}$. The dimensionless proportionality factor depends only on the geometry of the force application. Atomic Force Microscopy (AFM) studies of viral capsids confirm this linear dependence [8,12], which provides further support for the applicability of continuum theory to viral shells.

In FIG.2, we show full numerical force-indentation curves - in scaling form - beyond the linear response regime of icosahedral elastic shells resting on a flat surface and deformed by a spherical tip of the same radius as the shell [9]. The shell was oriented with a five-fold axis perpendicular to the flat surface [10].

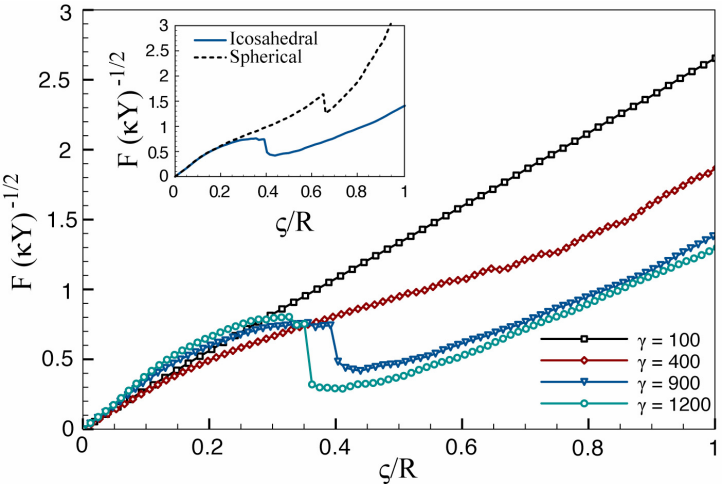

FIG. 2. Force-indentation curves of an icosahedral shell with isotropic elastic properties deformed by a spherical tip. The force F and the indentation (i.e., the reduction in diameter along the indenting axis) ζ are expressed in dimensionless units, with R the equivalent radius of shell and tip, Y the two-dimensional Young's modulus and κ the bending modulus. The dimensionless control parameter $\gamma = YR^2/\kappa$ determines whether the curve has a snap-through discontinuity. The inset compares the force-indentation curves of spherical and icosahedral shells with $\gamma = 900$.

For lower values of γ, the force-indentation curves are nearly linear and agree with linear response theory, but for larger values of γ the curves become increasingly non-linear and then develop *discontinuities* [11]. Note that the development of the discontinuity resembles that of a first-order transition near a critical point. The discontinuity occurred at larger ζ values during loading than during unloading, which is indicative of bistability. It should be noted γ must significantly exceed the buckling threshold γ_B in order for discontinuities to develop.

The right side of FIG. 1 (bottom) shows the shape of a shell with $\gamma = 1200$ immediately after the discontinuity has taken place: one of the twelve five-fold symmetry sites of the icosahedral shell has buckled and *inverted*. Inversion can be viewed as an example of a localized, non-linear instability focused on a geometrical defect - the five-fold sites in the present case - that characterize the failure of elastic shells. FIG. 2 shows that - unlike the critical indentation - the *critical force* for the discontinuity is indeed only weakly dependent on γ and hence on shell size. The discontinuity in the force-indentation curve of a shell having a *spherical* reference state - and thus no "defects" - but otherwise with the same elastic constants indeed takes place at a much larger indentation force (see FIG.2, inset).

We have examined the failure under elastic stress of actual capsid shells of the Cowpea Chlorotic Mottle Virus (CCMV) by AFM nano-indentation. Measured force-displacement curves of empty CCMV capsids are shown in FIG. 3 for two different p*H* values. The linear force-displacement curves recorded for the cantilever in direct contact with the glass substrate (black lines) serve as reference and were shifted so their onsets correspond to those of the curves corresponding to indentation of the virus (red for loading, blue for unloading). The horizontal distance between the glass curve (dashed arrow) and the capsid curves represents the actual depth of capsid indentation at a given force. In effect, the virus indentation curves arise from two springs in series, that of the cantilever and that of the capsid (the spring constant for the cantilever is determined by an independent calibration).

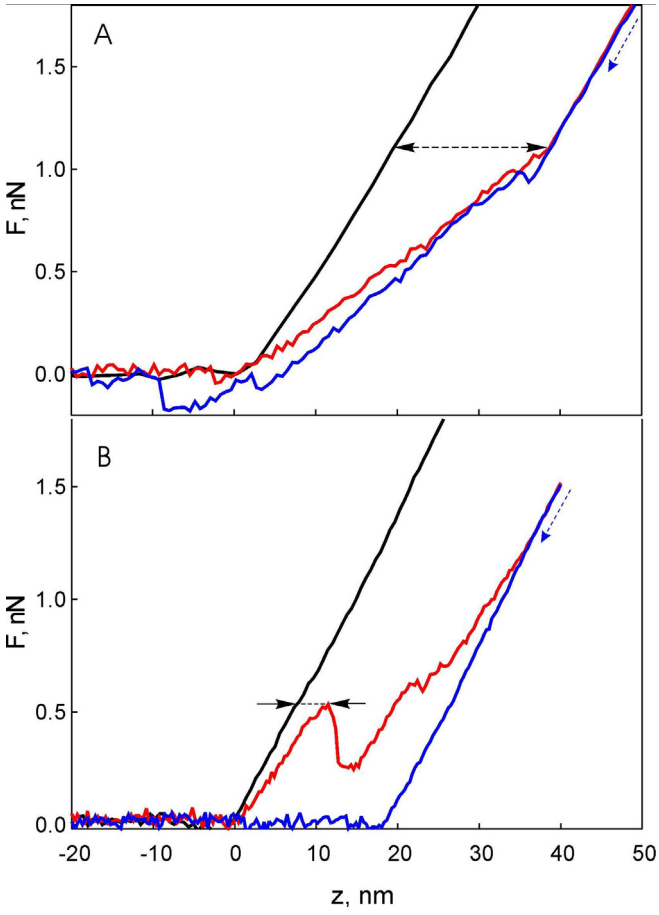

FIG. 3. Force-displacement curves for empty CCMV capsids. The abscissa measures the vertical position of the sample support which is lifted against the AFM tip. The point of contact between sample and tip is set to $z = 0$. The ordinate measures the force exerted by the tip on the sample, which is derived from the cantilever deflection using a calibration factor. The measurements are carried out in the appropriate buffer. See reference 12 for full experimental details. Black lines: cantilever directly against the glass substrate; Colored lines: capsid indentation (red for loading, blue for unloading). Top: pH 6; Bottom: pH 5. The horizontal distance (dashed arrow) between the black and colored curves represents the actual depth of indentation at a given force. The measurements were performed on different CCMV capsids ($N > 9$).

Details of the measurements and analysis can be found in Michel et al [12] and Ivanovska et al. [8] As noted in reference 12, the effect of capsid orientation on force-indentation character was not discernible at pH 5; the same is also true at pH 6.

For p*H* 6, the force-indentation curve is linear for indentations up to 70% of the capsid diameter (or 1.5 times the radius), in agreement with the theoretical force-indentation curves at small γ shown in FIG. 2. At this point there is a sharp change in slope and the curve parallels that of the glass curve, meaning that the capsid has become essentially incompressible. At an indentation of 20 nm, the capsid is compressed to only 6 nm high. Since the capsid wall can be as thick as 3.8 nm [16], at this "touch-down" indentation the two inner surfaces have come into contact. Remarkably, the entire force curve can be repeatedly retraced with minimal hysteresis and remains fully reversible.

This highly reversible, elastic behavior at p*H* 6 must be compared with the force-displacement of CCMV capsids at p*H* 5, (FIG. 3B), measured earlier by Michel et al. [12] . For indentations that are less than about 30% of the capsid radius, the force-displacement curve is linear and completely reversible for multiple indentations [13]. The slope of the p*H* 5 curve is about three times larger than that of the p*H* 6 curve. Since, according to linear response, this slope should be proportional to $\sqrt{\kappa Y}/R$, the p*H* increase must have produced a *nine-fold* decrease in the product of Young's and bending moduli. For indentations larger than 30% of the initial diameter, there are one or more sharp drops in the curve, associated with irreversible, structural failure. Images of the capsid taken after one of these sharp drops show that its height has decreased, although there is a partial relaxation after about 20 min. A failure threshold with ζ/R in the range of 0.4 would correspond to FvK numbers around 900 (see FIG.1) [14].

The remarkable, p*H* induced, softening of the CCMV capsid is likely related to the fact that it undergoes a reversible, radial swelling[15] by 10% when the p*H* is increased from 5 to 7 [16]. Magnetic resonance [17] and small-angle X-ray scattering measurements [18] show that the swelling largely takes place over the p*H* range 6.5–7.5. A detailed normal mode analysis of CCMV by Tama and Brooks [19] (TB) demonstrated that the swelling is preceded by the

development of a non-degenerate *soft mode* of the shell. The soft mode, which has a predominant radially outward character, is due to an increase in the electrostatic repulsions between just a few residues. According to Ginzburg-Landau theory, the elastic energy H of a weakly deformed spherical elastic shell of radius R subject to a soft mode instability with scalar symmetry can be expressed as [20]:

$$H \cong \int dS \left\{ \tfrac{1}{2}\kappa(\Delta\zeta)^2 + Y\left(\frac{\varsigma}{R}\right)^2 + \tfrac{1}{2} r\eta^2 + \Gamma\eta\left(\frac{\zeta}{R}\right) \right\} \qquad (1)$$

with $\zeta(\vec{r})$ the indentation profile and $\eta(\vec{r})$ the amplitude of the soft mode. According to the TB analysis, the stiffness modulus r in Eq.1 of the soft mode amplitude decreases with increasing p*H*; Γ is the coupling between the (scalar) soft mode and the local compressive elastic strain. Minimization of H with respect to $\eta(\vec{r})$ gives $\eta = -\frac{\Gamma}{r}\left(\frac{\zeta}{R}\right)$ which, if inserted in Eq.1, produces the elastic energy of an elastic shell with a *reduced* effective Young's modulus Y^* given by:

$$Y^* = Y - \frac{\Gamma^2}{2r} \qquad (2)$$

Minimization of this effective elastic energy under an applied external force F reproduces the linear force-indentation relation $\zeta(F)/R \propto F/\sqrt{\kappa Y^*}$, but with the renormalized Young's modulus. We thus indeed should expect the shell stiffness to decrease as the p*H* is increased. If only the Young's modulus were affected by the soft mode, then the FvK number should reduce from around 900 at p*H* 5 to around 100 at p*H* 6.

The fact that continuum theory appears to provide a profitable framework for the interpretation of mechanical indentation studies of nanometer-sized viral capsids is surprising. Unlike, say, the capsid of the *Herpes* virus, the size of a CCMV capsid is comparable to that of the constituent hexamer and pentamer protein capsomers. The recent results of Vliegenthart and Gompper [21] suggest that indeed the buckling behavior for small capsids may differ from that predicted by continuum model. The thickness of the CCMV shell (2-4 nm) also is not negligible compared to the shell diameter. Moreover, X-ray studies of CCMV show that no obvious change in faceting accompanies the swelling of the capsid [16], whereas FIG.1 (left panel) would lead us to expect a shape change if the FvK number

increases from 100 to 900. This may indicate that the applicability of the FvK number as an indicator for the *elastic response* of a viral shell is more general than its interpretation in the context of shape change. This, of course, would have to be confirmed by a detailed modeling study of viral shells under external force that does full justice to the molecular structure of the constituent proteins. Furthermore, detailed models would perhaps offer better quantitative agreement with experiments. In particular, the shape of the force-indentation curves below the discontinuity is quite sensitive to the geometry of the indenter and shell; a model reflecting the nonuniform thickness of the capsid might better capture the linearity of the experimental curves. We conclude by noting that a self-assembling protein container with p*H* - tunable elastic properties may have materials applications, in particular in view of the fact that the pH 6 shell appears not to fracture at all under mechanical stress.

Acknowledgements. This work was supported by DMR Grant 0404507, by Grant CHE-04 00363 from the US National Science Foundation, by the Foundation for Fundamental Research on Matter (FOM), and by a Vernieuwingsimpuls Grant from the Netherlands Organization for Scientific Research. RB would like to thank Thomas Guérin for helpful discussions.

References

[1] See, for example, M. Arnoldi, M. Fritz, E. Bäuerlein, M. Radmacher, E. Sackmann, & A. Boulbitch, (2000) *Phys. Rev. E* **62**, 1034 (2000).

[2] For the failure of microtubules under applied stress: P.J. dePablo, I.A. Schaap, F., MacKintosh, & C. Schmidt, *Phys. Rev. Lett*. **91**, 098101-1 (2003).

[3] A.C. Ugural & S. K. Fenster, *Advanced Strength and Applied Elasticity* (Prentice Hall, Saddle River, NJ, 2003).

[4] C. R. Calladine, *Theory of Shell Structures* (Cambridge, New York, 1983).

[5] J. Lidmar, L. Mirny and D. R. Nelson, Phys. Rev. **E68**, 051910 (2003).

[6] Reference 5 finds $\gamma_B \approx 154$, whereas T.T. Nguyen, R. F. Bruinsma, W. Gelbart, *Phys Rev E*, **72**, 051923 (2005) found $\gamma_B \approx 250$ using a different numerical procedure.

[7] L. D. Landau & E. M. Lifshitz, *Theory of Elasticity* (Pergamon, New York, 1986).

[8] I. L. Ivanovska, P. J. de Pablo, B. Ibarra, G. Sgalari, F. C. MacKintosh, J. L. Carrascosa, C. F. Schmidt & G. J. Wuite, *Proc. Natl. Acad. Sci. USA* **101**, 7600 (2004).

[9] The curves were computed numerically by finite element analysis using triangular subdivision-surface shell elements (W.S. Klug, in preparation). These subdivision elements define a smooth computational surface with C^1 continuity from local basis functions related to cubic box-splines: F. Cirak, M. Ortiz, and P. Schröder, *Int. J. Numer. Meth. Engrng*, **47**, 2039-2072 (2000).

[10] The force-indentation behavior is qualitatively similar for icosahedral shells oriented along 5-fold, 3-fold, and 2-fold symmetry axes with some variation in the precise quantitative details. In particular, buckling events for the 3-fold and 2-fold oriented shells involve simultaneous inversion of multiple 5-fold sites.

[11] There can be multiple discontinuities, depending on the geometry of the force application and the orientation of the shell.

[12] J. P. Michel, I. L. Ivanovska, M. M. Gibbons, W. S. Klug, C. M. Knobler, G. J. L. Wuite and C. F. Schmidt, *Proc. Nat. Acad. Sci*, USA **103**, 6184-6189 (2006).

[13] In our measurements, the cantilever and the capsid act essentially like two springs in series, one of which is linear. As a result, a small amount of nonlinearity in the response of the capsid, as predicted by the calculations for large γ in FIG. 2, could be masked.

[14] Since we also know the value of $\sqrt{\kappa Y^*}/R$ from the initial slope of the force-indentation curve in FIG. 3, we can obtain separate estimates for κ - about 70 k_BT - and Y^* at pH 5 - about 450 k_BT/nm^2 - which are in the same range as earlier estimates [12]. However, it must be noted that, in repeated measurements we obtained a broad *distribution* of failure thresholds so this is not very reliable as a method for measuring elastic moduli.

[15] J. B. Bancroft, G. J. Hills and R. Markman, *Virology* **31**, 354-79 (1967).

[16] J. A. Speir, S. Munshi, G. J. Wang, T. S. Baker and J. E. Johnson, *Structure* **3**, 63-78 (1995).

[17] G. Vriend, M. A. Hemmingga, B. J. M. Verduin and T. J. Schaafsma, *FEBS Lett*. **146**, 319-21 (1982).

[18] A. Gopal, private communication.

[19] F. Tama and C. L. Brooks III, *J. Mol. Biol*. **318**, 733-47 (2002).

[20] The derivation of Eq.1 assumes $\zeta << \sqrt{\kappa / Y} << R$. See also Z. Zhang, H.T. Davis, and D.M. Kroll, *Phys. Rev. E*, **48** R651 (1993) for the elastic energy of a shell without a soft mode. For a full discussion: T. Guérin and R. Bruinsma, in preparation.

[21] G. A. Vliegenthart and G. Gompper, *Biophys. J.*, **91**, 834-841 (2006)

CHAPTER 5

"There might be some sense in your knocking,' the Footman went on without attending to her, *`if we had the door between us. For instance, if you were INSIDE, you might knock, and I could let you out, you know."*

From *Alice's Adventures in Wonderland*
by *Lewis Carroll*

Deconstructing viral shells to understand its building blocks

I. L. Ivanovska*, X. Agirrezabala§, J. L. Carrascosa§, C. F. Schmidt*, G. J. L. Wuite*

*Faculty of Exact Sciences, Department of Physics and Astronomy, Vrije Universiteit, Amsterdam, 1081 HV, The Netherlands;
§Department of Structure of Macromolecules, Centro Nacional de Biotecnologı´a, Consejo Superior de Investigaciones Cientı´ficas, Campus Universidad Auto´noma de Madrid, 28049 Madrid, Spain

To be submitted

Abstract

Bacteriophages are known to carry their highly compressed genome under pressure in nanometer sized protein containers (capsids). ϕ29 is a double-stranded DNA *Bacillus subtilis* phage whose capsids are prolate icosahedrons elongated along a 5-fold symmetry axis. The prohead is an assembly intermediate that is made by a reduced number of structural components.. To withstand the considerable internal stresses, the prohead combines unexpected strength and resilience despite the fact that only weak protein-protein interactions are keeping the capsids structure together. Here we use Scanning Force Microscopy to study the mechanical properties of shell proteins as a function of their position with in the prohead. While gently probing the capsid, causing small deformations, we observe changes in the local elasticity revealing pentameric structures. When we break the shells in a controlled fashion we find that the capsids fracture along well-defined lines. The observed fracture lines are analyzed and classified according to the known monomer organization from the recently solved pseudoatomic structure. We found that the mechanically coherent building block of the protein shell is a trimer of monomers, organized according to the triangulation net of the icosahedron. Moreover, we find that the interactions between proteins in the equatorial belt are nearly twice weaker than the interactions within the icosahedral end-caps. The results suggest that proheads have evolved from a spherical prohead to an elongated one in order to accommodate a longer genome while compromising its structural integrity.

Introduction

ϕ29 is a well characterized bacteriophage with double-stranded DNA that infects *Bacillus subtilis*. The capsid is based on prolate icosahedron, elongated along the 5-fold axis, with a triangulation number T=3, Q=5 (Tao et al., 1998; Ibarra et al., 2000). During its life circle the viral genome is packed into a preformed capsid, the prohead, using a portal motor which consist of head-tail connector protein (gp10), a specific viral-coded RNA (pRNA) and the ATPase protein gp16 (1-4). It consists of only one type structural protein gp8, head fibers (gp 8.5) and its assembly require the presence of the gp10 connector and a scaffolding protein (gp7) (5-7). Gp8 follows the Caspar and Klug quasi–equivalence organization (8) of pentameric and hexameric protein arrangements around the 5-fold and quasi-six fold centers of the icosahedron (Fig1B). The elongated prohead shape stems from the insertion of a belt of 10 hexamers between the two hemispheres of the icosahedron. The resulting structure is 45 nm wide and 54 nm long but has only a thickness of 1.6 nm (1, 4, 5, 9) (Fig.1A).

Recently the pseudo atomic structure of ϕ 29 was solved with a 12.7 A resolution (6). Inspection of the structure shows that each gp8 subunit consists of a thin, wedge-like domain and a ridge-like domain (BIG2). The wedge domains pack tightly against one another to form the pentagons and hexagons at the 5- and 6-fold symmetry axes of the capsid, respectively. The BIG2 domains protrude from the surface of the particle and extend across the capsomeric borders, and contact neighboring capsomers at the quasi- and icosahedral 2-fold symmetry axes. The spatial arrangement of gp8 across the shell surface results in 5 distinct interaction environments, 3 quasi-equivalent ones in the icosahedral caps and 2 more because of the equatorial insertion. They are shown schematically in figure 1b.

This heterogeneous organization of identical subunits may lead to local differences in the mechanical properties of the viral shells. We previously performed a detail study of the deformation behavior and material properties of ϕ29 bacteriophage proheads using atomic force microscopy (AFM) manipulation (10) . We found indeed a bimodal distribution of the elasticity of shell, which we attributed to local soft areas on the capsid surface in combination with global deformation of the object. In this paper we

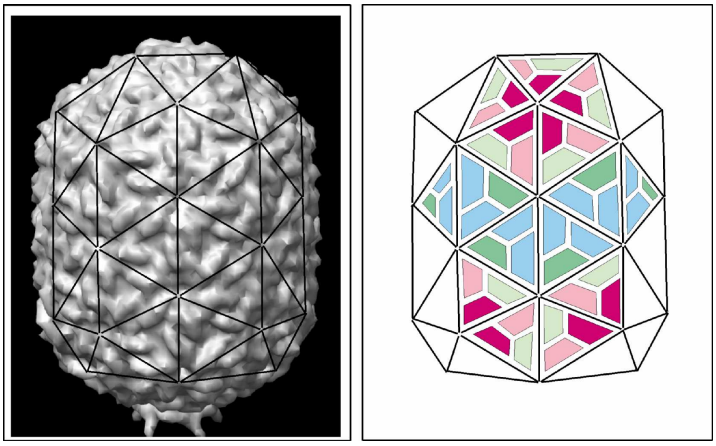

Figure 1. a) Pseudoatomic structure of ϕ 29 (6) 3D image reconstruction of fiberless prohead with superimposed the corresponding triangulation net, viewed perpendicular to the 5-fold axis of the particle [EBI database] b) schematic representation of gp8 monomers organization on the triangulation net of ϕ 29 prohead. The monomers involved in intra-pentameric interactions are in magenta. The hexameric units interacting with a pentameric subunit are presented in pink, and those one interacting with hexameric units are in light green. Furthermore, there are the equatorial positioned subunits which generate two additional conformations (dark green) and (blue).

investigate the nature of these local soft areas. Moreover, by inducing in a controlled fashion fractures in the proheads, we study the relative strength and functional organization of the of the monomer interactions. Finally, we discuss the consequences of our result in relation to the assembly of proheads.

Results and discussion

Local elasticity of proheads. Empty proheads deposited on a glass surface are imaged in jumping mode in liquid as described previously (10). The main relevant feature of this imaging mode is that the applied load is maintained constant during the scan because feedback is performed on the preset bending of the cantilever (11). In that way a local change of the elasticity could be visualized using adequate sharp tip and an appropriately chosen applied

force. Figure 2a shows a low magnification image of the derivative of the topography of virus particles. The measured height of these shells is as expected from EM studies, which indicates that the shells are not deformed in vertical direction. Pentameric plates with 3 or more pronounced edged sides can be observed on the top of the particles. Figure 2c show an example of pentameric structure on a prohead deposited on its side and figure 2d one standing upright. The observed edges in the 3D AFM images can not be topographical features, since they are not present in proheads (Fig 1a, 2b) (6) Footnote[1]). In fact, simultaneously recorded normal force maps show that sharp changes in the surface images occur when the tip is indenting deeper. This can also be seen in the profile of the cross-section of a shell surface where the shell deformation and the corresponding drop in the normal force are plotted together (Fig. 2d). Therefore the ridges are the result of changes in the local stiffness of the capsids. The average size of the measured sides of the observed pentameric figures is 20.8 ± 0.5 nm (N=12, SD=1.6 nm). Due to tip-sample convolution the capsids as well as its features appear broadened. The tips used in the experiments are conical with spherical apex with radii of 17 nm (SD=5 nm). From simple geometrical consideration one can write the relation between the apparent broadening halfwidth (w_h), tip radius (R_t), object radius (r_o) and the height (h) from the top point to the position where the width is measured as, $w_h = \sqrt{2h(R_t + r_0) - h^2}$. Using this formula we can correct the measured length of the observed pentameric edges, resulting in a length of 15 ± 1 nm. The characteristic size of one side of a pentamer of monomers is ~9.5 nm, so the boundaries between those oligomers are unlikely candidates for the observed edges in the SFM images. More likely are the observed pentamers shown in dotted lines in figure 2b where the protruding ridge domains interact with their neighbors at the 2 - fold quasi-symmetry axis. In this case trimers of monomers form the observed pentamers. The size of the side of this pentamer of equilateral triangles calculated from the shell geometry is ~ 16 nm, in agreement with the size which we measure from the

[1] *Gp8.5 head fibers are dispensable structural elements, as fiberless virus is as estable as wild type.. In fact, the proheads are labile structures. They are made originally by gp8, gp8.5, gp7 and gp10. During long storage, there is a continuous lose of gp7 and gp8.5. In order to have a quantitative estimation, we should have done an electrophoretic analysis of the particles to compare them with fresh prohead controls. The best approximation we can assume is that ϕ29 proheads that you estudied were made by gp8, a variable amount of gp8.5*

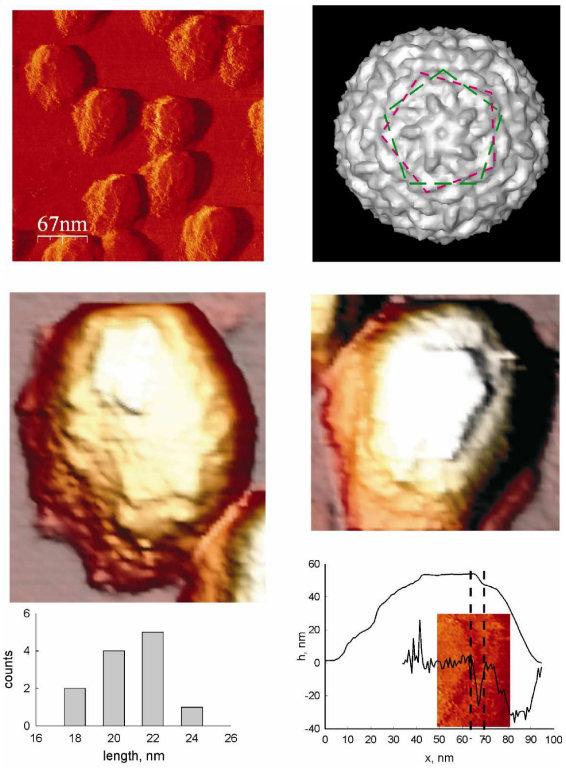

Figure 2. Features of proheads. a) Low resolution image of proheads - normal force map b) Pseudo-atomic structure ϕ 29 - top view on the icosahedral cap. With the dashed lines are outlined two complex pentameric features i) with line in green are connected the icosahedra vertices ii) in red are shown the boundaries across the protruding domains of the monomers involved in the interactions at 3-fold-quasi symmetry positions. The structure is similar in size as the pentameric feature formed from the vertices but slightly skewed in respect of the last one c) High resolution image of prohead attached on its side, imaging force 130 pN. d) Same as panel c but for upright prohead with the corresponding profiles of the topography and normal force map at the shown cross section. e) Distribution of size of observed pentamers sides including tip convolution (N= 12, std. dev.=1.6 nm .

SFM images. Within our tip resolution the five trimers of monomers thus seem to form a composite plate with continuous mechanical properties which is easier to deform in the middle area but display stiffer edges. It is difficult to determine in our images if the boundaries of the pentameric plates we observe are determined by the BIG2 domains or the wedge domains since there is only a slight skew between the two possibilities (Fig 2b) (6). But the protein-protein interactions subjected to applied load seem to respond differently to applied force depending on their position within the capsid (Fig. 1b). This should be the result of differences in interaction strength and distances between the 5 different protein environments.

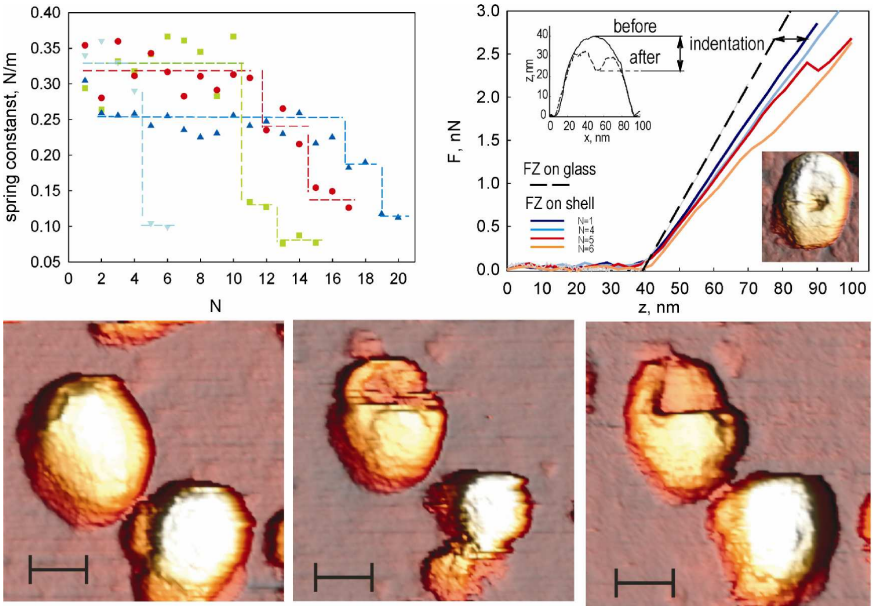

Figure 3 Fracturing proheads. a) Spring constants development during repetitive pushing. Spring constants calculated from the linear part of force distance curves (10). The dotted lines are the mean values of the elastic states in order to guide the eye to the different elastic levels of disintegrating shells. The loading rate is comparable to imaging mode (~10 msec per loading cycle). Similar behavior was found for 9 more viral capsids. b) Applied load on the capsids. Discrete fracture events can be seen after several rounds of indentation. c) Imaging with 170 pN of force. d) The shell fracture during imaging with 370 pN. Imaging at 130 pN shows the observed fracture lines. The scale bar is 35 nm.

Breaking virus shells.

The stiffness of the interactions between the subunits depends on their local environment but is there also a correlation between the monomer position in the capsids and the maximal force it can withstand? In a previous study it was shown that proheads break due to the application of a high force (>3 nN) or due to repeated tapping (<1 nN) on the capsid . In order to determine the relative strength of the 5 different protein-protein interaction environments, we indent shells with an AFM tip until they fracture and image the resulting damage afterward with a low applied-load in jumping mode. Often we

observe holes in the capsid with clearly observable (straight) boundaries around the location where the tip was positioned during the push. Even though such broken shells have multiple disrupted protein-protein interactions or even missing gp8 proteins, they still keep most of their original shape and keep responding elastic to external loads. The used AFM tips have a radius comparable with the proheads and the resulting contact area is in the order of the monomer size. Therefore the resulting stresses due to an indentation are concentrated in the contact region, and as seen in our experiments fracturing occurs indeed within this region.

However, we want to test the relative strength of all the protein-protein interactions, therefore each bond should be given an equal chance to fail under controlled conditions. It was shown that repeated pushing on a capsid results in failure (10). This failure occurs in a stepwise fashion presumably due to discrete disruption of protein-protein connections (Fig 3), which causes defects in the shell thus weakening its elastic response. As a result we can break capsids in a controlled way by imaging them repeatedly since imaging results in a gentle indentation during every tip contact at all positions on the capsid. Figure 3c-e shows 3 topographical images at different applied forces demonstrating the controlled breaking of a capsid. In the first image the prohead appears intact, after several rounds of imaging the shell breaks revealing fracture lines. Note that the outlines of a hexameric structure can be seen on the surface. Imaging at low force shows that the damage is permanent and that the fractures are pronounced. Breaking shells with imaging has the obvious additional advantage that we see the resulting fractures immediately. Most of the objects we have investigated, display straight fracture lines and geometrical shaped features (Fig 4). Two types of damage can be observed on 13 analyzed objects: indentation lines (N = 20) (Fig 4a) and completely separated proteins (N = 53) (Fig 4b, c, d). A cross section of an indentation line shows that those lines exhibit vertical displacements of about 3 to 5 nm. The proteins seem permanently moved but it is unclear if the bonds between the adjacent proteins are broken or still intact. The histogram of measured angles between fractures gives distinct peaks at 60 and 120 degrees, which are the angle expected from triangular faces of an icosahedral lattice (Fig 4c, top inset). The length of fracture lines which have well defined ends (32% of

complete fracture lines) is 20 ± 1 nm (Fig 4d, top inset), which is the same size as the observed pentameric features in the intact shells. The fractures have many different shapes but all with the typical length scale of trimers of gp8 monomers. Therefore, fracturing primarily takes place along the borders of these trimers indicating that protein interaction at the 3-fold symmetry axis in the triangular faces are the most robust within the proheads.

In all viruses, the edges of the capsid proteins have to participate in extensive interactions with its neighboring capsomers (electrostatic, van der Waals and hydrogen). In addition, many phages have adopted a strategy of connecting their subunits around the 3-fold symmetry axis by insertion of additional proteins (as in T4), or by swapping of domains between neighboring subunits (HK97). A particular mechanism is exhibited by HK97, where there is an additional covalent crosslinking between different domains of neighboring subunits (12-15). In ϕ29, there is no crosslinking, the interfaces around the 3-fold axis appear relatively strong, and they are probably reinforced by the extension of the BIG2 domain of one subunit across the capsomeric boundary (Morais et al., 2005). This suggests that the trimers of monomeric gp8 subunits are the building block from which the elongated shell is assembled. Other viruses have been shown to assemble in trimers as well (ref). Note that these trimers have to interact with each other in 4 different configurations (Fig 1b).

Trimer interactions.

Taking the gp8 trimers as the (un)building block of these proheads, we can analyze the fracture lines in terms of the protein (trimer) organization within a capsid with triangulation number T=3 and Q=3 (Fig 1, black lines; Fig 4, lower insets) (see materials and methods).The fracture lines which can not be clearly identified with in this trimer framework are not considered in the further analysis. Those lines constitute less than 25% of the total of fractures counted (N = 92). The identified lines can be grouped according to the 4 different interaction environments of the trimers and normalized according to the frequency of occurrence of these interactions (see materials and methods). In Figure 5 it can be seen that the interactions between the proteins in the 2-fold symmetry position on the equatorial belt fail nearly twice as often as the

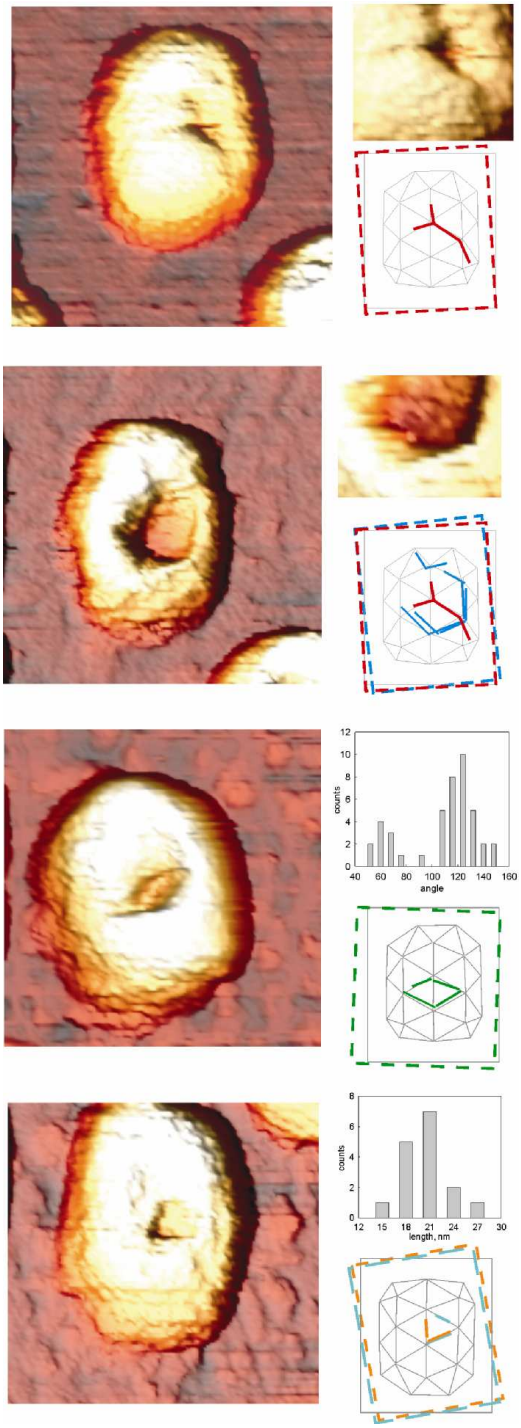

Figure 4. Fractured proheads. a) Fracture lines on the surface of a prohead, inset top, enlargement of feature, inset bottom, estimated location of fracture. b) Same prohead as shown in panel a after another round of imaging. Fractures have evolved into a complete displacement of a hexameric structure, inset top, enlargement of feature, inset bottom, estimated location of fracture. c) Missing triangles, inset top, histogram of measured angles, inset bottom estimated location of fracture. d) Missing triangle, inset top, histogram of measured length lines with clearly visible ends, inset bottom estimated location of fracture. The images are presented in 3D with insets for panel a and b in different views in respect of the light source position.

interaction within the icosahedral end-caps.[2,3]

The observation that the elongated shell is weaker in the equatorial region could suggest that the expansion of the ϕ29 prohead might have taken place during a later stage of its evolutionary development presumably to accommodate a larger genome. By the addition of a ring of gp8 trimers the number of interaction between these building blocks doubled. These additional interactions constrains also have to be met but the result seem to be a bigger yet weakened capsids structure. Also, prohead are formed in the presence of scaffolding protein which interacts with the subunits around the equatorial belt. Mutants lacking the scaffolding protein form regular icosahedrons. The reason is probably the diminish interaction strength between the trimers in the equatorial belt.

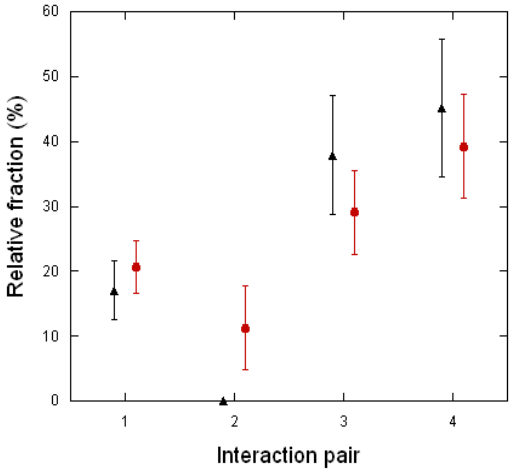

Figure 5. Normalized failure rate of trimer interactions. Interaction 1 to 4 represent the orange-pink, light green-light green, dark green–light green and blue-blue interactions between gp8 trimers (Fig 1b). Triangles, fraction of identified complete protein separations. Circles, as triangles including indentation lines.

[2] *Footnote 2: The tip exerts pressure on the surface shell which varies across the surface due to the capsid curvature. The equatorial region is cylindrical with a curvature in respect to the short axis. The end-caps have additional curvature along the other axis. However, due to the small indentations, the change of the normal component of the force due to the curvature is rather small and is comparable with the change in the force due to the experimental noise.]*

[3] *Footnote3: The proheads are originally assembled by gp8, the scaffolding protein (gp7) and the connector (gp10). The absence of the connector leads to icosahedral capsids, thus implicating this component in the definition of the prolate meridional elongation. The scaffolding protein is loosely attached to the interior of isolated proheads, and it is released after prolonged storage, resulting in scaffolding-less proheads. (Thus, the most likely protein composition of our proheads is gp8+gp10(*variable amount of gp8.5)).*

Materials and Methods

AFM Imaging

Most images are made with force of approximately 100 pN which can vary from experiment to experiment by about 50 pN depending of the conditions of the cantilever – sample engagement. All the images are made with Scanning Probe Microscope (Nanotec Electronica) operating in jumping mode.(11). In this mode the AFM performs a fast execution of force–distance curves at every point of the topographical image in a raster fashion. The maximum normal force exerted on the tip is set as a feedback parameter. In that way the force applied on every scanned sample point is constant and known. The tip is moved in lateral direction while is out of contact with the sample so the shear forces are avoided. The cantilevers spring constants are calibrated using the method of Sader (16). Both the topographical image and the corresponding normal force map were recorded. The proheads are purified as described in (1). The AFM samples are prepared and treated as described in (10). All experiments are performed in liquid in buffer condition.

Data analysis

To describe our observations in the AFM images we use a mesh of triangles where the triangle area will be split on three trapezoids to depict the protein monomers (Figure 1b). All proheads analyzed are deposited on the glass surface along their long axis. Using such 3D-mesh on the AFM images we found that it described the observed fracture features well. 2 different of attachments of the shell to the surface can be distinguished: they are rotated 18 degrees on the z-axes in respect to each other. To scale and align the different proheads in respect to each other a box was drawn around each image, which represents the image including tip convolution. The fracture lines are identified from the AFM images as follows: First the orientation of the prohead on x-y plane is obtained from a rectangular box around the image. Lines are drawn over the first image following the visible fracture lines. Then the pattern is placed on a different view (change in light angle) of the object and additional lines are added when necessary. In that way we are averaging the lines position, minimizing the displacement in their projection due to a possible z-distortion of the edges. The resulting pattern is positioned on different conformations of the 3D mesh and the best fit is chosen (Fig 4,

lower insets). 75% of protein-protein fractures and indentation can be matched with this procedure. Normalization of the trimer interface is performed by counting the number of different interactions within the two attachment configuration that are probed by the AFM tip. The average angle of our tip is 64 ± 11 degrees (N=14) and determines the surface actually contacted by the tip. The relative occurrence of interaction 1 to 4 following this approach is, 45%, 10%, 25% and 20% of the exposed surface (see Fig 5).

References

1. Ibarra, B., Caston, J. R., Llorca, O., Valle, M., Valpuesta, J. M. & Carrascosa, J. L. (2000) *Journal of Molecular Biology* **298,** 807-815.
2. Simpson, A. A., Tao, Y. Z., Leiman, P. G., Badasso, M. O., He, Y. N., Jardine, P. J., Olson, N. H., Morais, M. C., Grimes, S., Anderson, D. L., Baker, T. S. & Rossmann, M. G. (2000) *Nature* **408,** 745-750.
3. Valpuesta, J. M. & Carrascosa, J. L. (1994) *Quarterly Reviews of Biophysics* **27,** 107-155.
4. Guasch, A., Pous, J., Ibarra, B., Gomis-Ruth, F. X., Valpuesta, J. M., Sousa, N., Carrascosa, J. L. & Coll, M. (2002) *Journal of Molecular Biology* **315,** 663-676.
5. Tao, Y. Z., Olson, N. H., Xu, W., Anderson, D. L., Rossmann, M. G. & Baker, T. S. (1998) *Cell* **95,** 431-437.
6. Morais, M. C., Choi, K. H., Koti, J. S., Chipman, P. R., Anderson, D. L. & Rossmann, M. G. (2005) *Molecular Cell* **18,** 149-159.
7. Morais, M. C., Kanamaru, S., Badasso, M. O., Koti, J. S., Owen, B. A. L., McMurray, C. T., Anderson, D. L. & Rossmann, M. G. (2003) *Nature Structural Biology* **10,** 572-576.
8. Caspar, D. L. D. & Klug, A. (1962) *Cold Spring Harbor Symposia on Quantitative Biology* **27,** 1-&.
9. Wikoff, W. R. & Johnson, J. E. (1999) *Current Biology* **9,** R296-R300.
10. Ivanovska, I. L., Pablo, P. J. C., Ibarra, B., Sgalari, G., MacKintosh, F. C., Carrascosa, J. L., Schmidt, C. F. & Wuite, G. J. L. (2004) *Proceedings of the National Academy of Sciences of the United States of America* **101,** 7600-7605.
11. de Pablo, P. J., Colchero, J., Gomez-Herrero, J. & Baro, A. M. (1998) *Applied Physics Letters* **73,** 3300-3302.
12. Duda, R. L., Hempel, J., Michel, H., Shabanowitz, J., Hunt, D. & Hendrix, R. W. (1995) *Journal of Molecular Biology* **247,** 618-635.
13. Fokine, A., Leiman, P. G., Shneider, M. M., Ahvazi, B., Boeshans, K. M., Steven, A. C., Black, L. W., Mesyanzhinov, V. V. & Rossmann, M. G. (2005) *Proceedings of the National Academy of Sciences of the United States of America* **102,** 7163-7168.
14. Popa, M. P., McKelvey, T. A., Hempel, J. & Hendrix, R. W. (1991) *Journal of Virology* **65,** 3227-3237.
15. Wikoff, W. R., Liljas, L., Duda, R. L., Tsuruta, H., Hendrix, R. W. & Johnson, J. E. (2000) *Science* **289,** 2129-2133.
16. Sader, J. E., Larson, I., Mulvaney, P. & White, L. R. (1995) *Review of Scientific Instruments* **66,** 3789-3798.

CHAPTER 6

"'Take some more tea,' the March Hare said to Alice, very earnestly.

`I've had nothing yet,'* Alice replied in an offended tone, *`so I can't take more.'

`You mean you can't take LESS,'* said the Hatter: *`it's very easy to take MORE than nothing."

From *Alice's Adventures in Wonderland*
by *Lewis Carroll*

Internal DNA pressure modifies stability of wild-type phage

Irena Ivanovska[1], Gijs Wuite[1], Bengt Jönsson[2], and Alex Evilevitch[3]

1. Physics of Complex Systems, Division of Physics and Astronomy, Vrije Universiteit, De Boelelaan 1081, 1081 HV, Amsterdam, The Netherlands.

2. Department of Biophysical Chemistry, Center for Chemistry and Chemical Engineering, Lund University, Box 124, S-221 00 Lund, Sweden.

3. Department of Biochemistry, Center for Chemistry and Chemical Engineering, Lund University, Box 124, S-221 00 Lund, Sweden.

Accepted in ***PNAS,*** April ***2007***

Abstract

dsDNA in bacteriophages is highly stressed and exerts internal pressures of many atmospheres on the capsid walls. We investigate the correlation between packaged DNA length in phage λ (78 – 100 % of wt DNA) and capsid strength using an Atomic Force Microscope indentation technique. We show that phages with wt DNA are twice as strong as shorter genome mutants, which behave like empty capsids regardless of high internal pressure. Our analytical model of DNA-filled capsid deformation shows that due to DNA-hydrating water molecules, an osmotic pressure exists inside capsids which increases exponentially when the packaged DNA density is close to wt phage. This osmotic pressure raises the wt capsid strength and is approximately equal to the maximum breaking force of empty shells. This result suggests that the strength of the shells limits the maximal packaged genome length. Moreover, it implies an evolutionary optimization of wt phages allowing them to survive greater external mechanical stresses in nature.

Introduction

The majority of viruses have spherical protein shells (capsids) with icosahedral symmetry, with radii varying between 10 and 100 nm, and with thicknesses of few nm, corresponding to a single protein layer. Viral capsids protect genomes that can be tens of microns in contour length. In prokaryotic viruses (bacteriophages), capsid proteins first assemble in empty capsids before the genome is actively packaged by a molecular motor which is part of the capsid(1, 2). Matching the capsid size and genome length is of great importance for efficient packaging and viral infectivity. For example, wild-type (wt) phage λ infects E. coli cells and has its DNA (48,502 bp) contained in an icosahedral T=7 capsid to which a flexible, noncontractile tail is attached. The mature capsid has an outer diameter of 63 nm and a shell thickness of between 1.8 and 4.1 nm(1, 2). λ phages can be packaged with DNA lengths in the range of 78-106% of wt DNA and remain infectious(3). If the genome is shorter than 78% of the wt-DNA, then the phage fails to infect. When the DNA is longer than 106% of wt length, packaging does not occur. It was recently shown that dsDNA inside many phages is highly stressed due to electrostatic repulsion and the bending energy of the packaged DNA chain, resulting in internal pressures of several tens of atmospheres(4-12). This suggests that the infection is in part driven by the internal DNA pressure. Thus, if DNA is significantly shorter than wt, the internal pressure becomes too low and is therefore incapable of injecting enough DNA into the bacteria. On the other hand, if the DNA is longer than wt, the internal pressure might be too high, and the force that builds up in the capsid could exceed either the strength of the packaging motor(4, 13) or the maximum internal force the capsid can withstand. Thus the capsid size and strength might limit the extent to which the genome can be pressurized in the capsid.

In this work we investigate the physical coupling between packaged genome length and capsid size by measuring capsid deformation as a function of the externally applied force using Atomic Force Microscope (AFM) tips. We compare the properties of empty λ phages, λ phages filled with wt DNA, and phages partially filled with DNA. We found that wt λ had a spring constant nearly double that of the other λ phages, and could withstand forces twice as high before irreversible damage occurred. Using an

analytical model, we show that *only* the packaging density of the wt phage λ provides a "DNA pressure" that, remarkably, makes the capsid stronger. These results seem to indicate that wt λ phages have optimized their dimensions with regard to internal pressure and capsid strength. Considering that the λ phage host (E. coli cell) often adheres to surfaces exposed to a significant shear stress(14) suggests an answer to why genetically modified mutants, which are identical in structure but differ in DNA length, are infectious but not abundant in nature. This behavior seems to mirror biological cells, where osmotic pressure also creates strength against external mechanical deformation.

Results and Discussion

The mature heads of λ phage capsids are built of 415 copies of gpE protein (40 kDa) and 405-420 copies of gpD protein (11.4 kDa). gpE forms the actual shell and is clustered in hexamers and pentamers. gpD decorates the shell and six trimers surround each hexamer (1, 2). We imaged empty and (partially) full λ phage capsids repeatedly and with high resolution by AFM in jumping mode (Fig. 1). The 173 nm tail, which is attached to one of the icosahedral 5-fold vertices of the capsid (15), is easily dislodged during AFM imaging. Detachment of the tail is usually followed by the complete disintegration of the capsid. With high resolution imaging in jumping mode (16, 17), individual capsomers can be seen, presumably due to differences in height and lateral stiffness as a result of the gpD decoration (Fig 1d).

We determined the (non-) elastic response of intact mature λ capsids with different amounts of packaged DNA (0%, 78%, 94%, and 100% of 48,502 bp wt DNA) by nano-indentation using AFM cantilevers as described in (16). Note that all different DNA length phages and the empty capsid have identical mature capsids with the same number of gpD proteins (18-20). The empty shells have been emptied of their genetic content after maturation (see experimental procedures). We also confirm that result with high-resolution cryo-electron microscopy, by averaging many phage particles together and performing radial average (Fig 2). The packaged genome length (in every phage sample) was verified by extracting DNA from the capsids and determining its length with pulse-field gel electrophoresis. DNA length in

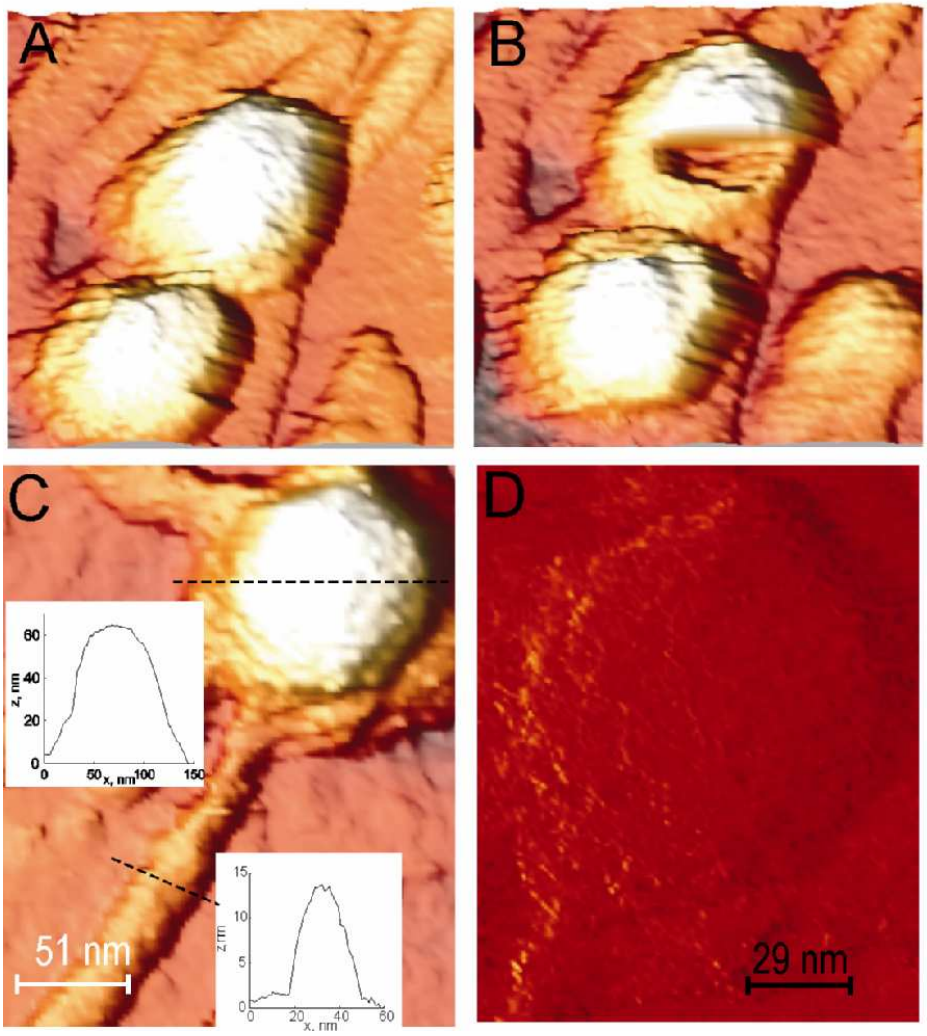

Figure 1: High-resolution imaging of λ capsids (3-d with shadow): A) intact phage λ, B) same phage as in panel A but after breakage, C) cross sections of intact phage, D) high-resolution normal mode image of capsomers on capsid surface.

each case, corresponded to that of a single DNA length population of phage particles (37.7, 45.7, or 48.5 kbp DNA). For each of the capsid conditions we recorded the applied force as a function of piezo-related displacement of the sample towards the tip (FZ curves) for 10-15 individual objects. The typical

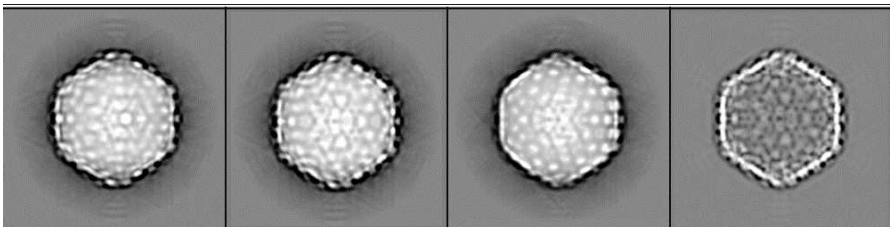

Figure 2: Cryo electron microscopy images of 100, 94, 78% DNA filled and empty phage λ capsids. Images are made by averaging many of the phage particles together and performing a radial average. No difference in the capsid diameters and thickness was observed.

features of the FZ curves are the following: i) the moment the tip touches the virus shell (contact point), ii) a linear reduction of the shell height with applied force, iii) sudden nonlinear response of the shell (capsid breakage or collapse), iv) retraction of the tip (Fig. 3a & b). Figure 3c, shows an example sequence of FZ curves of a shell. These curves reveal a repetitive linear response with no hysteresis or shifting of the contact point. Such response, which was seen for all capsids, indicates that the shells respond elastically without plastic deformation up to indentations of ~25% of the capsid radius. After several indentations, however, the capsid starts to show nonlinear behavior and breaks irreversibly. This kind of material fatigue was also observed for ϕ29 proheads and CCMV capsids but typically, only after many more rounds of pushing (16, 17). λ phages thus seem more fragile. One possible explanation is the existence of the long tail in mature λ phages. They appear to break off rather easy as can be concluded from many detached tails observed on the glass surface. Repetitive deformation of the capsids by the AFM tip might cause the tail to fall off quickly hence inducing an irreversible defect. Irreversible shell collapse or breakage can also be induced by a single push in which the AFM cantilever flattens the capsid against the glass surface. We note here that in all cases before deforming the phage capsid with an AFM tip, we always confirmed that the tail is attached to the capsid by imaging the entire phage under very small forces (as shown in Figure 1). As mentioned above, without tails, capsids were either partially or completely disintegrated, and those capsid parts had a significantly different, nonlinear deformation response compared to the intact shells. However, we also

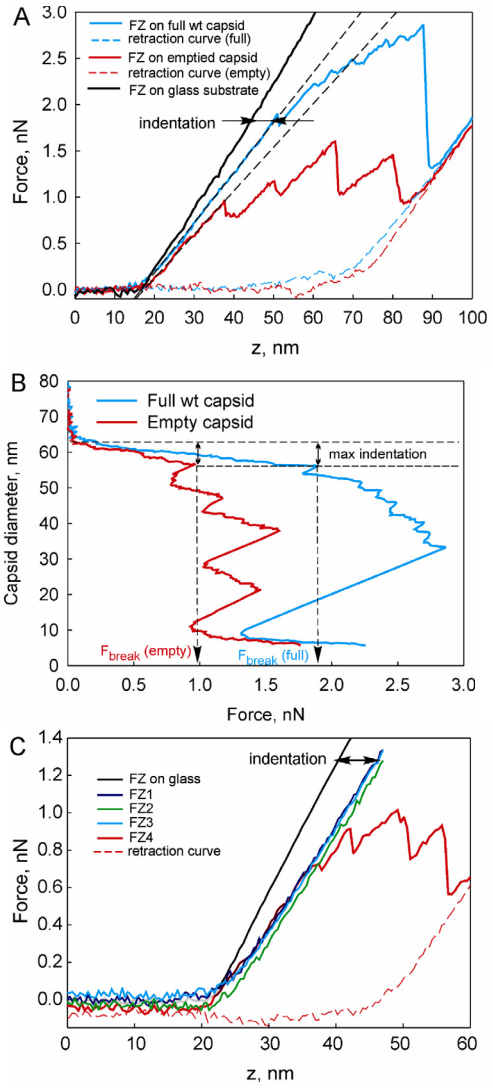

Figure 3: Indenting λ capsids. A) Force distance curves full wt versus empty phage λ. Black dashed lines represent the fit of the linear part of the FZ curves. FZ curves for filled and empty capsids are solid but the dashed parts show the areas when the capsid breaks, and there is a discontinuity in the curve. The capsid breaks stepwise; that is why we observe several "jumps" in the FZ curves without any FZ data between these gaps. B) The data in panel A displayed as observed capsid height vs. force. The deformation of the capsid is linear until a critical deformation is reached, whereafter a sudden decrease in capsid height can be observed. The dashed line with an arrow is inserted to guide the eye, since there is no data recorded between these gaps. C) A sequence of FZ curves performed on a phage capsid containing 94% of the wt genome.

observed for a large number of phage particles, that upon AFM cantilever-induced deformation, the capsid would partially disintegrate while the tail would remain attached to the capsid remains (Fig. 1b). We always confirmed that the capsid was broken by imaging the surface after breaking the phage.

From the FZ curves of the various capsids we extract the following parameters: the spring constant of the linear region, and the force and indentation depth at which the shell starts to respond nonlinearly (Figs. 4 and

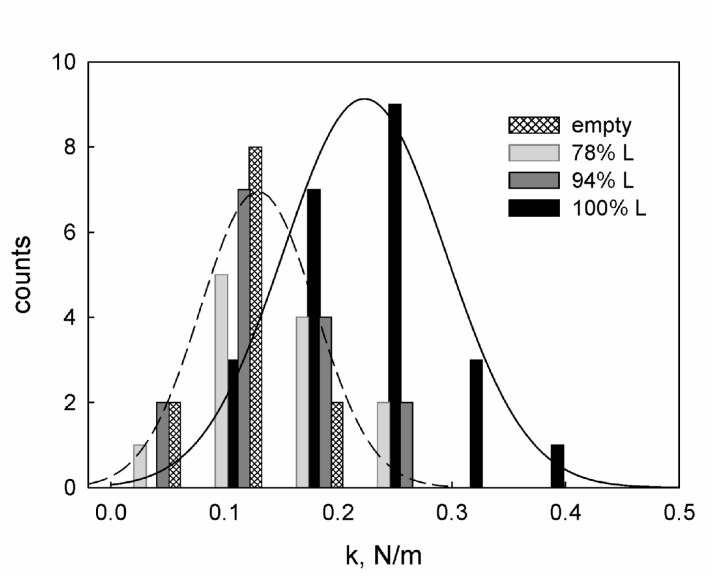

Figure 4: Histogram of spring constants for wt, 94%, 78% filled and empty phages. The data are statistically compared using unpaired t-test to determine the statistical significance of the difference between the means within different groups. The calculated p-values for the difference between the wt capsids and 78%, 94% filled capsids are respectively 0.0027 and 0.00011 (both below the common threshold value of 0.05 for statistical significance). The data for empty phages and the mutants shows no statistical significance with p-values 0.406 and 0.336, respectively. The solid line is a fit to wt phage data and the dashed line is a joint fit to 94%, 78%, and empty phage data.

Table

Table 1, Spring constant of the linear region, and the force and indentation depth at which the shell starts to respond nonlinearly.

Genome length %	Spring constant k, N/m	Std. dev.	Std. error	Fbr, nN	Std. dev.	Std. error	Indent. nm	Std. dev	Std. error
0	0.13	0.04	0.01	0.8	0.4	0.1	5.7	2	0.6
78	0.15	0.07	0.02	0.9	0.4	0.1	6.1	2	0.7
94	0.14	0.05	0.01	1.0	0.3	0.1	6.6	2	0.5
100	0.23	0.06	0.01	1.6	0.6	0.1	7.6	3	0.6

5, Table 1). From these figures and the table, it is clear that capsids containing wt DNA are almost twice as stiff and as strong as the other ones. The maximal indentation wt lambda shells can withstand also shows some increase (~25%), which might stem from a difference in deformation shape of the capsid due to the DNA "pressure" (i.e. less buckling and more flattening than the partially filled and empty capsids). Nevertheless, the actual failure of the shell is probably related to a critical protein-protein separation independent of the amount of DNA inside the capsid. Therefore reaching the threshold of this separation might determine the tensile strength of the capsids.

A continuum theory of elasticity for thin homogeneous shells (21) and finite element analysis can be used to describe the mechanical properties of empty capsids measured using force-distance curves (16, 17). In the continuum model approximation, the spring constant, k, can be related to the Young's modulus, E, of the protein capsid with $k = \alpha E h^2 / r_0$, where h is the capsid thickness, r_0 is the capsid radius, and α is the geometry-dependent proportionality factor. Using finite element simulations for empty phage λ capsids, we obtained a Young's modulus of 1.0 GPa (average capsid radius, r_o, of 29.5 nm; thickness of the gpE shell ≈1.8 nm). From this simulation, we found the capsid geometry-dependent proportionality factor, α, to be around unity (16, 17, 21). This Young's modulus value is close to that reported for ϕ29 proheads, a virus that also keeps its genome under pressure (4, 16). The average force to break an empty λ capsid is 0.8 nN (Table 1), a value similar to that found for empty CCMV, but half the breaking force of ϕ29 at loading rates comparable to these experiments (~1.5 nN at 1500 pN/s). Thus, even though ϕ29 proheads have the same thickness as the gpE shells of λ capsids, they are able withstand higher deformation forces. On the other hand, λ capsids are considerably more elastic than ϕ29 proheads (0.13 N/m vs. 0.31 N/m). As a result, the relative deformation before failure of both capsids is about the same (20-25%). Thus, the difference in strength seems to be caused primarily by the difference in rigidity of the capsids. This result indicates that the energy potential of the capsomer-capsomer interactions in λ phages is lower, and that the mechanical properties of empty viral capsids seem to depend strongly on these local interactions (22). Although it should be noted

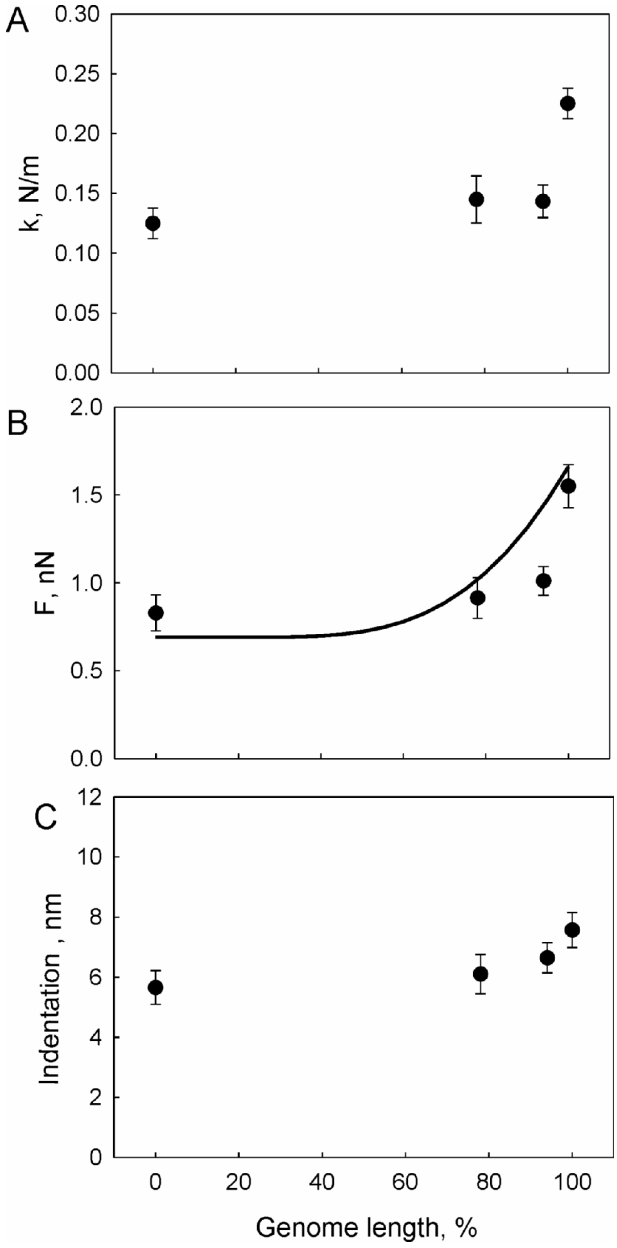

Figure 5: A) Capsid spring constant versus genome length, B) breaking force versus genome length (experimental data shown by circles and model calculation with a line) C) deformation versus genome length. Error bars are shown as standard errors.

that failure of the λ capsids could also be triggered by the loss of the capsid's tail, resulting in a lowering of the apparent maximal strength.

Recently, the effect of packaged DNA length on the internal pressure in λ phage capsids has been investigated both theoretically (4-6, 8, 9, 12) and experimentally (7, 10, 11, 13). It was found that internal DNA pressure increases monotonically, and significantly as the DNA packaging progresses to completion. Eventually, internal pressures reach tens of atmospheres in the λ capsid (10). We have investigated the effect of DNA internal pressure on capsid strength in response to an external deformation (Fig. 4, Table 1). The surprising difference in strength and elasticity between the wt (100% DNA filled) capsids and the partially filled ones (78% and 94%) exists in spite of the fact that DNA in the partially filled capsids still exerts high internal pressure on the capsid walls (~20 atm, ~40 atm, respectively (6, 13)). In fact the partially filled shells responded to external deformation like an empty capsid. Only wt phage with an internal pressure of ~60 atm is approx. twice as stiff and thus, twice as resilient to external forces.

Could this unexpected behavior be the result of DNA hydration forces when the capsids are deformed? It has been shown that the interaction of water-soluble molecules can be described through the interaction of these molecules with the water (23). Using the osmotic stress method, hydration forces were measured between phospholipids bilayers (24), between polysaccharides(24), and between DNA double helices (25). Condensed DNA was seen to be packed into a lattice with well-defined interaxial spacing, d, that decreases with the concentration of the added polymer (osmotic pressure). The force of DNA compression, given by the polymer's osmotic pressure, is equal and opposite to the interhelical repulsion at a given spacing between DNA strands (25). It was found that at separations below 35Å, the repulsive force between DNA molecules varies exponentially and cannot be described by the electrostatic theory. These forces were termed "hydration forces". The hydration force represents the work of removal of water from the vicinity of the surface of the DNA molecule. Likewise, X-ray diffraction studies on phages (26-28) showed that the interhelical distance between packaged DNA strands in bacteriophage heads is in the same range of distances measured using the osmotic stress method. From both results, an

empirical relation was determined for the resulting internal pressure of DNA , P(d), on the walls of the phage capsid (6, 12, 25):

$$P(d) = \Pi(d) = F_0 \exp\left(-\frac{d}{c}\right) \quad (1)$$

where $\Pi(d)$ is the osmotic pressure, and F_0 and c are constants that depend on the nature, charge, and concentration of ions present in the solution. For the ionic conditions of our experiment (10 mM $MgSO_4$), F_0 = 1.2 x 10^4 pN/nm^2 and c = 0.30 nm(12, 25, 29). As shown in ref.(12), the relation between the interaxial spacing, d, the genome length, L, and the capsid volume, V, can be reasonably described by:

$$d = \sqrt{\frac{2V}{\sqrt{3}}}\frac{1}{\sqrt{L}} \quad (2)$$

Now if the volume of a capsid is changed due to AFM indentation, DNA cannot leave the capsid while water can do so. As a result, the change in capsid volume requires dehydration of DNA, which increases the DNA-DNA hydration force exponentially. In order to determine if this force is significant in our AFM measurements, we need to compare the additional work due to the hydration forces with the work of deforming empty capsids.

Dockland et al. (1) proposed from their structural study of λ phage that capsid proteins of λ do not seem to interact directly with the packaged DNA. Therefore, in our model we describe the force of capsid deformation as a sum of the force required to deform an empty capsid and the force required to deform the DNA inside the capsid. From a thermodynamic perspective, the work (w) exerted by the external force, F, on the capsid is given by:

$$w = \int_0^D F(D)\cdot dD = \int_0^D dG_{\text{empty capsid}} + dG_{\text{surface area}} + dG_{\text{osmotic}} \quad (3)$$

where D is distance of deformation in the z-direction, $dG_{\text{empty capsid}}$ is the work of deformation of an empty shell (bending and stretching), $dG_{\text{surface area}}$ is the work of capsid area change due to capsid stretching induced by the packaged DNA, and dG_{osmotic} is the work induced by osmotic pressure change due to the capsid volume modification. The work required for small mechanical deformations of the capsid shell is:

$$w = dG_{\text{empty capsid}} + dG_{\text{surface area}} \approx k_1 \cdot D \cdot dD + k_2 \cdot dA \quad (4)$$

where dA is a change in the capsid surface area due to the deformation distance dD and parameters k_1 and k_2 are material-specific constants for the capsid proteins. k_1 corresponds to k_{empty} (0.13 N/m) the spring constant for an empty λ capsid (Table 1). The deformation dD also gives rise to a volume change, dV, which in turn leads to an osmotic work $\left(dG_{osmotic} = -\Pi_{osmotic} \cdot dV\right)$. The force of deformation F(D) can thus be expressed as:

$$F(D) = k_{empty} \cdot D + k_2 \cdot \frac{dA}{dD} - \Pi_{osmotic} \cdot \frac{dV}{dD} \tag{5}$$

By setting the capsid area constant (dA / dD = 0), a value which, considering the Young's modulus of the capsids, is expected to be small, we show in the supplemental data that, independent of the deformed capsid shape (oblate or a truncated sphere depending on the assumed AFM cantilever tip shape and size), $\frac{dV}{dD} \approx \frac{\pi \cdot r_0}{2} \cdot D$. Thus the total deformation force F(D) can be expressed as:

$$F(D) \approx k_{empty} \cdot D + \Pi_{osmotic}(c_0 \cdot V_0 / V) \cdot \frac{\pi \cdot r_0}{2} \cdot D \tag{6}$$

where $\Pi_{osmotic}(c_0 \cdot V_0 / V)$ is the osmotic pressure of DNA in the deformed capsid with the volume changed from V_0 to V, c_0 is DNA concentration in the undeformed capsid, and $c_0 \cdot V_0 / V$ is the DNA concentration in the deformed capsid with volume change $V_0 / V \approx 1 + \frac{3}{16 \cdot r_0^2} \cdot D^2$ (derived from equations A2 and A4 in the supplemental data section). This volume change before a capsid breaks is almost negligible for small deformations (in our case, ΔV ~1% at maximum deformation D_{max} = 7.6 nm). Therefore the osmotic pressure $\Pi_{osmotic}(c_0 \cdot V_0 / V) \approx \Pi_{osmotic}(c_0) \approx constant$ during the entire deformation before the capsid breaks. This explains why we observe a linear deformation for all DNA-filled λ capsids even though the DNA is under high pressure.

By setting $k_{empty} \cdot D$ = 0.7 nN in equation 6 (the lower estimate of the breaking force for empty capsids) and by using the maximal indentation averaged over all measured values (D = 6.5 nm), we can calculate the maximal force a capsid can withstand as a function of DNA length (solid line in Fig. 5b) using V_0 = 87114 nm^3 and r_0 = 29.5 nm. Even though it shows a small overestimation, the theoretical prediction in Fig. 5b shows good agreement

between the calculated values and the measured data, in particular when one considers that there are no fitting parameters used in this model. The overestimation of the data can be explained by the fact that in our model, we have set the capsid area constant. However, some change in the area upon deformation should be expected, which would imply a smaller change in the volume and thus a smaller contribution from the volume-dependent osmotic force term to the total force F(D). Equation 6 thus provides an upper limit of the deformation force.

These results show that the packaging density of wt DNA (or close to its length) in λ phage is capable of providing a significant internal support to the mechanical strength of the capsid with the help of DNA hydration forces. We suggest that it is not coincidence, but rather the evolutionary energy optimization by nature that has selected and optimized the wt DNA phages, which can survive external mechanical stresses in the environment that are twice as high, in comparison to its mutants. Such an assumption is supported by the fact that E. coli cells which are infected by λ are often found colonizing the surfaces experiencing high shear forces due to the laminar liquid flows (14). Since the phage needs, in turn, to adhere to the E. coli cell surface in order to infect, it will also experience this mechanical stress. Indeed, practical experience shows that phages have a limited life due to mechanical breakage induced by the shear forces in the solution (30). From our own experience, wt λ phages seem to lose their infectivity more slowly than their shorter genome mutants, which we confirmed by titering wt phage and its 37.7 kbp mutant before and after two weeks storage at 4ºC.

Finally, we performed AFM indentation experiments on the wt phage λ in 1 mM spermine tetrahydrochloride. Spermine is a tetravalent cation that is known to cause DNA condensation by introducing attractive interactions between the DNA strands (24). Capsid deformation response was again linear but the capsid breaking force was now similar to the empty capsid. Indeed, we have shown earlier that 1 mM spermine will significantly reduce forces between packaged DNA strands within the capsid, since spermine cations permeate the capsid (7,10). Rau et. al. (24) showed that hydration forces between DNA strands will significantly decrease in the presence of polyvalent ions such as spermine. Therefore this experimental observation confirms our

above model interpretation that the osmotic force inside wt phage under standard buffer conditions will contribute to the capsid's strength against external mechanical deformation.

Our data analysis also shows that in the wt phage, the osmotic force contribution to maximum deformation force (~0.8 nN) is nearly equal to the breaking force of an empty capsid. This result suggests that the mechanical strength of the capsid sets the upper limit to the amount of DNA that can be packaged (i.e. the maximal internal force due to the osmotic pressure). Although there is no lower limit of DNA length that can be packaged into phage λ (as long as phage does not have to infect the cells and multiply), there is, however, an upper limit (106% of the wt genome) which could be related to the strength of the capsids (3). This balance between the internal DNA pressure and the capsid strength has also been discussed in the context of osmotic shock experiments (31). Therefore we expect the packaging density of DNA to be optimized to the capsid strength and to be the key parameter in phage stability and infectivity.

Experimental Procedures

Bacteriophage strain and preparation of phage stock.

Wild-type bacteriophage λ cI857, with genome length 48.5 kbp, and its shorter mutant, with 45.7 kbp, were produced by thermal induction of lysogenic Escherichia coli strains AE1 and AE2 derived from S2773 and S2739 strains (generously provided by Stanley Brown, Dept. of Molecular Cell Biology, Copenhagen University). The AE1 and AE2 strains were modified to grow without LamB protein expressed on its surface in order to increase the yield of phage induced in the cell. The culture was then lysed by temperature induction. Phage λ λb221 with 37.7 kbp was extracted from single plaques. Phage purification details are described elsewhere (7). All phage samples were purified by CsCl equilibrium centrifugation and dialyzed from CsCl against TM buffer (10 mM $MgSO_4$ and 50 mM Tris-HCl/pH 7.4). The final titer was $\approx 10^{12}$ virions/ml determined by plaque assay (32).

Empty phage particles were prepared by incubating wt phage with its extracted LamB receptor for 1 hour at 37°C, which causes all phages to eject their DNA. The ejected DNA was digested by DNase I and empty phage

"ghosts" were purified by filter centrifugation.

Preparation of LamB phage λ receptor.

The receptor was the LamB protein purified from pop 154, a strain of *E. coli* K12 in which the *lamB* gene has been transduced from *Shigella sonnei* 3070(33, 34). This protein has been shown to cause complete in-vitro ejection of DNA from λ at 37°C, in the absence of the added solvents required with the wild-type *E. coli* receptor (35, 36). Purified LamB was solubilized from the outer membrane with the detergent octyl polyoxyethylene (octyl-POE).

AFM

All SFM experiments are performed with SFM (Nanotec Electronica, Madrid, Spain) operated in jumping mode using WSxM software (www.nanotec.es <http://www.nanotec.es/>). Detailed description of the method and apparatus can be found elsewhere (37). Both imaging and force-distance curves are done in buffer conditions at room temperature. The SFM sample is prepared as is described in Ivanovska et. al. (16). The virus particles are deposited for adsorption on preliminary cleaned, hydrophobic glass coverslips. Rectangular gold-coated cantilevers (Olympus, Tokyo) were used with tip apex nominal value < 20 nm. The cantilevers' spring constants are calibrated using the method described in (38) and are found to be 0.07 N/m, varying by ~15 % in a wafer unit.

Acknowledgements

We greatly acknowledge William M. Gelbart, Charles M. Knobler, Christoph F. Schmidt and Michael Feiss for valuable discussions and advice. We are grateful to Gabriel Lander and John E. Johnson for taking EM images of lambda capsids. We thank Stanley Brown for providing bacterial strain for phage growth and Caroline Fraysse for providing the strain for LamB production. This work was supported by the European Laser Center at Vrije University, Amsterdam and the Swedish Research Council (VR) (to AE), and by the Dutch organization for Fundamental Research of Matter (FOM) and the Netherlands Organization for Scientific Research (NWO) (to GJLW).

References:

1. Dokland, T. & Murialdo, H. (1993) *J Mol Biol* 233, 682-94.
2. Yang, F., Forrer, P., Dauter, Z., Conway, J. F., Cheng, N., Cerritelli, M. E., Steven, A. C., Pluckthun, A. & Wlodawer, A. (2000) *Nat Struct Biol* 7, 230-7.
3. Feiss, M., Fisher, R. A., Crayton, M. A. & Egner, C. (1977) *Virology* 77, 281-93.
4. Smith, D. E., Tans, S. J., Smith, S. B., Grimes, S., Anderson, D. L. & Bustamante, C. (2001) *Nature* 413, 748-752.
5. Kindt, J., Tzlil, S., Ben-Shaul, A. & Gelbart, W. M. (2001) *Proceedings of the National Academy of Sciences of the United States of America* 98, 13671-13674.
6. Tzlil, S., Kindt, J. T., Gelbart, W. M. & Ben-Shaul, A. (2003) *Biophys. J.* 84, 1616-1627.
7. Evilevitch, A., Lavelle, L., Knobler, C. M., Raspaud, E. & Gelbart, W. M. (2003) *Proc. Nat. Acad. Sci. USA* 100, 9292–9295.
8. Purohit, P. K., Kondev, J. & Phillips, R. (2003) *Proc. Nat. Acad. Sci. USA* 100, 3173-3178.
9. Purohit, P. K., Kodnev, J. & Phillips, R. (2003) *Journal of the Mechanics and Physics of Solids* 51, 2239-2257.
10. Evilevitch, A., Castelnovo, M., Knobler, C. M. & Gelbart, W. M. (2004) *J. Phys. Chem. B.* 108, 6838-6843.
11. Evilevitch, A., Gober, J. W., Phillips, M., Knobler, C. K. & Gelbart, W. M. (2005) *Biophysical Journal* 88, 751-756.
12. Purohit, P. K., Inamdar, M. M., Grayson, P. D., Squires, T. M., Kondev, J. & Phillips, R. (2005) *Biophys J* 88, 851-66.
13. Grayson, P., Evilevitch, A., Inamdar, M. M., Purohit, P. K., Gelbart, W. M., Knobler, C. M. & Phillips, R. (2006) *Virology* 348, 430-6.
14. Thomas, W. E., Trintchina, E., Forero, M., Vogel, V. & Sokurenko, E. V. (2002) *Cell* 109, 913-23.
15. Hendrix, R. W. (1983) (Cold Spring Harbor, N.Y. : Cold Spring Harbor Laboratory.
16. Ivanovska, I. L., de Pablo, P. J., Ibarra, B., Sgalari, G., MacKintosh, F. C., Carrascosa, J. L., Schmidt, C. F. & Wuite, G. J. (2004) *Proc Natl Acad Sci U S A* 101, 7600-5.
17. Michel, J. P., Ivanovska, I. L., Gibbons, M. M., Klug, W. S., Knobler, C. M., Wuite, G. J. & Schmidt, C. F. (2006) *Proc Natl Acad Sci U S A* 103, 6184-9.
18. Kellenberger, E. & Edgar, R. S. (1971) in *The Bacteriophage Lambda*, ed. Hershey, A. D. (Cold Spring Harbor Laboratory), pp. 271-295.
19. Hendrix, R. W. & Tsui, L. (1978) *Proc Natl Acad Sci U S A* 75, 136-9.
20. Hendrix, R. *personal communication* (2007).
21. Landau, L. D. & Lifshitz, E. M. (1986) *Theory of Elasticity* (Pergamon, NewYork).
22. Zandi, R. & Reguera, D. (2005) *Phys Rev E Stat Nonlin Soft Matter Phys* 72, 021917.
23. Leikin, S., Parsegian, V. A., Rau, D. C. & Rand, R. P. (1993) *Annu Rev Phys Chem* 44, 369-95.
24. Rau, D. C. & Parsegian, V. A. (1992) *Biophys J* 61, 260-71.

25. Rau, D. C., Lee, B. & Parsegian, V. A. (1984) *Proc Natl Acad Sci U S A* 81, 2621-5.
26. Earnshaw, W. C. & Harrison, S. C. (1977) *Nature* 268, 598-602.
27. Earnshaw, W. C., King, J., Harrison, S. C. & Eiserling, F. A. (1978) *Cell* 14, 559-68.
28. Earnshaw, W. C. & Casjens, S. R. (1980) *Cell* 21, 319.
29. Parsegian, V. A., Rand, R. P., Fuller, N. L. & Rau, D. C. (1986) *Methods Enzymol* 127, 400-16.
30. Maniatis, T., Fritsch, E. F. & Sambrook, J. (1983) *Molecular Cloning A Laboratory Manual* (Cold Spring Harbor Laboratory.
31. Cordova, A., Deserno, M., Gelbart, W. M. & Ben-Shaul, A. (2003) *Biophys J* 85, 70-4.
32. Silhavy, T. J. (1984) *Experiments with gene fusions* (Cold Spring Harbor, N.Y. : Cold Spring Harbor Laboratory.
33. Roa, M. & Scandella, D. (1976) *Virology* 72, 182-194.
34. Graff, A., Sauer, M., Van Gelder, P. & Meier, W. (2002) *Proceedings of the National Academy of Sciences of the United States of America* 99, 5064-5068.
35. Randall-Hazelbauer, L. & Schwartz, M. (1973) *J. Bacteriol.* 116, 1436-1446.
36. Roa, M. (1981) *FEMS Microbiology Letters* 11, 257.
37 de Pablo, P. J., Colchero, J., Gomez-Herrero, J. & Barro, A. M. (1998) *Appl. Phys. Lett.* 73, 3300-3302.
38. Sader, J. E., Chon, J. W. M. & Mulvaney, P. (1999) *Rev. Sci. Instrum.* 70, 3967-3969.

CHAPTER 7

Have you guessed the riddle yet?' the Hatter said, turning to Alice again.

`No, I give it up,'* Alice replied: *`what's the answer?'

`I haven't the slightest idea,' said the Hatter.

`Nor I,' said the March Hare.

From *Alice's Adventures in Wonderland*
by *Lewis Carroll*

CONCLUSIONS

Introduction

Bulk chemical assays as well as electron microscopy and crystallography experiments have been used to study viral systems over many years, and a wealth of information has come from such experiments. However the bulk assays provide information only on averaged properties of viruses. On the other hand, although the EM can achieve atomic resolution, biological specimens either require staining or image averaging. Over the past decades Atomic Force Microscopy has demonstrated great potential as a technique which can generate both high-resolution images and can probe the interactions between macromolecules under natural conditions for the biological structures. Despite all what is known about viruses: their assembly, structure and subunit organization, there is little known about their material properties and their behavior in response to mechanical stresses. The familiar images of viruses, built from protein building blocks in a highly precise manner, brings up associations with small machines with their parts, such as containers, motors, springs etc. Particularly the protective shells of viruses, which are self-assembled from protein monomers, interacting usually by weak molecular forces such as van der Waals and electrostatic forces, are very intriguing objects. Are they brittle like crystal balls or elastic like rubber ones? Is there a difference between empty and full viral shells? How do their mechanical properties reflect their biological specialization? Can the laws of continuum mechanics describe structures as small as their subunits? This thesis attempts to answer some of these questions.

Experimental achievements

Biggest challenges of AFM experiments on viruses are finding the appropriate attachment conditions on the surface and avoiding the destructive tip-sample interactions. This is the reason why early attempts to perform AFM experiments on viruses were done either in ambient conditions (1, 2) or with a fixating agent. A number of viruses have been previously studied (2) under physiological conditions but within crystal lattices. Moreover, they are often deformed in the used imaging conditions. The experiments described in this

thesis overcome all these disadvantages due to the use of jumping mode imaging and optimization of the surface attachment. In jumping mode the tip is in contact with the sample with a controlled force and it is out of contact during the lateral movement of the sample thus avoiding shear forces. In that way the viral shells are imaged with high resolution (1nm) without deformations (3-6). During imaging we can record simultaneously the normal force. The surface attachment we pioneered is non-specific and works well for a variety of the capsids (ϕ 29, CCMV, λ phage). Even though it provides a very stable attachment, it is not stronger than the intramolecular interactions among the capsid subunits. Therefore it is unlikely to influence the particle properties. This enables us to study the molecular interactions by breaking capsids in a controlled manner (5).

Nanoindentation experiments:

Linear regime: The spring constant and indentations

The main physical property which we measured in nanoindentation experiments is the spring constant of the capsid obtained from the slope of FZ distance curves. The continuum model of elasticity of thin homogeneous shell predicts a linear elastic response for small deformations as a function of external applied force. AFM experiments validate such response for protein shells even though they are certainly non-homogeneous and their building blocks are not much smaller than the size of the capsid structure itself. We also demonstrate that there is a linear elastic response far beyond the regime of small deformation (in order of the magnitude of the shell thickness), a surprising result considering the theoretical predictions. For example the maximal indentation ϕ29 proheads can sustain at high loading rates is found to be 12 nm ± 3 nm which is 50% of its radius along the short axis. This is large compared with the shell thickness of ~1.6 nm. Another surprising case of an unexpectedly large linear elastic response is measured for CCMV capsids at a specific transitional state, induced at a specific pH. In this state the shell can be deformed essentially till the top and bottom part of the shell touch each other.

Young's modulus

The measured spring constant allow us to compare the properties of capsids with the same or similar geometry. Because the spring constant of a shell depends on its shape, radius and thickness, we also use more universal material characteristics such as the Young's modulus, *E*, to compare different kinds of viruses. Treating a capsids as a thin spherical shell we can obtain this Young's modulus from the relation: $k_{cap} = \alpha E h^2 / R$, where h the wall thickness, R is shell radius and α is a geometry-dependent proportionality factor. At the same time Finite Element Analysis (FEA) is also used to obtain and confirm this value. With these tools we found for instance that ϕ29 immature empty capsids have a Young modulus of 1.8 ± 0.2 GPa and λ bacteriophage empty mature shells have a modulus of 1 ± 0.2 GPa. Both values are similar to other structural biological molecules like actin and tubulin. ϕ29 capsids are not known to undergo a process of expansion or thinning during maturation. Therefore its geometrical characteristics stay the same, but it seems that there is a change in its internal structure because the spring constant for full ϕ29 phages is found to be ~30% smaller than the immature capsids (data not published). A surprising result considering that the mature particle contains DNA kept under considerable pressure. Although they can not be directly compared this result suggests that the Young's modulus of the shell might decrease at the final stage of maturation. The Young modulus of the RNA virus CCMV is approximately one order of magnitude smaller than ϕ29 and λ. This result is interesting considering that ϕ29 and λ are double-stranded DNA bacteriophages which are known to carry their genome under a large pressure (tens of atmospheres). This pressure is used at the initial stages of injection of the genome during bacterial infection. In contrast CCMV carries RNA and the capsid is self-assembled around it. Certainly such different biological mechanisms would require different physical properties and it is quite understandable that the strength of a phage capsid is many times more than the strength of the plant virus shell. During the preparation of this thesis a similar work has been published (7) on the study of an animal virus murine leukemia virus (MLV), which, similarly as CCMV, carries RNA integrated into the capsid during the

process of self-assembly. The found Young's modulus is 0.23 GPa, close to that of CCMV confirming this result.

Effect of biologically induced changes in the shells

Other important aspect in spring constant measurements and material properties extraction is the insight they can give from a bioengineering perspective. The wild type CCMV capsid is known to self-assemble both in the absence and in the presence of RNA under appropriate conditions. CCMV capsids can also assemble spontaneously around a variety of anionic polymers. In addition a number of mutants have been made with substitutions and/or deletions of residues in the capsid protein. To asses the effect of protein-RNA interactions and mutations in the shell protein on the shell properties, full, empty and SubE mutant capsids properties are measured and compared. The results demonstrate that a single point mutation in capsid protein can measurably enhance the mechanical stability of the capsid. The SubE mutant has a spring constant of 0.19 ± 0.02 N/m (SEM) versus 0.15 ± 0.01 N/m (SEM) for the empty wild type capsid. The presence of RNA inside the capsid also leads to reinforcement of the shell resulting in a similar shell stiffening possibly due to RNA binding to the inside surface of the capsid. A similar effect has been recently reported for parvovirus MVM capsids (8).

Nanoindentation experiments: Nonlinear regime

Breaking force. Ultimate stresses. Failure of viral capsids.

For all capsids subjected to nanoindentation experiments a linear elastic response was found for small indentations (3, 4, 6). After repetitive indentations or with high applied loads the capsids usually break, displaying a catastrophic drop in the recorded force distance curves. Such a catastrophic drop is difficult to be unconditionally associated with a breakage or buckling since both phenomena are associated with a sudden instability of the shell followed by a sharp change in the force-distance response. Buckling can be proven when it is reversible. Then the all FZ curves stay essentially the same. Among all the studied objects indication for such an event has been found only for ϕ29 empty capsids probed with high load rates. Usually FZ curves

which display a sudden drop in the force are followed by FZ curves with decreasing slopes. This is a clear indication of a decrease in elastic energy due to bond(s) disruption. Moreover, when imaged afterwards the capsids appear broken or cracked. The threshold forces for shell failure of different viruses cannot directly be related to each other, because they depend on the tip-sample contact area i.e. stresses distribution which in turn is dependent on the shell size. With FEA simulations, however, we can compare the ultimate stresses. The tensile strength of many known materials is in the range of 5 to 10 % of their Young's modulus. The lowest estimated value of the ϕ29 tensile stress (~0.3 GPa) already more than exceeds this common expectation. For CCMV where the stresses are obtained from simulations the tensile strength is approximately half of the Young modulus. This is a value typical for highly elastic materials such as rubber and elastin. We can thus conclude that the viral capsids are highly elastic yet strong.

Change in the local elasticity

Viral shells are not homogeneous and although a continuum model can describe the deformation behavior well, the elasticity of the shell is expected to vary spatially. In order to probe a difference in local elasticity AFM tips with an appropriate size are required. When the tip-shell contact area has the same scale as the elastic heterogeneity then it can be measured. Local soft spots have been detected in the equatorial region of ϕ29 capsid resulting in a bimodal distribution of the spring constant in this area. We also show that sharp changes in stiffness can be seen in images based on normal force mapping. The already mentioned study on MVM virus also reports anisotropic spring constants which depend on the symmetry axis along which the stiffness is measured. The authors explain their finding arguing that the capsids get reinforcement due to specific attachment of DNA to the inner walls.

Material fatigue

The different viruses handle repetitive indentation differently but they all display material fatigue eventually. For example ϕ29 capsids can sustain many more force deformation cycles than λ phage using similar loading rates.

This might be a reflection of the protein–protein interactions across the shell surface. For example after several indentations λ phage often disintegrates completely, while ϕ29 often displays cracks and gaps but keeps its general shape. Repetitive indentation of CCMV capsids usually does not visibly affect the shell. This suggests that the capsomers of the CCMV shell might have a greater possibility to rearrange without bond-bond disruption. This is supported by the fact that one of the main features of CCMV is the swelling due to a change of the ionic conditions. This swelling is associated with protein subunits rearrangement and increases the diameter by about 10%.

Breaking lines

The fact that ϕ29 capsids can be broken in a controlled manner allows us to study the mechanical coherence of this shell. The pentamers and hexamers at the 5 and 6-fold symmetry vertexes are built from monomers, but they appear not to be the mechanical building blocks of the shell structure. We show that the most stable mechanical unit across the shell surface is the trimer of monomers at the 3-fold symmetry positions of the capsid. Another interesting result came from the analysis of the break lines across the surface of prohead shells. The shells appear to be weaker in the equatorial region. It is interesting to speculate that the elongation of ϕ29 capsids happened in a later stage of the evolutionary development of ϕ29 in order to accommodate a longer genome while losing some of its strength.

Empty versus full capsids under pressure

The fact that bacteriophages keep their genome densely packed raised the question: "What is the mechanical response of capsid filled with DNA?" We investigated this question and found that the deformation of full capsids is again linearly related to the applied force. However, the presence of DNA can be detected as the result of stiffening of the shell. It is known that DNA pressure exerted on the inner walls of a virus shell depends exponentially on the space between the DNA strands. Therefore when this spacing becomes very small the DNA can be felt during an indentation experiment. We demonstrate this effect in experiments on λ phages.

Virus shell modeling

FEA is used to obtain the Young modulus of viral shells. For ϕ29 and λ phage a thin homogeneous shell resting on a surface and subjected to a point force is used. The shape of the ϕ29 is approximated with an ellipsoid and that of λ with a sphere. Since both shells are thin (< 2 nm, and $h/R \ll 1$), a thin shell approximation and a point force are reasonable assumptions for small deformations. FEA allows us to mimic the experimental conditions such as the position of applied force and supporting surface constrains. In order to determine the Young's modulus, E, with the simulation, we adjust E till we obtain a match with the experimentally measured spring constant. For the CCMV capsid, (which is clearly not a thin shell with $h/R \sim 0.3$) the simulation were more involved to understand the effect of a thick shell subjected to a large deformation with a realistic tip shape. Those simulations closely resemble the experimentally observed behavior of the shell until the point that irreversible deformation occurs. The next level of viral simulation would be to model a capsid not as a homogenous shell but with a variable thickness and stiffness. Besides the use of a continuum elastic model for a quantitative description of viral shell deformation, some other models can be found in the literature. The first one is a discrete bead-spring model, in which the authors show that for small capsids the force deformation behavior deviates from the predictions of the continuum elastic model (9). The other study (10) models the capsid as pentameric and hexameric capsomers interacting with a Lenard-Jones potential. The study investigates the stress distribution, and mechanically and thermodynamically induced failure of the capsid. The study provides the same estimates for the above mentioned stresses as we have found in the presented work.

References

1. Falvo, M. R. et al. Manipulation of individual viruses: Friction and mechanical properties. Biophysical Journal 72, 1396-1403 (1997).
2. Kuznetsov, Y. G., Malkin, A. J., Lucas, R. W., Plomp, M. & McPherson, A. Imaging of viruses by atomic force microscopy. Journal of General Virology 82, 2025-2034 (2001).
3. Ivanovska, I. L. et al. Bacteriophage capsids: Tough nanoshells with complex elastic properties. Proceedings of the National Academy of Sciences of the United States of America 101, 7600-7605 (2004).

4. Michel, J. P. et al. Nanoindentation studies of full and empty viral capsids and the effects of capsid protein mutations on elasticity and strength. Proceedings of the National Academy of Sciences of the United States of America 103, 6184-6189 (2006).
5. I. L. Ivanovska, X. A., J. L. Carrascosa, C. F. Schmidt, G. J. L. Wuite. Deconstructing viral shells.
6. I. L. Ivanovska, G. J. L. W., B. Jönsson and A. Evilevitch. Internal DNA pressure modifies stability of wild-type phage.
7. Kol, N. et al. Mechanical properties of murine leukemia virus particles: Effect of maturation. Biophysical Journal 91, 767-774 (2006).
8. Carrasco, C. et al. DNA-mediated anisotropic mechanical reinforcement of a virus. Proceedings of the National Academy of Sciences of the United States of America 103, 13706-13711 (2006).
9. Vliegenthart, G. A. & Gompper, G. Mechanical deformation of spherical viruses with icosahedral symmetry. Biophysical Journal 91, 834-841 (2006).
10. Zandi, R. & Reguera, D. Mechanical properties of viral capsids. Physical Review E 72 (2005).

SUMMARY

Viruses are highly regular, minimalistic in design biological organisms with intriguing biological and physical properties. Virus shells are self-assembled nanocontainers made of proteins which protect and carry viral genetic information from host to host for further infection. This thesis focuses on studying the mechanics of different viral systems by using Atomic Force Microscopy (AFM). AFM has been demonstrated to be a powerful method both for high resolution imaging and manipulation of biological systems under their natural environmental conditions. In **Chapter 2** is described our approach of studying mechanical properties of viruses by using AFM in liquid and the utilization of the method to reveal different spatial and temporal characteristics of their mechanics. Bacteriophages are known to carry their highly compressed genome under considerable pressure in nanometer sized protein containers (capsids). The mechanical properties of ϕ29 capsid are probed by applying point forces by the AFM tip. We show that empty shells withstand high (nanonewton) forces while being indented up to 30% of their height. The elastic response varies across the surface, reflecting the arrangement of shell proteins. Finite element analysis (FEA) of the deformation of homogeneous thin elastic shell is performed and Young's modulus (~ 1.8 GPa) comparable to that of hard plastic is obtained. We also observe fatigue and breakage of capsids after probing them repetitively. In **Chapter 3** we extend our studies to different type of virus (CCMV) – plant virus which is known to self-assemble both in the absence and in the presence of RNA under appropriate conditions. Studies have been carried out on wild-type capsids, both empty and RNA full, as well as on bioengineered mutants. Full capsids resist indentation more than empty ones but all of them are highly elastic. A single point mutation in the capsid protein increases the capsid stiffness. The experiments are compared with FE simulations of the deformation of a homogeneous thick elastic shell. The estimated Young's moduli are approximately one order of magnitude smaller than those obtained for bacteriophages. We also observe catastrophic drop in the Force distance (FZ) curves, associated with capsid failure. In **Chapter 4** is presented a combined theoretical and experimental study of the structural failure of

viral shells under mechanical stress. We found that discontinuities in the FZ curve associated with capsid failure should appear when the so-called Föppl-von Kármán (FvK) number exceeds a critical value. Our indentation experiments on CCMV viral shell subject to a soft-mode instability confirms the predicted onset of failure as a function of the FvK number. A pH induced softening of CCMV makes its capsid remarkably elastic – it can be repeatedly squeezed till its inner wall surfaces come into a contact. **Chapter 5** is focused on more detailed study of the problem of how bacteriophage capsid breaks under externally applied forces. While gently probing the capsid, causing small deformations, we observe changes in the local elasticity revealing pentameric structures. When we break the shells in a controlled fashion we find that the capsids fracture along well-defined lines. The observed fracture lines are analyzed and classified according to the known monomer organization from the recently solved pseudoatomic structure. We found that the mechanically coherent building block of the protein shell is a trimer of monomers, organized according to the triangulation net of the icosahedron. Finally in **Chapter 6** we investigate the correlation between capsid strength and packaged DNA length in phage lambda (78 – 100 % of wt DNA). We show that phages with wt DNA are twice stronger than shorter genome mutants, which behave like empty capsid regardless of high internal pressure. Our analytical model of DNA-filled capsid deformation shows that due to DNA-hydrating water molecules an osmotic pressure exists inside capsids which increases exponentially when the packaged DNA density is close to wt phage. In **Chapter 7** all the results are summarized and the mechanical properties of the different viral systems and their elastic and nonelastic behavior are compared and discussed in the context of their biological functioning.

SAMENVATTING

Virussen zijn zeer regelmatige, minimalistische biologische organismen met intrigerende biologische en fysische eigenschappen. Virushulzen zijn zelf-assemblerende nanocontainers van eiwitten die het genetische materiaal bevatten om zo de ene na de andere gastheercel te infecteren. Dit proefschrift gaat over de studie naar de mechanische eigenschappen van verschillende virussen met behulp van 'atoomkrachtmicroscopie' ('atomic force microscopy' of AFM). Deze technologie wordt veel gebruikt om met hoge resolutie afbeeldingen te maken van biologische systemen en deze te manipuleren in hun natuurlijke omgeving. In **Hoofdstuk 2** staat onze methode beschreven om de mechanische eigenschappen van virussen te bestuderen met AFM in vloeistof. Van *bacteriofagen* weten we dat ze hun samengepropte DNA onder aanzienlijke druk met zich meevoeren in eerdergenoemde eiwitcapsules ('capsids'). De eigenschappen van de capsule van de faag genaamd ϕ29 zijn bestudeerd door met de AFM-naald op één punt op de faag te drukken. We laten zien dat lege virushulzen hoge krachten kunnen weerstaan, terwijl we ze indrukken tot 30% van hun hoogte. De elasticiteit varieert over het oppervlak, veroorzaakt door de ordening van de eiwitten. Zogenaamde 'Finite Element' (FE) analyse leert ons dat de Young's modulus van de huls vergelijkbaar is met die van hard plastic. We zien ook 'materiaalmoeheid' en uiteindelijk het uiteenvallen van de virussen na herhaalde metingen. In **Hoofdstuk 3** zijn we een ander soort virus gaan bestuderen: CCMV – een plantvirus dat zowel met als zonder RNA kan zelf-assembleren. We hebben experimenten gedaan op wild-type virussen (zowel leeg als vol met RNA), alsmede op genetisch gemodificeerde mutanten. Volle virussen weerstaan de indrukking met de AFM-naald beter dan lege, maar beide zijn ze zeer elastisch. Eén enkele puntmutatie blijkt de stijfheid verder te vergroten. De FE-analyse laat zien dat de Young's modulus ongeveer tien keer zo klein is als voor bacteriofagen. We zien ook een forse sprong in de gemeten zogenaamde FZ-curves, wat te maken heeft met het uiteenvallen van de virussen. In **Hoofdstuk 4** staat zowel theoretisch als experimenteel onderzoek beschreven van dit uiteenvallen van viruscapsules onder mechanische druk. We hebben gevonden dat de voornoemde sprong in de

FZ-curves zou moeten plaatsvinden wanneer het zogenoemde 'Föppl-von Kármán (FvK)' getal een kritische waarde overstijgt. De metingen aan het CCMV-virus bevestigen deze afhankelijkheid van het FvK-getal. Wanneer we de CCMV-virussen zachter maken onder invloed van veranderende pH worden deze opvallend elastisch: we kunnen ze herhaaldelijk zo ver samendrukken dat de binnenwanden elkaar raken. **Hoofdstuk 5** gaat over een meer gedetailleerde analyse van hoe de capsules van bacteriofagen breken onder invloed van druk. Als we de virussen zachtjes indrukken, zien we veranderingen in de lokale elasticiteit die *pentamerische* structuren in het virusoppervlak blootleggen. Wanneer we de virussen op een gecontroleerde manier breken, zien we dat dit gebeurt langs vaste breuklijnen. Door nauwkeurige analyse van deze breuklijnen en een vergelijking met de recent gepubliceerde virusstructuur, kunnen we concluderen dat de bouwsteen van de viruscapsule een cluster van drie eiwitten ('trimeer') is, die samen een *icosaëder* (veelvlak-figuur van twintig driehoeken) vormen. Tenslotte beschrijft **Hoofdstuk 6** de samenhang bij 'lambda' bacteriofagen tussen hun sterkte en de hoeveelheid ingepakt DNA (tussen 78 en 100% van de normale lengte). We laten zien dat volledig gevulde virussen twee keer zo sterk zijn als gedeeltelijk gevulde, die zich gedragen als lege virushulzen. Ons model laat zien dat er door DNA-hydraterende watermoleculen een osmotische druk ontstaat in de virussen die exponentieel toeneemt wanneer de virussen bijna geheel gevuld zijn met DNA. In **Hoofdstuk 7** worden alle resultaten samengevat, en worden de mechanische (elastische en niet-elastische) eigenschappen van de verschillende virale systemen vergeleken en bediscussieerd in relatie tot hun biologische context.

`But I don't want to go among mad people,' Alice remarked.

`Oh, you can't help that,'* said the Cat: *`we're all mad here. I'm mad. You're mad.'

`How do you know I'm mad?' said Alice.

`You must be,'* said the Cat, *`or you wouldn't have come here.'

From *Alice's Adventures in Wonderland*
by *Lewis Carroll*

ACKNOWLEDGMENTS

Now when the work is done, and the thesis is written I have the pleasure to express my gratitude to the people who were part of my professional and personal life during all these years.

First of all I would like to thank my supervisor Gijs Wuite. Years ago when I came to Amsterdam you believed in me and gave me the opportunity to start this research and I am really grateful for that. Thank you, Gijs for your constant help, for the useful discussions, for the support to my ideas and for the given freedom in my research. I enjoyed very much working with you and it was a privilege to have you as supervisor.

My gratitude goes also to my promotor Christoph Schmidt. I was happy to work in a stimulating and enjoyable atmosphere in so competitive group. Thank you for your support, your valuable suggestions and interest in my research.

During these years I have been lucky enough to work in collaboration with wonderful scientists.

From the very beginning till the end of my research project the expertise of Jose Carrascosa and his group on ϕ 29 has been always greatly appreciated. I would like to thank Borja, Xabi and Roberto for the purification of the bacteriophage and their helpful advices in that matter. Pepe, thank you for your insightful input in my work.

I learned a lot from the close collaboration we had with Fred MacKintosh. From a scientific text to a Christmas party, you are doing everything with such a stile. Thank you, Fred for all your advices and help.

I would like to acknowledge the fruitful collaboration with the people from UCLA - Jean-Philippe Michel, Melissa Gibbons, William Klug, Robijn Bruinsma, Bill Gelbart, Chuck Knobler. Dear Chuck, besides everything else, you made my visit (my first visit in USA) at UCLA unforgettable –thank you for that.

When I met for the first time Alex Evilevitch, I was so sure that we can do together a wonderful work. Alex – we did it! Thank you for that. Thank you and your family also for the care and your warm hospitality during my visit in Lund.

My special thanks to Pedro de Pablo, who first introduced me to the exiting world of the Atomic Force Microscopy.

I would like to thank all CoSy group members during these years, for the enjoyable, creative and friendly atmosphere which I will never forget. Thank you, guys for your help, support and friendship. If I have to mention all of you and express my feelings I have to write another book, please forgive me that I am not mentioning all of you in person. With some of you I spent a long period in my life. Thank you Bram, thank you Maarten, thank you Erwin, thank you Sander, thank you Lucas, thank you Karen, for being such wonderful colleagues. Thank you, Misha for your friendship. Thank you Remus for our conversations – professional or personal, they were always of great value for me. Maryam, you became my closest dearest friend, what can I say more than that?

From all my heart I like to express my gratitude to Joost and Iwan. You know guys how special you are to me. Joost, whatever I will say, whatever I will write, it will never be enough. From software problems to moving nightmares, you have been always there to help me. I enjoyed talking and discussing with you not only science, not only life but you are the person with whom I shared some of my deepest feelings. Iwan - from the very beginning, during all this years I was sharing my AFM experience with you – bad days and troubles, joyful moments and "bright" ideas. Your help in the AFM/Bio Labs and your opinion on (non)scientific problems were invaluable for me. Sometimes your sense of humor was the only thing to cheer me up at the end of the day.

Joost and Iwan! My paranimfs! Thank you!

I was very happy to have a lot of my old Bulgarian friends here in Netherlands. Thank you guys for your help whenever is necessary and for the nice time we had together. And I was very lucky to meet new friends when I came in Netherlands – Dessy and Yasha. Thank you for being there for me and my family in difficult or joyful moments.

Finally I would like to thank my all family for their constant support and for their belief in me. Without your love I would never make it.

My mother, my brother Stavro and my sister Sofiya, sacred words of gratitude to you are written in my heart. Dad I wish you were here. I dedicate this thesis to your memory.

Yana – my baby, my blessing! Before you I thought I knew what is happiness. I was wrong.

Marko! If I have to write acknowledgments for this period of my life in one word, that will be your name.

LIST OF PUBLICATIONS

Publications related to the work described in this thesis:

1. **I. L. Ivanovska**, P.J. de Pablo, B. Ibarra, G. Sgalari, F.C. MacKintosh, J.L.Carrascosa, C.F. Schmidt and G.J.L. Wuite *Bacteriophage capsids: tough nano-shells with complex elastic properties* Proc. Natl. Acad. Sci. U. S. A. 101: 7600-7605 (2004)

2. J. P. Michel, **I. L. Ivanovska***, M. M. Gibbons, W. S. Klug, C. M. Knobler, G. J. L. Wuite and C. F. Schmidt *Nanoindentation studies of full and empty viral capsids and the effects of capsid protein mutations on elasticity and strength* Proc. Natl. Acad. Sci. U. S. A. 103: 6184-6189 (2006)

* shared first co-author

3. W.S. Klug, R.F. Bruinsma, J.P Michel, C.M. Knobler, **I. L. Ivanovska**, C.F. Schmidt, G.J.L. Wuite *Failure of Viral Shells* Phys. Rev. Letters 97: 228101 (2006)

4. **I. Ivanovska** , G Wuite, B Jönsson, A. Evilevitch *Internal DNA pressure modifies stability of wild-type phage* Proc. Natl. Acad. Sci. U. S. A. April (2007) (accepted)

5. Roos W. H., **Ivanovska I. L**., Evilevitch A. and Wuite G. J. L. *Viral capsids: mechanical characteristics, genome packaging and ejection mechanisms* Cell. Mol. Life Sci, epub 18 April (2007)

6**. I. L. Ivanovska**, X. Agirrezabala, J. L. Carrascosa, C. F. Schmidt, G. J. L. Wuite *Deconstructing viral shells to understand its building blocks* (to be submitted)

Other publications

Arnaudov, L.; Denkov, N. D.; **Surcheva, I**.; Durbut, P.; Broze, G., Mehreteab, A. *Effect of Oily Additives on Foamability and Foam Stability. 1. Role of Interfacial propertie* Langmuir 17(22): 6999-7010 (2001)

Curriculum Vitae

Irena Lambrova Ivanovska was born on October 27, 1972 in Sofia, Bulgaria. She studied at high school "Georgi Bakalov", Sofia. After finishing her high school in 1990 she passed her entrance exam and was admitted to study engineering physics in the Faculty of Physics, Sofia University "Kliment Ochridski", Bulgaria. She graduated in 1995 from the Faculty of Physics, with an MSc in applied optics. The same year she started two years graduate specialization as an international TEMPUS student in the Laboratory of Thermodynamics and Physicochemical Hydrodynamics, Faculty of Chemistry, Sofia University. During that study she spent 5 months in the laboratory of Prof. Paul Joos in University Insteling Antwerpen, Antwerp, Belgium. From 1997 until 2001 she worked as a research associate in the Laboratory of Thermodynamics and Physicochemical Hydrodynamics at Sofia University. In September 2001 she started her PhD at the Department of the Physics of Complex Systems, Vrije Universiteit, Amsterdam. The results of her PhD research are presented in this thesis.